ISTANBUL TECHNICAL UNIVERSITY ★ GRADUATE SCHOOL OF SCIENCE ENGINEERING AND TECHNOLOGY

DEVELOPMENT OF HIGH-PERFORMANCE AND CHLORINE-RESISTANT THIN-FILM COMPOSITE MEMBRANES WITH ZWITTERIONIC SURFACES FOR SEAWATER DESALINATION

Ph.D. THESIS

Jalal-Al-Din SHARABATI

Environmental Engineering Department

Environmental Sciences Engineering and Management Program

JANUARY 2019

ISTANBUL TECHNICAL UNIVERSITY ★ GRADUATE SCHOOL OF SCIENCE ENGINEERING AND TECHNOLOGY

DEVELOPMENT OF HIGH-PERFORMANCE AND CHLORINE-RESISTANT THIN-FILM COMPOSITE MEMBRANES WITH ZWITTERIONIC SURFACES FOR SEAWATER DESALINATION

Ph.D. THESIS

Jalal-Al-Din SHARABATI
(501142703)

Environmental Engineering Department

Environmental Sciences Engineering and Management Program

Thesis Advisor: Prof. Dr. İsmail KOYUNCU

JANUARY 2019

İSTANBUL TEKNİK ÜNİVERSİTESİ ★ FEN BİLİMLERİ ENSTİTÜSÜ

DENİZ SUYU DESALİNASYONUNDA KULLANILACAK ZWİTTERİYONİK KATKILI YÜKSEK PERFORMANSLI VE KLOR DİRENCİNE SAHİP İNCE FİLM KOMPOZİT MEMBRANLARIN GELİŞTİRİLMESİ

DOKTORA TEZİ

Jalal-Al-Din SHARABATI
(501142703)

Çevre Mühendisliği Anabilim Dalı

Çevre Bilimleri Mühendisliği ve Yönetimi Programı

Tez Danışmanı: Prof. Dr. İsmail KOYUNCU

OCAK 2019

Jalal-Al-Din Sharabati, a Ph.D. student of İTU Graduate School of Science Engineering and Technology student ID 501142703, successfully defended the dissertation entitled "DEVELOPMENT OF HIGH-PERFORMANCE AND CHLORINE-RESISTANT THIN-FILM COMPOSITE MEMBRANES WITH ZWITTERIONIC SURFACES FOR SEAWATER DESALINATION", which he prepared after fulfilling the requirements specified in the associated legislations, before the jury whose signatures are below.

Thesis Advisor : **Prof. Dr. İsmail KOYUNCU**
Istanbul Technical University

Jury Members : **Doc. Dr. Derya YÜKSEL-İMER**
Istanbul Technical University

Prof. Dr. İzzet ÖZTÜRK
Istanbul Technical University

Prof. Dr. Bülent KESKİNLER
Gebze Technical University

Prof. Dr. Yusuf MENCELOĞLU
Sabanci University

Date of Submission : 11 December 2018
Date of Defense : 02 January 2019

To my family,

FOREWORD

First and foremost praise is to God the most gracious, the most merciful on whom ultimately we depend for sustenance and guidance. I thank the Almighty for giving me the determination and strength to conclude my research work and compose this thesis. Furthermore, I would like to express my gratitude to all the people who supported me in this course, including all of my family, Prof. Dr. İsmail KOYUNCU, Dr. Derya YÜKSEL-İMER and last but not least all of my colleagues at the National Research Center on Membrane Technologies.

Obtaining drinking water with different membrane technologies is becoming a global trend in our time. Reverse osmosis is currently the most efficient technology for the desalination of seawater. One of the major drawbacks of current seawater desalination membranes is their poor resistance to chlorine. A fundamental understanding of the membrane structure-property relationship and the development of novel and innovative membrane materials is, therefore, critically needed. This thesis aims to contribute to the development of innovative membranes with a novel approach that involves the production of zwitterionic polymers with both positively and negatively charged functional groups. The approach was proposed in the research project "Fabrication of novel forward osmosis and reverse osmosis desalination membranes and modules for application in drinking water production" in cooperation with Sabanci University, Yalova University and the Esan corporation. The project was financed by the Scientific and Technological Research Council of Turkey (TUBITAK) under grant number 113Y356. My part of the project was conducted at the MEM-TEK National Research Center for Membrane Technologies, where I worked together with the master students Şeyma YİLMAZ, Farzin SAFFARIMIANDOAB, Çisil ERİŞ and other researchers. My special thanks go to all the participants of this project.

As an outcome of the collaboration between the universities we were able to modify the standard method for the production of desalination membranes by including the polymerization of zwitterionic silanes in the interfacial polymerization process. In this course we filed a patent for our unique method of organic/inorganic hybrid membrane fabrication. My main tasks in the project were split into membrane fabrication in

laboratory and pilot scale, membrane characterization, membrane performance tests under seawater desalination conditions and chlorination experiments. The optimal fabrication parameters and post treatment steps had to be found and the optimal monomer concentration ratios had to be investigated. This thesis demonstrates that membrane performance can be significantly increased by using zwitterionic monomers in the membrane production process. The advantages of the novel zwitterionic membranes over commercial seawater desalination membranes were, moreover, discussed in several conferences. One of the most important achievements of this work is the reduced sensitivity of the novel membranes to the exposure of chlorine, which is the Achilles heel of current desalination membranes.

January 2019 Jalal-Al-Din SHARABATI

TABLE OF CONTENTS

Page

ABBREVIATIONS

APS	**:** (3-aminopropyl)trimethoxysilane
ATR	**:** Attenuated total reflectance
CSA	**:** (+)-10-camphor sulfonic acid
DI	**:** Deionized
DMAPS	**:** (N,N-Dimethylaminopropyl)]trimethoxysilane
EDS	**:** Energy dispersive spectroscopy
FTIR	**:** Fourier transform infrared
IPC	: Isophthaloyl chloride
MPD	**:** m-phenylenediamine
NIPS	**:** Nonsolvent-induced phase separation
NMP	: 1-methyl-2-pyrrolidinone
NMR	**:** Nuclear magnetic resonance
PEI	: Polyethylenimine
PVA	**:** Polyvinylalcohol
PVP	**:** Polyvinylpyrrolidone
RO	**:** Reverse osmosis
SCADA	**:** Supervisory control and data acquisition
SEM	**:** Scanning electron microscopy
SDS	**:** Sodium dodecyl sulfate
SPPT	**:** (3-sulfopropylbetaine-propyl)-trimethoxysilane
TDI	: Toluene diisocyanate
TEA	**:** Triethylamine
TFC	**:** Thin-film-composite
TMC	**:** Trimesoyl chloride
V	**:** Volume
W	**:** Weight

SYMBOLS

A_m	: Effective membrane surface area
A_s	: Cross-section area of the streaming channel
C_F	: Salt concentration in feed
C_P	: Salt concentration in permeate
J	: Permeate flux
n_1	: Refractive index
L_s	: Length of the streaming channel
P	: Pressure
R	: Salt rejection
R_e	: Electrical resistance
Δt	: Time for collecting permeate
ΔV	: Volume of permeated water
ζ	: Zeta potential
η	: Dynamic viscosity
ε_0	: Vacuum permittivity
ε_r	: Dielectric constant
ρ	: Density
φ	: Streaming potential

LIST OF TABLES

Page

LIST OF FIGURES

Page

DEVELOPMENT OF HIGH-PERFORMANCE AND CHLORINE-RESISTANT THIN-FILM COMPOSITE MEMBRANES WITH ZWITTERIONIC SURFACES FOR SEAWATER DESALINATION

SUMMARY

Thin film composite (TFC) membranes are usually produced by the interfacial polymerization method. The TFC fabrication method allows one to use different polymers as active and support layers. A TFC membrane with a polyamide active layer provides a good separation barrier for reverse osmosis (RO) and can, therefore, be used for seawater desalination. However, these membranes allow only moderate water fluxes and the polyamide active layer can be damaged when it is exposed to chlorine. This thesis describes the fabrication of novel TFC membranes by using zwitterionic monomers (reactants with both positively and negatively charged functional groups) during the interfacial polymerization process for the production of the membrane active layer. In theory, oppositely charged salts in the feed should be repelled electrically by the fixed ionic groups of a zwitterionic active layer. Furthermore, zwitterionic polymers are highly hydrophilic and thus provide an ideal pathway for water. This thesis aims give a deeper insight into the mentioned effects of zwitterionic groups on membrane performance and desalination technology. It will be argued that the zwitterionic properties have a positive effect on salt rejection, water flux and chlorine resistance.

After an introduction into early and recent TFC membrane development efforts in the first chapter of this thesis, the research work is presented in the following two chapters. The second chapter describes the fabrication of the optimal support layer by the phase inversion technique. Commercial RO membranes with high performance for seawater desalination usually have polyamide active layers, which are produced on top of a compaction resistant polysulfone support layer by interfacial polymerization with m-phenylenediamine (MPD) in aqueous and trimesoyl chloride (TMC) in organic phase. In this work, the impact of the support layer pore size on the polyamide active layer polymerization was investigated and the fabrication conditions were optimized. Therefore, six different TFC membrane types with support layers having average pore sizes ranging from 18 nm to 120 nm were fabricated on which the active layers were polymerized. The third chapter of the thesis describes the use of the zwitterionic functional trialkoxysilane monomer (3-sulfopropylbetaine-propyl)-trimethoxysilane (SPPT) as an additional monomer to MPD in the aqueous phase. An interpenetrating polysiloxane-polyamide network is polymerized by using these two monomer for interfacial polymerization with TMC in the organic phase. To find the optimal fabrication conditions, membranes were produced at different monomer concentration ratios and compared to control membranes prepared without silane monomers.

Several characterization methods were used including Fourier transform infrared (FTIR) spectroscopy, contact angle measurements, streaming zeta potential measurements of the membrane surface and scanning electron microscopy (SEM) coupled with energy dispersive spectroscopy (EDS). Cross flow RO tests were performed under seawater desalination conditions (3.2% NaCl feed; 55.2 bar operating

pressure) and salt rejection was calculated from permeate conductivity. Chlorination experiments were performed under the same conditions but with addition of 500 ppm active chlorine to the feed.

The SEM micrographs in the second chapter show that the polyamide ridge-and-valley structure is more pronounced for active layers of TFC membranes prepared with support layers having larger pores. Cross-flow RO tests reveal that the salt rejection of polyamide TFC membranes systematically increases from 80.5% to 99.0% with decreasing support layer pore size. Convective monomer transport during interfacial polymerization is discussed as a possible reason behind the formation of ear- and ridge-like protuberances, of which the latter can apparently be damaging to the inner active layer.

In the third chapter, SEM micrographs of the polysiloxane-polyamide hybrid membranes fabricated with the additional zwitterionic monomer reveal that at high SPPT concentrations the ridge-and-valley structure of the polyamide active layer appears to be filled out with another polymer that has a brittle structure. In the EDS analysis of the scanned areas, the amount of silicon in the modified membranes was measured above the value of the polyamide membrane. The silicon contents of the membranes prepared with higher SPPT/MPD ratios indicate thus a higher incorporation of polysiloxane into the polyamide layer. Comparison of streaming zeta potential measurements display a pH-independent behavior of the zwitterionic membranes due to their strongly acidic and basic functional groups. Membranes produced with a SPPT/MPD ratio of 1 to 10 exhibit an increase in permeate flux from 25 L m^{-2} h^{-1} to 33 L m^{-2} h^{-1} when compared to the control membrane prepared without SPPT, which is an increase of 31%. Furthermore, salt rejection is not compromised, but slightly increases from 98.8% to 98.9%. On the other hand, the highest resistance to chlorine is observed for membranes produced with a SPPT/MPD ratio of 1 to 1. The proposed electrostatic forces induced by the incorporated zwitterionic groups apparently affect the free volume in the active layer and the repulsion of mobile ions.

By using an in-situ polymerization method as in this work, the zwitterionic side groups can be produced not only on the surface but also inside the active layer. It is postulated that the ionic solvation of free water molecules induced by the incorporated zwitterionic groups creates a more hydrophilic pathway for water and a larger free volume in the polyamide network. As a consequence, a higher permeate flux is observed in the modified membranes. Furthermore, the diffusion path of solute ions through the membrane is longer due to electrostatic repulsion between the feed solution and the zwitterionic groups in the active layer. Ion shielding effects that would undermine the electrostatic repulsion are not expected on the permeate side of the active layer, because when solutes diffuse to the permeate side of the membrane, the ionic strength of the permeating solution becomes lower. Even though the free volume of the hybrid polymer is expected to be larger, a high salt rejection can be maintained due to the elongated diffusion path of sodium and chloride ions. Furthermore, an increased rejection of charged chlorine species that are present at high pH, such as hypochlorite (ClO^-) and trichloride (Cl^{3-}) is hypothesized. This effect is thought to shield chlorination of the underlying polyamide layer and thus improve the resistance of the membrane material against chlorine.

This thesis proposes for the first time the use of trialkoxysilane coupling reagents in interfacial polymerization to produce polyamide-polysiloxane hybrid networks. A review of the literature showed that neither zwitterionic functional trialkoxysilanes,

nor other functional trialkoxysilanes had been used as reactants for interfacial polymerization before. Because modification of the TFC membrane fabrication method resulted in the incorporation of zwitterionic polysiloxane polymers inside the polyamide active layer, it is fundamentally different from other methods that involve a coating layer on top of the active layer. An additional coating would result in an additional resistance to membrane flux. In contrast to these methods, the modified membranes produced in this work exhibit a higher flux at certain SPPT/MPD ratios. They also show a significant change in the membrane's active layer morphology, surface properties and chlorine resistance. The lack of a correlation between the streaming zeta potential of the membrane surface and the pH of the streaming solution is, furthermore, a strong indication for the successful integration of the zwitterionic groups into the membrane active layer.

DENİZ SUYU DESALİNASYONUNDA KULLANILACAK ZWİTTERİYONİK KATKILI YÜKSEK PERFORMANSLI VE KLOR DİRENCİNE SAHİP İNCE FİLM KOMPOZİT MEMBRANLARIN GELİŞTİRİLMESİ

ÖZET

Su kaynaklarındaki azalma ve artan enerji maliyetleri, içme suyu eldesinde tüm dünyada kullanılan desalinasyon sistemlerinde yeni çözümler ve işletim modellerinin araştırılması ve geliştirilmesi için yeni çalışma alanları yaratmıştır. Desalinasyon tesisleri Dünya'da 120'den fazla ülkede işletilmektedir ve suyun üretim maliyeti genellikle enerji tüketimi, kullanılan ekipmanın, membranların ve iş gücünün maliyeti ile orantılıdır. Bunun içerisinde en büyük katkıya enerji tüketimi sahiptir.

İlk yüksek performanslı ticari ters osmoz (TO) desalinasyon membranlar Cadotte tarafından üretilmiş poliamid aktif tabakalı ince-film kompozit (IFK) membranlardır. IFK membranları genellikle arayüzey polimerizasyon yöntemi ile üretilirler. IFK üretim yöntemi, aktif ve destek katmanları olarak farklı polimerlerin kullanılmasına izin verir. Poliamid aktif tabakalar, deniz suyu desalinasyonu için iyi bir ayırma verimliliği sağlar ancak ortalama su akısına sahiptirler ve klor direncinden kaynaklı membran hasarlarına eğilimlidirler. Membran sistemlerinde, membran materyalinin yapısal özellikleri, filtrasyon sisteminin tasarımında ve işletmesinde önemli bir etkiye sahiptir. Çünkü materyalin türü, kimyasal ve termal stabilite, ıslanabilirlik, adsorbsiyon ve membran kirlenmesi gibi yüzey özelliklerini etkiler ve filtrasyon performansını belirler. Buna ek olarak, membranın yıkanması aşamasında bazı kimyasal maddeler membranın polimer yapısına zarar verebildiği için kullanılan temizleme prosesinin seçimi de tamamen seçilen membran materyaline bağlıdır.

Yüksek performanslı membranların geliştirilmesi, uygun membran malzemesinin seçimi ve bu malzemenin istenilen membran yapısını oluşturmasının sağlanmasıyla gerçekleşir. Bununla birlikte, çoğu zaman membran performansını arttırmak için membran malzemesinin veya yapısının değiştirilmesi gerekmektedir. Genel olarak, modifiye edilen membranların modifikasyonlarındaki amaçlar şunlardır : (i) akı ve/veya seçiciliğin arttırılması ve (ii) kimyasal direncin (solvent direnci, klor direnci) arttırılmasıdır. Bu nedenle son yıllarda yenilikçi membranlar olarakta isimlendirilebilen birkaç malzemenin (organik-organik, organikinorganik) karıştırılmasıyla üretilen membranlarla ilgili çalışmalar önem kazanmıştır. Özellikle klor direnci yüksek kirlenme potansiyeli düşük malzemelerin desalinasyon membranlarının üretiminde kullanılması büyük avantaj sağlayacaktır.

Bu çalışma kapsamında yüksek performansli ve klor dayanımlı yeni nesil desalinasyon membranlarının üretilmesi hedeflenmiştir. Zwitteriyonik monomerlerin membran aktif tabakasının üretimi için ara yüzey polimerizasyon işlemi sırasında kullanımını ile üretilen özgün IFK membranları tarif etmektedir. Teoride, besleme suyundaki zıt yüklü tuzlar zwitteriyonik aktif tabakasındaki sabit iyonik gruplar tarafından elektriksel olarak itilmelidir. Ayrıca, zwitteriyonik özellikler su için daha hidrofilik bir

geçiş yolu oluşturmalıdır. Bu tez çalışmasında zwitteriyonik grupların genel olarak membran performansına ve özel olarak tuzdan arındırma teknolojisine etkisi hakkında daha geniş bir fikir verilecek, bu iki özelliğin membran akısı ve tuz giderimi üzerinde olumlu bir etkiye sahip olduğu ve hatta klor direnciyle ilgili membran hasarını azalttığı ileri sürülecektir.

İlk bölümde IFK membran üretimindeki ilk çalışmalar ve güncel çalışmalar anlatılırken sonraki iki bölümde bu tez çalışması anlatılmaktadır. Araştırma çalışması, faz inversiyon tekniği ile farklı gözenek boyutlarına sahip polisülfon destek tabakalarının üretimini kapsamıştır. Deniz suyu arıtımı için yüksek performansa sahip ticari RO membranları genellikle sulu faz içindeki m-fenilendiamin (MPD) ve organik faz içindeki trimesoil klorür (TMC) ile ara yüzey polimerizasyonu ile destek tabakasının üzerine üretilen poliamid aktif tabakalara sahiptir. Bu tez, zwitteriyonik fonksiyonel trialkoksisilan monomerin (3-sülfopropilbetain-propil) -trimtoksisilan (SPPT) 'nin sulu fazda MPD'ye ilave bir monomer olarak kullanımını tarif eder. Böylelikle, iç içe geçmiş bir polisiloksan-poliamid ağı, TMC ile ara yüzey polimerizasyonu sırasında polimerize edilebilir. Membranlar üç kopya olarak üretildi ve silan monomerleri olmaksızın hazırlanan kontrol membranları ile karşılaştırıldı. Membran karakterizasyonu, taramalı elektron mikroskopu (SEM) ile birleştirilmiş enerji dispersif spektroskopisini (EDS), fourier transform kızılötesi (FTIR) spektroskopisini, temas açısı ölçümlerini ve membran yüzey yükünün zeta potansiyel ölçümlerini içermektedir. Çapraz akışlı RO testleri deniz suyu desalinasyon koşulları altında (% 3.2 NaCI besleme; 55.2 bar çalışma basıncı) yapıldı ve süzüntü suyu iletkenliğinden tuz tutunumu hesaplandı. Klor deneyleri aynı koşullar altında besleme suyuna 500 ppm klor ilavesiyle yapıldı.

İkinci bölümdeki SEM görüntüleri, daha büyük gözeneklere sahip destek membranları üzerine hazırlanan TFC membranların aktif tabakalarında poliamidin girintili çıkıntılı yapısının daha belirgin olduğunu ortaya koymuştur. Çapraz akışlı RO testleri, poliamid TFC membranlarının tuz reddinin destek tabakasının gözenek boyutunun azalmasıyla sistematik olarak % 80.5'ten% 99.0'a yükseldiğini ortaya koymuştur. Girintili çıkıntılı kulak benzeri yapıların oluşumunun arkasındaki muhtemel sebebin arayüzey polimerizasyonu sırasında konvektif monomer taşınması olduğu düşünülmektedir ve bu durum aktif tabakanın yapısına zarar verebilir.

Üçüncü bölumde yüksek SPPT konsantrasyonlarında üretilen membranların SEM görüntüleri, aktif tabakanın sırt-vadi yapısının, nodüler poliamid yapısına belirgin bir şekilde farklı olan, kırılgan bir yapıya sahip başka bir polimer ile doldurulduğunu ortaya koymaktadır. Taranan alanların EDS analizinde, modifiye edilmiş zarlardaki silikon miktarı, poliamid membranın değerinin üzerinde ölçülmüştür. Daha yüksek SPPT / MPD oranlarıyla hazırlanan membranların silikon içeriği, poliamid tabakasına daha yüksek bir polisiloksan katılması olduğunu göstermektedir. Zeta potansiyel ölçümlerinin karşılaştırılması, kuvvetli asidik ve bazik fonksiyonel gruplarından dolayı zwitteriyonik membranların pH-bağımsız davranışını göstermiştir. SPPT / MPD oranı 0.1 ile üretilen membranın akısı kontrol membranlarına kıyasla 25 $Lm^{-2}saat^{-l}$'den 33 Lm^{-2} $saat^{-1}$'e kadar %31 oranında artmıştır. Ayrıca, tuz tutunumunda herhangi bir azalma gözlenmemiştir ancak % 98.8'den % 98.9'a hafifçe artmıştır. Diğer taraftan, klor direnci en yüksek olan membran SPPT/MPD oranı 1/1 olarak üretilmiştir. Anlatılan zwitteriyonik grupların neden olduğu önerilen elektrostatik kuvvetler, aktif tabakadaki serbest hacmi ve hareketli iyonların itilmesini etkilemektedir.

Bu çalışmada kullanılan in-situ polimerizasyon yöntemi, sadece yüzeyde değil aktif katmanın içinde de zwitteriyonik yan gruplar oluşturur. Birleştirilmiş zwitteriyonik gruplar tarafından tesir edilen serbest su moleküllerinin iyonik solvasyonunun, daha hidrofilik bir su yolu ve poliamid ağında daha büyük bir serbest hacim yaratması önerilmiştir. Sonuç olarak, daha yüksek bir süzüntü akısı gözlenir. Ayrıca, çözünen iyonların membran boyunca yayılma yolu, besleme çözeltisi ile aktif tabakadaki zwitteriyonik gruplar arasındaki elektrostatik itme nedeniyle daha uzun olacaktır. Çözücüler, membranın süzüntü tarafına yayıldığı zaman, nüfuz eden çözeltinin iyonik gücü, besleme çözeltisinden daha düşüktür ve bu nedenle, aktif tabakanın süzüntü tarafında elektrostatik itmeyi zayıflatacak iyon koruyucu etkiler beklenemez. Sadece besleme tarafında bu etki gözlenebilir. Hibrid polimerin serbest hacminin daha büyük olması beklenmekle birlikte, sodyum klorür iyonlarının uzatılmış difüzyon yolundan dolayı yüksek bir tuz tutunumu sağlanabilmektedir. Ayrıca hipoklorit (ClO^-) ve triklorür (Cl_3^-) gibi yüksek pH'ta mevcut olan yüklü klorlu türlerin tutunduğu hipotezi de kurulmuştur. Bu etkinin altta yatan poliamid tabakanın klorlanmasını engellediği ve böylece membran malzemesinin klora karşı direncini arttırdığı düşünülmektedir. Üretilen membranların sularda bulunan veya kimyasal yıkama aşamasında ortama katılan klora karşı olan dayanıklılıkları özellikleri belirlenmiştir.

Mevcut çalışmada olduğu gibi, poliamid-polisiloksan hibrit ağları üretmek için arayüzey polimerizasyonda trialkilsiyalan birleştirme reaktiflerinin kullanımı literatürde daha önce önerilmemiştir. Ne zwitteriyonik fonksiyonel trialkoksisilanlar, ne de başka fonksiyonel trialkiloksilanlar, arayüzey polimerizasyonu için reaktifler olarak kullanılmamıştır. IFK membran üretim yönteminin modifikasyonu, poliamid aktif tabakanın içine zwitteriyonik polisiloksan polimerlerin dahil edilmesine yol açtığından, esas olarak, aktif tabakanın üstünde bir kaplama tabakası içeren diğer yöntemlere göre farklıdır. İlave bir kaplama, membran akışına karşı ek bir direnç ile sonuçlanır. Bu yöntemlerin aksine, bu çalışmada üretilen modifiye edilmiş membranlar, belirli SPPT / MPD oranlarında daha yüksek bir akı sergilemiştir. Ayrıca, membranın aktif tabaka morfolojisinde ve yüzey özelliklerinde de önemli bir değişiklik göstermektedir. Çözelti pH'ı ve membran yüzeyinin zeta potansiyeli arasında bir korelasyon olmaması, ayrıca zwitteriyonik grupların başarılı bir şekilde bütünleştiğini gösteren güçlü bir göstergedir.

Bu çalışma, 113Y356 ana proje kodu ile Türkiye Bilimsel ve Teknolojik Araştırma Kurumu (TÜBİTAK)-Çevre, Atmosfer, Yer ve Deniz Bilimleri Araştırma Destek Grubu (ÇAYDAG) Öncelikli Alanlar Ar-Ge Projeleri Destekleme (1003) programı tarafından desteklenmiştir.

1. INTRODUCTION

Today, the most efficient method for the desalination of seawater is reverse osmosis (RO) with semipermeable membranes. Since the first introduction of membrane based RO systems, their energy consumption has declined dramatically, reaching almost the practical minimum energy for an ideal RO stage [1]. Still, one of the major drawbacks of current desalination membranes is their poor resistance to chlorine [2]. Moreover, their rough surface properties diminish process efficiency and necessitate energy expensive pre-treatments [3–6]. Thus, a fundamental understanding of the membrane structure-property relationship and the development of chlorine-resistant membrane materials are critically needed in advancing membrane technology.

1.1 Purpose of Thesis

This thesis investigates the structure-property relationship of high–performance membranes and describes the development of a novel method for the fabrication of seawater desalination membranes with new properties and improved performances, including an improved resistance to active chlorine species. The method is based on the polymerization of zwitterionic monomers, which are reactants that possess both positively and negatively charged functional groups. The monomers are used during the production of the membrane active layer along with other monomers in order to create an interpenetrating network of two polymers with hybrid properties. The purpose of this study is to understand the effects of electrostatic forces on free volume and mobile ion rejection during the desalination process. This understanding is of great importance for the development of efficient membranes.

1.2 Literature Review

Several factors contribute to the successful fabrication of high performance membranes. Materials with the appropriate properties must be selected depending on the separation task. For desalination a dense, water-permeable but effectively salt-

impermeable material is needed. The challenge is to manufacture this material as a robust, thin and defect-free membrane. The World Health Organization (WHO) guidelines for drinking-water quality [7] state that "the palatability of water with a total dissolved solids (TDS) level of less than about 600 mg/l is generally considered to be good". In order to produce a permeate of 500 mg/L NaCl from a synthetic seawater feed of 35 g/L NaCl with a 30% recovery, a membrane is needed that rejects at least 99.0% of the salts. Considering that desalination membranes loose approximately 0.3% rejection over a 3-year life time, a membrane with at least 99.3% rejection is needed for seawater desalination. In order to achieve a high salt rejection, the membranes have to be defect free.

1.2.1 Early development of interfacially polymerized membranes

In the early 1960's, an important discovery transformed membrane separation from a laboratory to an industrial process: the Loeb–Sourirajan method for making high-flux, anisotropic RO membranes. These cellulose acetate based membranes consisted of an ultrathin, selective surface layer on a thicker microporous support, which provides the mechanical strength [8]. For the first time, membrane water flux was high enough to make RO a potential technology for the effective desalination of seawater. Later on, the commercialization of RO membranes played a key role in the development of ultrafiltration, microfiltration and other membrane technologies [9]. Building on the original Loeb–Sourirajan method, alternative membrane formation processes were developed for high-performance membranes. In principal, membranes that have thin selective layers should be fabricated to allow high flux, while maintaining mechanical strength of a thick support layer. This approach lead to the utilization of the interfacial polymerization technique, which brings two reactants together at an interface between two immiscible phases, where a thin and dense polymer film is produced [10]. When this layer is formed on a microporous support layer, an anisotropic membrane is produced, which is called thin film composite (TFC). The nature of the reaction is self-inhibiting. Passage of a limited supply of reactants through the already formed layer results in a film of extremely low (~100 nm) thickness. A scheme of the different anisotropic membranes is given in Figure 1.1.

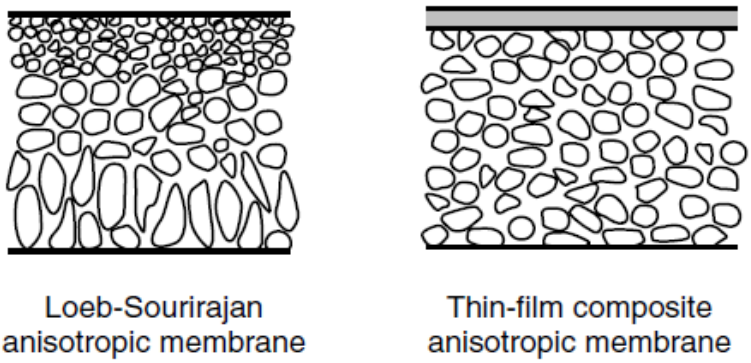

Figure 1.1 : Schematic diagrams of principle types of anisotropic membranes [11].

A review from 1981 by Cadotte & Petersen [12] - two pioneers in the field of composite membrane fabrication - gives an account of the developments leading up to the commercialization of high performance RO membranes. They described how the idea of turning away from low flux Loeb-Sourirajan cellulose based RO membranes to TFC membranes, lead to the development of polysulfone support layers with higher fluxes and resistance to compaction. Interestingly, the Loeb-Sourirajan method continued to be an essential membrane fabrication method, because it was found that the support layer of the TFC membrane should be Loeb-Sourirajan type in order to provide small pores on the support skin with a much thicker and more permeable microporous structure on the support backside to provide the mechanical strength. In a patent for TFC membranes by Cadotte [13] it was stated that only as long as the pores on a support surface have an average diameter of about 20 nm, the active layer can bridge over the pores and provide a relatively defect-free reverse osmosis layer. Therefore it was revealed that Loeb-Sourirajan type anisotropic membranes should be used as support layers for TFC membranes, since it was able to achieve the described characteristics with a sufficiently high water flux, in contrast to isotropic membranes. The high molecular polysulfone UDEL-3500 from Union Carbide was identified as having the best combination of compaction resistance and surface microporosity. Casting this polymer over a woven or non-woven polyester fiber backing would produce a sponge like structured support membrane, where finger-like macro cavities are not observed.

Several materials have been fabricated as RO membranes since their first introduction in the 1960's. First, cellulose-acetate-based membranes and later on TFC membranes were developed by utilizing the interfacial polymerization method. The turn away from cellulose (polysaccharide) type membranes was decisive. Cadotte and coworkers

found that even if TFC membranes were fabricated with a very thin cellulose active layer, the improved membrane flux was still not sufficient. Therefore they started to develop membranes based on polymers other than cellulose and named their membranes with the prefix NS, which stands for non-saccharide e.g. NS-100, NS-101 and NS-200. Cadotte & Petersen documented how they and other researchers started to use polymerization techniques on top of polysulfone supports to further improve membrane water flux, which at that time was not sufficiently enough to make membrane technology economically feasible to desalinate seawater [12]. In the course of this evolution it was found that interfacial polymerization is an excellent method to produce thin and defect-free active layers.

Figure 1.2 excerpted from source [10] illustrates the early developments of different active layers and their polymerization reactions. Rozell et al. in 1967 [14], described the preparation of the first interfacial polymerized TFC membranes, which at that stage had only low salt rejections. They developed later in 1970 the NS-100 as the first high salt-rejecting membrane from polyethylenimine (PEI). The active layer of the membrane was produced by interfacial polymerization of PEI in aqueous solution and toluene diisocyanate (TDI) in the organic solution [15]. The polymeric PEI reacts with the monomeric TDI and a cross-linked polyurea polymer is produced. Then the coated and drained polysulfone support had to be dried at high temperature in a post treatment step. A salt rejection greater than 99% could thereby be achieved for the produced composite membrane on a synthetic seawater feed at high pressure. For the NS-101, isophthaloyl chloride (IPC) was substituted for TDI as the cross-linker. The selective layer in this membrane consisted of a cross-linked polyamide thin-film and also demonstrated high permselectivity. However, in both membranes the mechanical stability was not high and the membranes were highly vulnerable to attack by chlorine. Riley et al. continued to develop membranes based on polyamide, which has been very promising. In 1975, they developed the PA-300 membrane, whose prefix stands for polyamide [27]. The sensitivity to chlorine could be reduced because they produced a polyamide polymer backbone without residual amines or amide functional groups, which are prone to chlorine attack. Later the development shifted from polymeric reactants to monomeric reactants, in order to have more controllable reactions. Eventually, the NS-300 was developed that was prepared from the reaction of the

monomeric piperazine with the trifunctional monomer, trimesoyl chloride (TMC) and in later variants with both TMC and IPC.

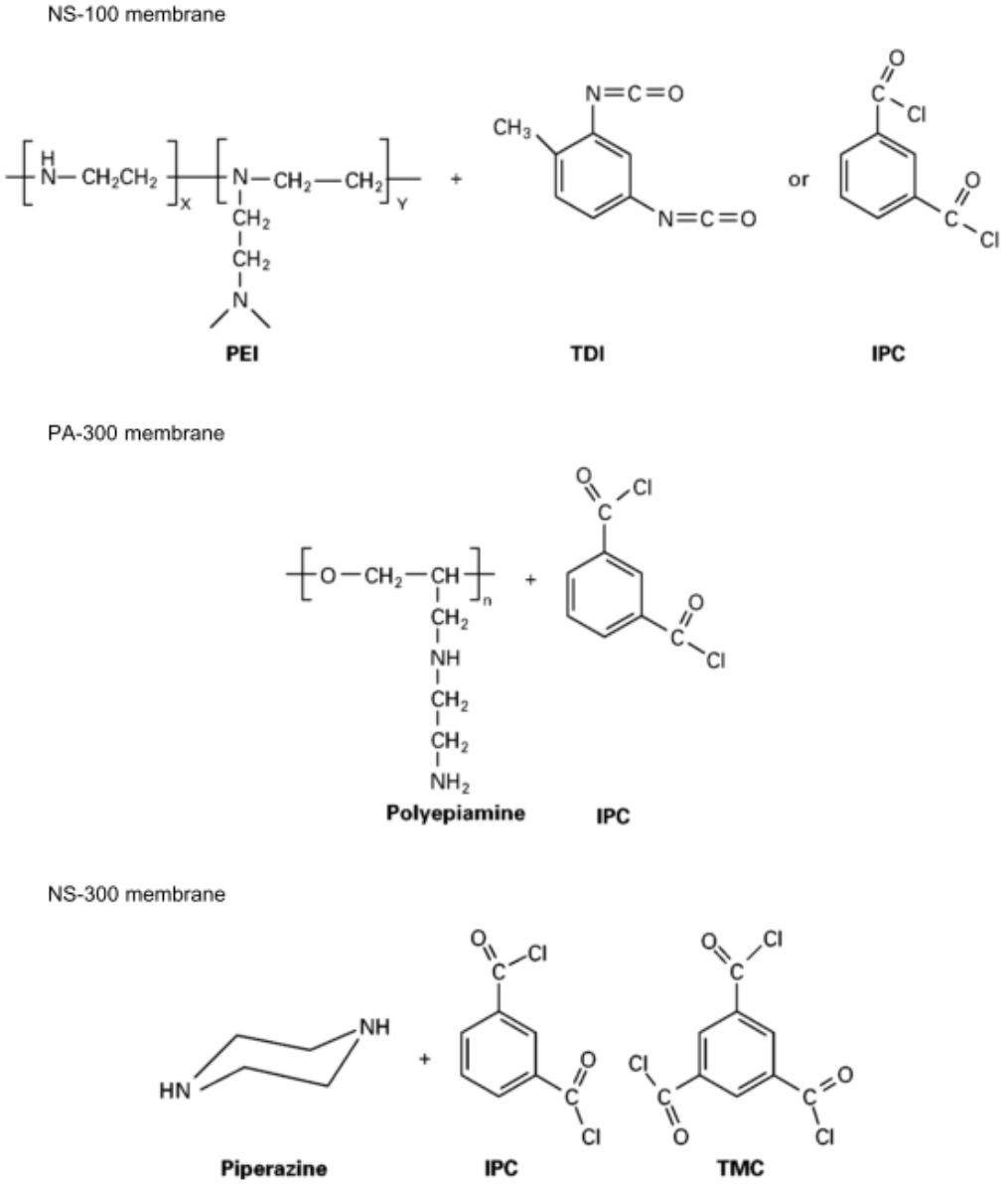

Figure 1.2 : Early developments in TFC membrane polymerization [10].

In 1978, Cadotte and his co-workers at FilmTec used a monomeric, aromatic amine, m-phenylenediamine (MPD) as a reactant instead of piperazine: the FT-30 membrane [13] was produced from the reaction of MPD with TMC, as shown in Figure 1.3a. Since then, this membrane has become the new industry standard until today. It exhibited even superior chlorine tolerances to its precursor models. However, the tolerance is still very limited as low chlorine levels in the ppm range can even destroy the polyamide layer after a certain time [10]. The FT-30 membrane structure and its original photomicrographs are presented in Figure 1.3b [12].

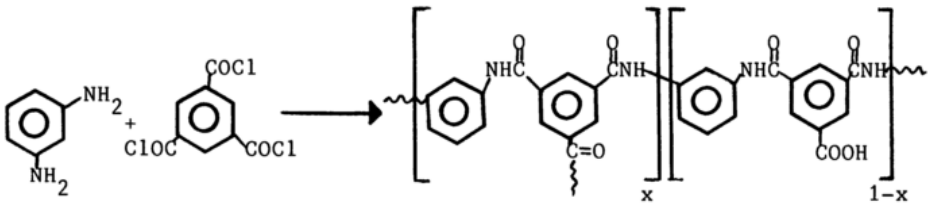

a)

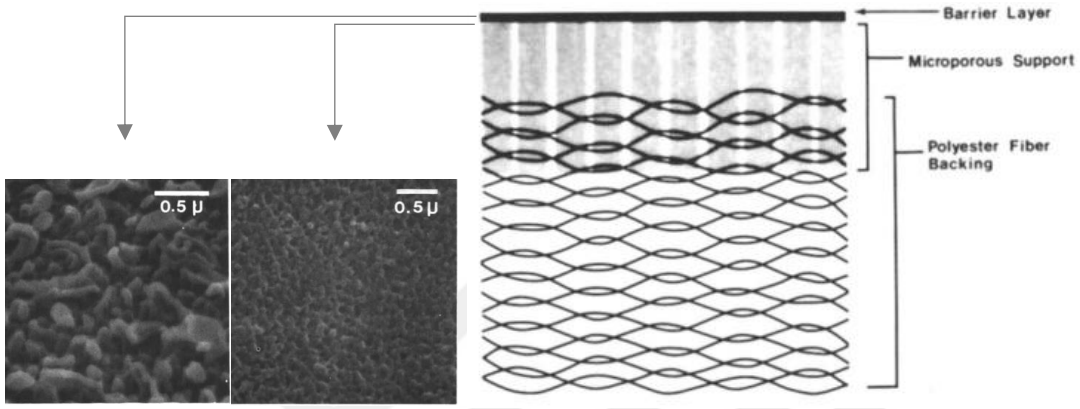

b)

Figure 1.3 : FT-30 membrane developed by Cadotte and coworkers [12]. a) Reaction between MPD and TMC for the production of the active (barrier) layer. b) Schematic structure (right) and surface photomicrographs of the active layer and the microporous support layer (left).

1.2.2 Recent development of desalination membranes

The previous section demonstrated how the TFC fabrication method allows one to use different polymers as active and support layers. Whereas early TFC membrane developments concentrated on finding suitable reactants for the polycondensation reaction (thereby producing different active layer polymers including polyamide, polyurea and polyurethane), nowadays development efforts are more focused on optimizing active layer chemistry and morphology, with a couple of known monomers. The experience that was gained from the development of seawater desalination membranes, lead to their successful commercial application. The fabrication of polyamide active layers from aromatic monomers remains until today the state of the art. The interfacial polymerization reaction is most commonly carried out with MPD in aqueous and TMC in organic phase or their derivates with one additional amine group and one missing chloride group respectively [16]. Seawater desalination membrane manufacturers most commonly use aromatic polyamide as the active layer,

because it has been revealed to be a very dense polymer with rejections over 99.3% for seawater desalination. By changing reaction and coating conditions the optimal structure is tried to be obtained, which should be translated in a performance increase by maximizing solvent passage and minimizing solute passage. Studies about the mechanism of solvent/solute transport in permselective polymers play thereby a very important role in order to understand the membrane structure-performance relationship. This is very difficult given the nanoscale nature of the thin film and the barrier thickness is not always related to flux. The relationship between amine monomer diffusivity/solubility and membrane morphology and crosslinking density is very important to understand in this regard.

In Cadotte`s patent [13] an important structure-performance relationship is described, which states that as long as pores on the support layer surface have an average diameter of about 20 nm, the active layer can bridge over these pores and form a relatively defect-free RO layer. However, limited scientific research has been published in the literature to give further insight into this relationship since then. Many approaches have been reported to analyze the structure and morphology of polyamide-TFC membranes; however, the effect of the support layer on the interfacial polymerization reaction has often been underestimated [17,18]. In recent studies, it has become more evident that the support layer has a substantial influence on the interfacial polymerization process and thus the properties of the resulting polyamide active layer [19–25]. It has been demonstrated that thickness, roughness and cross-linking degree of the polyamide layer depend on surface properties of the support layer including its pore size, porosity and hydrophilicity. Singh et al. [23] investigated the effect of support layer pore size on polyamide layer formation. Interfacial polymerization of MPD and TMC was performed on the surface of polysulfone support membranes with average pore size distributions of 70 nm and 150 nm, respectively. It was argued that polysulfone substrates with an average pore size of 150 nm resulted in the formation of a thinner polyamide layer than in the case of the 70 nm pore size support, causing a higher degree of defects and lower salt rejection. Misdan et al. [19,24] also reported that the thickness of the polyamide layer decreased with increasing surface pore size of the polysulfone support layer. Ghosh and Hoek [21] similarly found out that larger, hydrophobic pores of the support layer produced more permeable and rougher TFC membranes. However, these studies solely concentrated on brackish water desalination

membranes, which are distinctively different from seawater desalination membranes in terms of permeability, rejection and active layer morphology [26]. The effect of support layer pore size on high-performance RO membranes, as required for seawater desalination, has not yet been reported in the literature.

Factors that govern the interfacial polymerization reaction are expected to influence the structure and properties of the polyamide active layer as well. Due to the low solubility of most acid chloride monomers in water, a large excess of the amine monomer must be used. Xie et al. [27] investigated the influence of monomer concentrations on membrane performance. It was found that increasing the MPD concentration increases its partitioning and diffusion into the organic phase, where the active layer polymerizes. As a consequence, a thicker active layer and a lower water flux is observed. The type of the organic solvent can also influence partitioning and diffusion of the amine monomer and thus affect the resulting active layer morphology. The effect of the organic solvent on membrane performance and morphology was investigated in a study from Ghosh et al. [28]. The authors reported the mentioned correlation between diffusivity and partitioning on active layer thickness. However, film thickness and morphology were not found to intrinsically affect water permeability. The absence of a clear correlation lead the authors to conclude that membrane resistance is not solely determined by film thickness. Rather, separation would occur at a "dense inner barrier layer" and the visible polyamide morphology is a "byproduct of the polymerization reaction" [28]. These findings suggest that further studies are required to understand the structure-property relationship in TFC membranes.

Chlorination, i.e. the use of different chlorine species to oxidize and disinfect microorganisms is an integral part of seawater pre- and posttreatment [29]. This step must be followed by a dechlorination step, before feed water comes into contact with polyamide membranes, because otherwise the chlorine would cause membrane damage. The sensitivity of current polyamide membranes to chlorine comes from the high electron density of amide linkages in polyamide. Chlorine has a high potential to oxidize their N–H groups by converting them to N–Cl groups (N-chloroamide), which can also undergo intermolecular rearrangement to form various aromatic substitution products [30]. The risk of failure of the dechlorination system as well as higher costs and the limitation of disinfection strategies are problems encountered from the

sensitivity of current RO membranes to chlorine. Therefore, research efforts are made to reduce the chlorine sensitivity by modifying polyamide membranes or using alternative polymers [31]. Numerous studies have been conducted using different monomeric reactants to improve RO performance [2,32,33]. However, improving the water flux without sacrificing salt rejection at seawater desalination conditions was only achieved in few studies [34–37].

Zwitterionic structures, which have both positively and negatively charged groups such as sulfobetaine, carboxybetaine or phosphobetaine, have recently attracted the interest of membrane scientists [38–40]. By forming ionic bonds, water molecules tend to bind more strongly to such materials than to other hydrophilic materials that can only form hydrogen bonds [41]. While the water that is adsorbed by polar groups is referred to as hydrating water, the water surrounding the hydration layer can be referred to as free water due to its similar properties to liquid water [42–44]. Whereas the presence of hydrating water is observed in hydrophilic films, free water has been observed additionally in the matrix of zwitterionic films [45]. The interaction of the opposite charges of zwitterionic groups with the opposite poles of water molecules is thought to facilitate the formation of free water layers by electrostatic attractions. This effect can be attributed to the ionic solvation of free water molecules. Incorporation of zwitterionic groups into membranes could create a hydrophilic pathway to enhance water transport and provide electrostatic repulsion to increase salt rejection [37,38,46].

Incorporation of charged functional groups into TFC membranes can be achieved by addition of functional monomers during the interfacial polymerization reaction [47,48] or by modification of the membrane surface [40,41,49]. Zhao et al. [37] prepared high-flux RO membranes by adding the co-monomer, o-aminobenzoic acid-triethylamine salt (o-ABA-TEA), to the aqueous MPD solution to react with TMC during interfacial polymerization. The co-monomer has a negatively charged functional group and an exchangeable cation (TEA) attached to the functional group via an ionic bond. The synthesized membrane exhibited high permeate flux and salt rejection under seawater desalination conditions. Ma et al. [50] incorporated a zwitterionic diamine monomer, N-aminoethyl piperazine propane sulfonate (AEPPS), into polyamide RO membranes via interfacial polymerization. As a result, modified RO membranes exhibited an enhanced separation performance under brackish water conditions. However, high salt

rejections for seawater desalination have not been achieved yet with zwitterionic monomers.

1.3 Hypothesis

In the literature, there are fairly limited scientific works on the modification of TFC membranes with silanes, which are used as monomers for condensation reactions. Different studies are reported on the use of siloxane based polymers as materials for gas separation [51–56] and desalination membranes [57,58]. Studies of the Y. T. Lee research group comprised the coating of commercial polyamide RO membranes with functional trialkoxysilanes for an improved salt rejection [59], chlorine resistance [30] and antifouling properties [60]. In these modified commercial membranes, the essential of the modification is based on sol-gel condensation reactions of silane coupling agents on top of the polyamide surface (Figure 1.4a). However, coating of the membrane surface with a polymer creates additional resistance that reduces permeate flux. Instead of using a coating method, the approach of this thesis is to in-situ polymerize zwitterionic alkoxysilanes during interfacial polymerization with MPD and TMC. Prior to polymerization, the alkoxysilane monomers were functionalized to contain sulfobetaine zwitterionic groups (Figure 1.4b). The monomers do not only undergo the described condensation reactions, but also react with TMC. As a result, an interpenetrating and crosslinked polysiloxane - polyamide network with zwitterionic moieties is produced as the active layer of the TFC membrane.

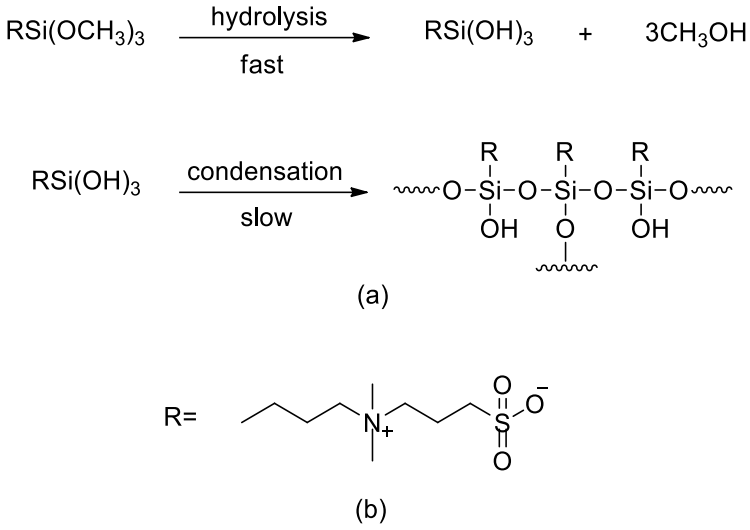

Figure 1.4 : a) Formation reaction of polysiloxane by sol-gel condensation of trialkoxysilane compounds. b) Zwitterionic functional group of the trialkoxysilane monomer used in this work.

In the light of the above, it is postulated that the use of zwitterionic polymers as the active layer of TFC desalination membranes, will increase the membrane desalination performance. In theory, the oppositely charged salts should be electrically repelled by the fixed ionic groups of the zwitterionic polymer. Furthermore, the zwitterionic properties of the produced active layer will create a more hydrophilic water pathway. These two properties will have a positive effect on membrane flux and rejection and furthermore will decrease chlorination related membrane damage by shielding the active layer from charged chlorine species. The study of these aspects provides a deeper understanding of electrostatic forces during solution diffusion and how zwitterionic structures effect free volume and mobile ion rejection. This understanding is of great importance for the development of efficient TFC membranes.

2. IMPACT OF SUPPORT LAYER PORE SIZE ON ACTIVE LAYER POLYMERIZATION AND SEAWATER DESALINATION PERFORMANCE

This chapter focuses on the structure-property relationship of interfacially polymerized thin-film composite (TFC) membranes. Since the structure of a membrane and its properties are correlated, a fundamental understanding of this relationship is required.

The impact of the polysulfone support layer on the polymerization of the polyamide active layer is investigated systematically and the resulting membrane surface morphology is related to RO separation performance under seawater desalination conditions. Six different TFC membranes with support layers having average pore sizes ranging from 18 nm to 120 nm were fabricated. Cross-flow RO tests reveal that salt rejection systematically increases from 80.5% to 99.0% with decreasing support layer pore size. Scanning electron microscopy at high resolution was used to show that the ridge-and-valley structure is more pronounced for active layers of TFC membranes prepared with support layers having larger pores. Convective monomer transport during interfacial polymerization is discussed as a possible reason behind the formation of ear- and ridge-like protuberances, of which the latter can apparently be damaging to the inner active layer. This understanding is very important for the development of novel TFC membranes.

2.1 Materials and Methods

2.1.1 Materials and reagents

Polysulfone Udel P-3500 NT LCD (molecular weight mw: 80-86 kDa) was purchased from Solvay Specialty Polymers (USA). N,N-dimethyl formamide (DMF) was purchased from Akkim Chemicals (Turkey). Polyvinylalcohol (PVA) (mw: 89-98 kDa; hydrolysis degree: 87–89%), polyvinylpyrrolidone (PVP) PVP10 (mw: 10 kDa), PVP40 (mw: 40 kDa), m-phenylenediamine (MPD) (99%), triethylamine (TEA) (99.5%), (+)-10-camphor sulfonic acid (CSA) (98%), 1,3,5-benzene tricarboxylic acid chloride or trimesoyl chloride (TMC) (98%) were obtained from Sigma–Aldrich (Germany). Sodium chloride (NaCl) salt Emprove and n-hexane Suprasolv were

purchased from Merck (Germany). CU424 type polyethylene terephthalate (PET) non-woven fabric (thickness: 90 μm; width: 1 m) from Neenah Papers (USA) were used as backing material. All chemicals and materials were used as received unless specified. Commercial RO membranes, TM810C and TM810V from Toray (Japan) were used for comparison with fabricated TFC membranes. 15 x 10 cm membrane samples were cut from opened 4 inch diameter modules. Both membranes are TFC type and consist of a polyester non-woven fabric, a polysulfone support layer and a polyamide active layer.

2.1.2 Fabrication of support layer

The nonsolvent induced phase separation (NIPS) method [61] was applied to produce support layer membranes with different average pore sizes using a pilot scale flat-sheet membrane fabrication machine. Polymer casting solutions were prepared in DMF with 18% (w/w) polysulfone polymer and varying amounts of PVP. Solutions were cast onto a polyester nonwoven fabric layer using a casting knife with a 130 μm gap at varying speeds and then coagulated in a water bath. Parameters such as PVP concentration, casting speed and coagulation bath temperature were varied in order to produce support membranes with different average pore sizes on the membrane surface. Final support layer membranes had sponge-like structures with thicknesses around 40 μm excluding the nonwoven fabric. Six different membranes were fabricated as the support layer for interfacial polymerization labeled from Type-1 to Type-6, as listed in Table 2.1.

Table 2.1 : Fabrication parameters for support membranes with different pore sizes.

	Casting solution composition			**Coagulation parameters**	
	Polysulfone (%w/w)	PVP10 (%w/w)	PVP40 (%w/w)	Casting speed (m/min)	Bath Temperature (°C)
Type-1	18	4.5	1.5	1.5	30
Type-2	18	4.5	1.5	1.5	25
Type-3	18	4.5	1.5	3	25
Type-4	18	4.5	1.5	3	20
Type-5	18	4.5	-	3	25
Type-6	18	4.5	-	3	15

2.1.3 Fabrication of active layer

The interfacial polymerization method was used for the preparation of TFC membranes in laboratory scale similar to a method from Xie et al. [27]. The method was modified by using increased monomer concentrations and additives in order to produce seawater desalination membranes. The support membrane surface was immersed for 5 min into a 2% (w/w) MPD solution with 2% (w/w) TEA, 5 % (w/w) CSA and 0.1 % (w/w) SDS as additives. After removing excess MPD solution on the surface by using a rubber roller and drying for 120 sec, the membrane was contacted with a 0.1% (w/v) TMC solution for 1 min. This was followed by an oven curing step at 70 °C for 10 min. Prepared TFC membranes were washed with distilled water and dipped into an aqueous 0.2% (w/w) PVA solution to adsorb a protective layer. Membranes were labeled TFC Type-1 to TFC Type-6 according to their support layer.

2.1.4 Evaluation of membrane performance

The cross-flow RO-system that was used to determine the desalination performance in this study is illustrated in Figure 2.1. It consisted of a feed tank with heat exchanger, cartridge filter, high pressure pump, membrane filtration cell, permeate collection vessel, computer with supervisory control and data acquisition (SCADA), flow meter, and pressure, pH, temperature and conductivity sensors. The effective filtration area of the membrane in the membrane filtration cell was 140 cm^2. The feed was subjected to coarse filtration by a cartridge filter (5 µm pore size) before entering the high pressure pumping system.

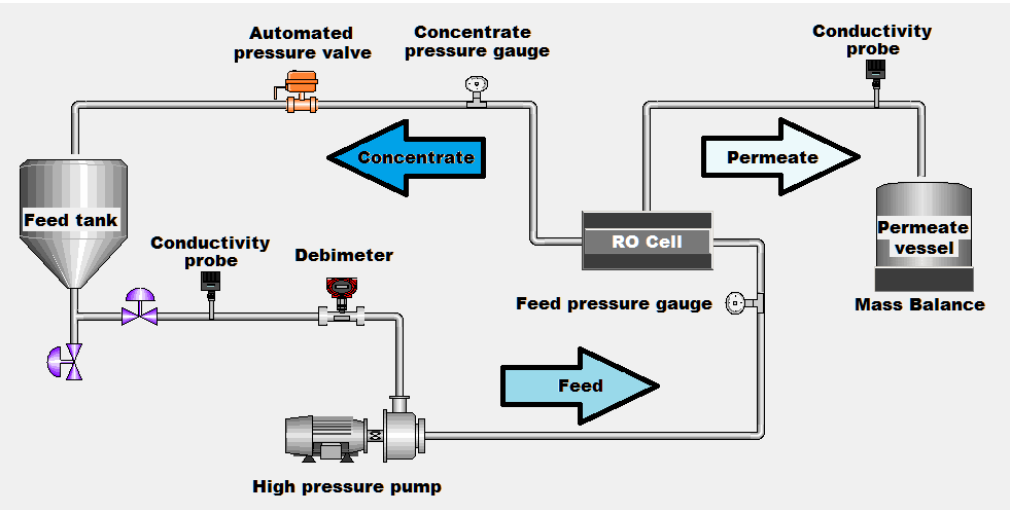

Figure 2.1 : Cross-flow RO filtration system used for the evaluation of desalination performances.

Membrane performances were determined by operating the cross-flow RO system with a synthetic seawater feed consisting of 3.2% (w/w) NaCl in deionized water with a pH of 5.9. Permeate flux and salt rejection of each membrane were measured after stabilization at 55.2 bar for 60 min. During the filtration, the concentrate was recirculated at a flow rate of 5 L/min to the feed the tank, and the temperature was cooled to 25 ± 1 °C. Permeate flux J in L m^{-2} h^{-1} was calculated from the measured permeate weight converted to volume of permeated water (ΔV), the time for collecting fixed volume water (Δt), and the effective membrane filtration area (A_m) according to equation (2.1):

$$J = \frac{\Delta V}{(\Delta t \times Am)} \tag{2.1}$$

Electrical conductivity of feed and permeate solutions were measured using a conductivity meter. A calibration curve was used to relate solution conductivity to salt concentration. Salt rejection (R) was calculated from salt concentrations in permeate (C_P) and feed (C_F) according to equation (2.2):

$$R = \left(1 - \frac{C_p}{C_F}\right) \times 100\% \tag{2.2}$$

Salt rejection and permeate flux were reported as averages of measurements from at least three separately produced membranes for each membrane type. Error bars represent the standard deviation from mean values.

2.1.5 Membrane characterization

Scanning electron microscopy (SEM) with FEI Quanta FEG 200 SEM was used to analyze the membrane surface. Membrane samples were coated with Gold and Palladium (Au-Pd) particles (5 nm diameter) with Quorum SC7620 ion sputtering equipment. Cross-sectional SEM samples were prepared by freeze fracturing with liquid nitrogen. Imaging software ImageJ was used to determine the average pore size of each support membrane. The obtained micrographs were processed first by converting the greyscale image into a binary (black and white) image. The software then identified each pore and quantified the pore area. The area of membrane pores were calibrated using the SEM image scale. The pore diameter d was then calculated from the pore surface area A_p according to formula equation (2.3):

$$d = 2\sqrt{\frac{A_p}{\pi}} \tag{2.3}$$

The pore size distribution was then used to calculate the average pore size and its standard deviation. The obtained results were statistically analyzed to interpret the influences of casting parameters on support layer pore size by analysis of variance (ANOVA) using Origin 8 statistical software.

Fourier transform infrared spectroscopy (FTIR) was performed using Perkin Elmer Spectrum 100 FT-IR spectrometer with a resolution of 4 cm^{-1}. The attenuated total reflectance (ATR) crystal is composed of a diamond ATR with a zinc selenide focusing element, which is in direct contact with the diamond and has a refractive index of 2.4. A background spectrum was taken to decrease instrumental and atmospheric contributions to a minimum level before each sample measurement.

2.2 Results and Discussion

2.2.1 Examination of commercial seawater desalination membranes

2.2.1.1 Seawater desalination performance

Two different state-of-the-art commercial RO membranes from Toray were examined, in order to have a comparison to laboratory fabricated membranes. Both membranes are of TFC type with a polyamide active layer. Table 2.2 lists the RO performance of the two commercial membranes as specified by the manufacturer and as measured from membrane sheets that were cut from opened modules in our laboratory. The TM810C membrane is referred to as a standard seawater RO membrane with a lower permeate flux than the TM810V membrane, which is described as a low energy seawater RO membrane. The performance data of the membranes tested in the laboratory cross-flow filtration setup did not match the specification, possibly because of membrane damage from oxidation during storage or from the extraction of membranes from modules.

Table 2.2 : RO-performance of two commercial polyamide TFC membranes at seawater desalination conditions (32,000 ppm NaCl; 55.2 bar).

Membrane code	Specifications given by manufacturer		Measured performance	
	Permeate flux[a] ($L\ m^{-2}\ h^{-1}$)	Salt rejection (%)	Permeate flux ($L\ m^{-2}\ h^{-1}$)	Salt rejection (%)
TM810C	27	99.8	37	97.7
TM810V	38	99.8	39	97.8

[a] calculated from product flow rate of membrane module and membrane area

2.2.1.2 Morphology

Morphological studies of the commercial membranes were performed with SEM after removing the non-woven fabric layer. As presented in Figure 2.2 and Figure 2.3 it is evident that the support layers of both TFC membranes have a sponge-like structure with a thickness around 40 μm. In contrast to finger-like structures, a sponge-like structure is more resistant to membrane compaction [62]. Higher magnification SEM images of the cross-section show the relatively rough front surface of the polyamide layer, which is described as a ridge-and-valley structure [63]. Surface roughness in terms of height and width of protuberances is observed to differ between the two membranes. The TM810V membrane appears to be rougher than the TM810C membrane, which was also confirmed by top surface micrographs. The ridge-and-valley structure is more pronounced in the TM810V membrane compared to the TM810C membrane, where the protuberances appear to be smaller. The TM810C membrane`s protuberances appear more spherical, whereas ear-like protuberances are encountered more frequently in the TM810V membrane. A closer examination of both membranes at higher magnification (200,000x) reveals that underneath the ridge-and-valley structure, a tightly packed nodular structure is present.

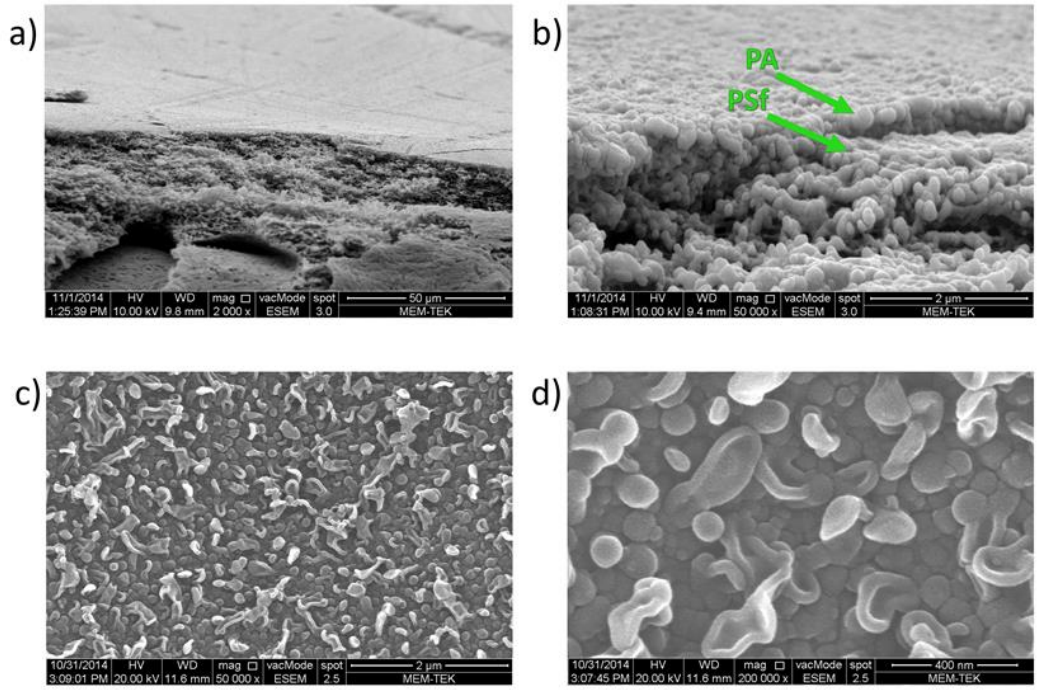

Figure 2.2 : SEM micrographs of the TM810C RO membrane from Toray. Cross-sectional views a) and b) exhibit the sponge-like structure of the polysulfone (PSf) support layer and the rough surface of the polyamide (PA) active layer. Top surface views c) and d) show the ridge-and-valley morphology.

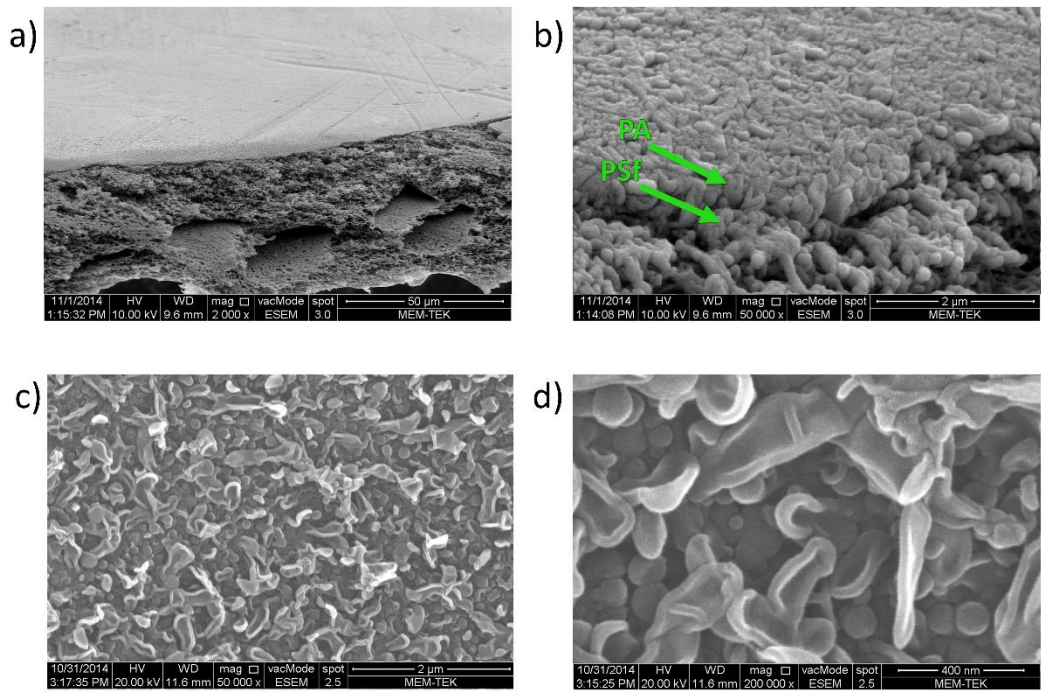

Figure 2.3 : SEM micrographs of the TM810V RO membrane from Toray. Cross-sectional views a) and b) exhibit the sponge-like structure of the polysulfone (PSf) support layer and the rough surface of the polyamide (PA) active layer. Top surface views c) and d) show the ridge-and-valley morphology.

2.2.1.3 Infrared absorbance

Figure 2.4 shows the ATR-FTIR absorbance spectrum of the TM810V membrane. Since the beam penetration depth (~1μm) is greater than the polyamide layer thickness (~100 nm) peaks corresponding to the underlying support layer are also observed. Several bands that can be attributed to polysulfone as the support layer and fully aromatic polyamide as the active layer were found in the spectrum.

The 1609 cm^{-1} (aromatic ring breathing) and 1542 cm^{-1} (amide stretching) bands are unambiguously selective for polyamide and the 1504 cm^{-1} (aromatic ring stretching) and 1081 cm^{-1} (sulfonate stretching) bands are unambiguously selective for polysulfone. Other studies [18,27] reported a characteristic band for polyamide at 1660 cm^{-1} (carbonyl stretching) in addition to the mentioned bands. However, the 1660 cm^{-1} band can also overlap with a very broad band around 1650 cm^{-1} arising from PVP [64,65], a common additive in polysulfone support layer casting solutions. Polysulfone supports with PVP additives prepared in this study confirmed the presence of this peak in the support layer and thus the 1660 cm^{-1} band cannot be attributed solely to polyamide.

The TM810C spectrum had similar peaks with different intensities. Since the relative absorbance intensities of the 1542 cm^{-1} band for polyamide and the 1504 cm^{-1} band for polysulfone depend on the penetration of the infrared beam, the ratio of the two absorbance bands was used as an indicative for the polyamide layer thickness for a better understanding of the structure of each TFC membrane.

In Figure 2.5 the average ratio of the two absorbance bands (1542 cm^{-1}/1504 cm^{-1}) is shown for the commercial membranes. The ratio is larger in the case of TM810V compared to TM810C, which indicates a thicker polyamide layer.

These results are in agreement with the morphological studies by SEM that revealed larger polyamide protuberances in the TM810V membranes than in the TM810C membrane.

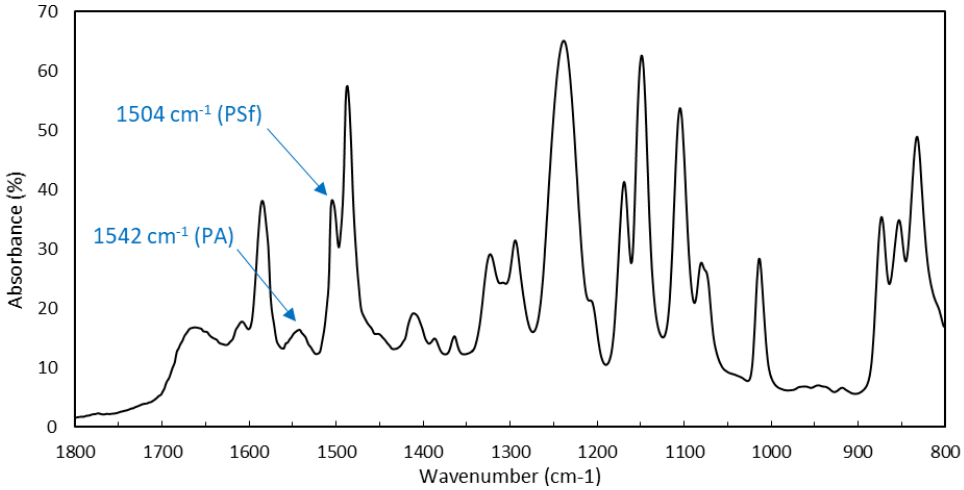

Figure 2.4 : ATR-FTIR spectrum of the TM810V membrane with characteristic polysulfone (PSf) and polyamide (PA) peaks selected to calculate the relative active layer thickness.

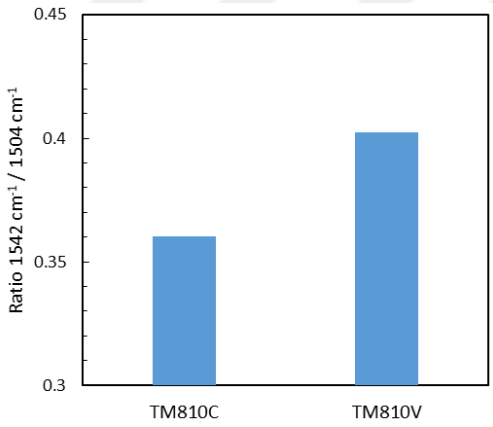

Figure 2.5 : Ratio of the 1542 cm^{-1} and 1504 cm^{-1} absorbance intensities corresponding to the TFC membrane's polyamide and polysulfone signals respectively. A higher ratio corresponds to a relatively higher amount of polyamide, which indicates a thicker active layer.

2.2.2 TFC membranes produced with support layers of varying pore size

2.2.2.1 Fabrication of support layers

Membranes with varying average pore sizes were produced from polysulfone casting solutions with PVP additives by the NIPS method. Six membrane types were chosen as support layers for interfacial polymerization. By changing phase inversion kinetics and thermodynamics, the average pore sizes could be arranged to values between 18-120 nm. Table 2.3 lists average pore size and distribution, cross-sectional thickness and water permeability values for produced support membranes. SEM surface images that were used to calculate pore sizes of the different support layers (Figure A.1) and a graph illustrating their pore size distributions (Figure A.3) can be found in the

appendix. Differences in the membranes' pore sizes are very distinct and can easily be noticed in SEM surface images. The pore size distribution of the Type-1 support membrane is very broad, with a distinctly larger average pore size than the other membranes. In general, narrower pore size distributions were observed with decreasing average pore size. The cross-sectional thickness of the support layers was found to be between 35 and 42 μm. In addition, cross-sectional SEM images presented in Figure A.2 in the appendix show sponge-like and thus compaction-resistant membrane structures with a finely porous top layer. It is important to note that no macrovoids were observed extending from underneath the top surface in the cross-sections. The water permeability value of the support membranes was found to decrease with decreasing average pore diameter, except for the Type-2 membrane.

Table 2.3 : Characterization of the fabricated support membranes.

	Average pore size (nm)	**Cross-sectional thickness** (μm)	**Water permeability** (L m^{-2} h^{-1} bar^{-1})
Type-1	120 ± 37	38 ± 2	618 ± 30
Type-2	79 ± 18	38 ± 3	474 ± 32
Type-3	42 ± 14	42 ± 9	512 ± 85
Type-4	35 ± 12	35 ± 7	486 ± 14
Type-5	30 ± 8	34 ± 6	463 ± 49
Type-6	18 ± 5	35 ± 3	331 ± 17

The influence of the casting parameters (Table 2.1) on the resulting support layer pore size can be interpreted by statistical means. Figure 2.6 reveals how the average pore size of membranes change with varying casting speeds, coagulation bath temperatures and PVP40 concentrations in the casting solutions. Statistical factor values calculated with ANOVA were found to be increasing in the order from PVP40 concentration, coagulation bath temperature to casting speed, with the last one showing the highest correlation. The R^2 correlation values of the logarithmic fitting equation were found to be high. The pore size distribution was found to be large; however, statistical calculations exhibit a high correlation between casting parameters and the average pore size, which can be used to demonstrate the effect of the support layer on salt rejection in the next chapter.

The position of the binodal (liquid-liquid) boundary on a ternary phase diagram for solvent, nonsolvent and polymer, at which the system divides into a polymer-rich and

polymer-poor phase, has already been studied intensively [66–68]. In summary, it is hypothesized that the top skin layer structure is primarily determined by the order of events during phase separation. When the precipitation pathway intersects the binodal at the high polymer concentration region (gelation boundary) before entering into the two-phase region, gelation will occur and the polymer begins to gel before phase separation occurs [69]. This would result in a high polymer concentration at the top surface and a dense skin layer with small pores.

In this study, relatively slow casting speeds of 3 m/min allowed the solvent to evaporate for 9 sec before the casting solution was immersed into the coagulation bath, causing a higher concentration of the polymer on top of the thin film of polymer solution. In addition, a relatively high polysulfone concentration of 18 % was chosen, which was increased by decreasing the concentration of the PVP additives. A higher concentration of the polymer in solution and thus the cast film is expected to result in smaller pores in the formed skin layers.

Polymer precipitation is another key phenomenon during the membrane formation process, which is affected by the rates of nonsolvent influx and solvent outflux to and from the polymer solution, respectively. The observed membrane morphology depends on the balance between the solvent–nonsolvent demixing rate and the polymer vitrification, defined as the process in which the casting solution solidifies crossing the glassy region in the phase diagram [69]. It is largely assumed that a delayed (less rapid) solvent-nonsolvent demixing rate is responsible for a sponge-like and thus compaction resistant structure [61]. In systems with a very low nonsolvent-polymer interaction as water and PSf, an instantaneous demixing is normally expected. As a consequence the formation of finger-like macrovoids is expected to occur and the mechanical stability of the membrane would be compromised.

In this study, a reduction of the demixing rate to obtain sponge-like structures was achieved by the choice of DMF as the solvent. Compared to other solvents such as 1-methyl-2-pyrrolidinone (NMP), DMF is a less favorable solvent for polysulfone and, hence, diffuses into the precipitation bath more quickly than NMP. As a consequence of the relatively fast outward flux, the nonsolvent influx into the precipitating film is slow. The formation of macrovoids is prevented, because the vitrification front moves more quickly relative to the nonsolvent front [69]. Furthermore, the sponge-like morphology is accompanied with the formation of a dense and thick skin layer. The

ratio of solvent outflow to nonsolvent inflow during NIPS can be increased gradually by lowering the coagulation bath temperature and by increasing the casting solution viscosity with high molecular weight additives such as PVP [67]. As a result, coagulation will take a path at high polymer concentrations, reaching the gel region before intersecting the binodal and thus a further decrease of the average pore size is observed.

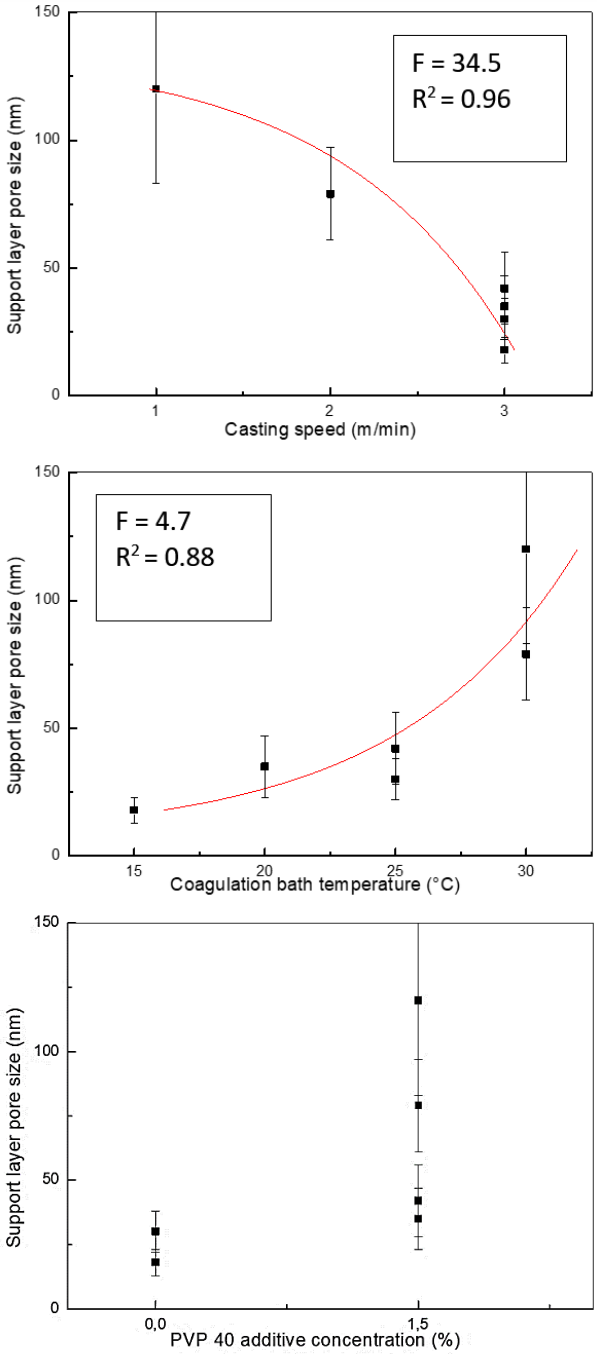

Figure 2.6 : Effect of different NIPS parameters on the average pore size of the support layer. F is the statistical factor value calculated with ANOVA and R^2 is the correlation value of the logarithmic fitting equation (red).

2.2.2.2 TFC membrane morphology

The interfacial polymerization technique to fabricate polyamide-TFC membranes was performed on top of six different support membrane types. In Figure 2.7, selected SEM micrographs of support and active layers of produced membranes are presented at a magnification of 200,000x. A comprehensive collection of SEM micrographs for all membrane types can be found in Figure A.1 in the appendix**,** where polyamide layers were also examined at a magnification of 50,000x to analyze a larger membrane area. The morphological characterization of produced TFC membranes reveals significant differences in terms of the length and width of polyamide protuberances. With increasing average support layer pore size, active layer surfaces appear to be rougher, with a more pronounced ridge-and-valley structure. Underneath the ridge-and-valley structure, a tightly packed nodular structure is observed, as it was the case with commercial membranes. The Type-1 and Type-2 support layers analyzed at 200,000x SEM magnifications have relatively large pores with averages of 120 nm and 79 nm, respectively. In their corresponding fabricated TFC membranes, it becomes clear that protuberances formed during interfacial polymerizations are at least as large as the smallest pore of their support layer. Large ear-like and even larger (200-600 nm diameter) ridge-like protuberances that exceed the pore size of the corresponding support layer multiple times are frequently observed for Type-1 and Type-2 TFC membranes. The same observation was made in Type-3 and Type-4 membranes but with smaller protuberances since support layer pores were smaller around 42 nm and 35 nm, respectively. The 50,000x magnification images show that there is a smaller number of ridge-like protuberances (100-400 nm diameter) in Type-3 and Type-4 membranes than in the former types. In the micrographs of membranes Type-5 and Type-6, ridge like protuberances (100-400 nm diameter) that are multiple times larger than the support layer pore size appear rarely. Only one or two ridge-like protuberances were observed in addition to several ear-like protuberances per scanned area at a magnification of 50,000x for these two membranes. As a consequence, the tightly packed nodular structure is more visible between protuberances.

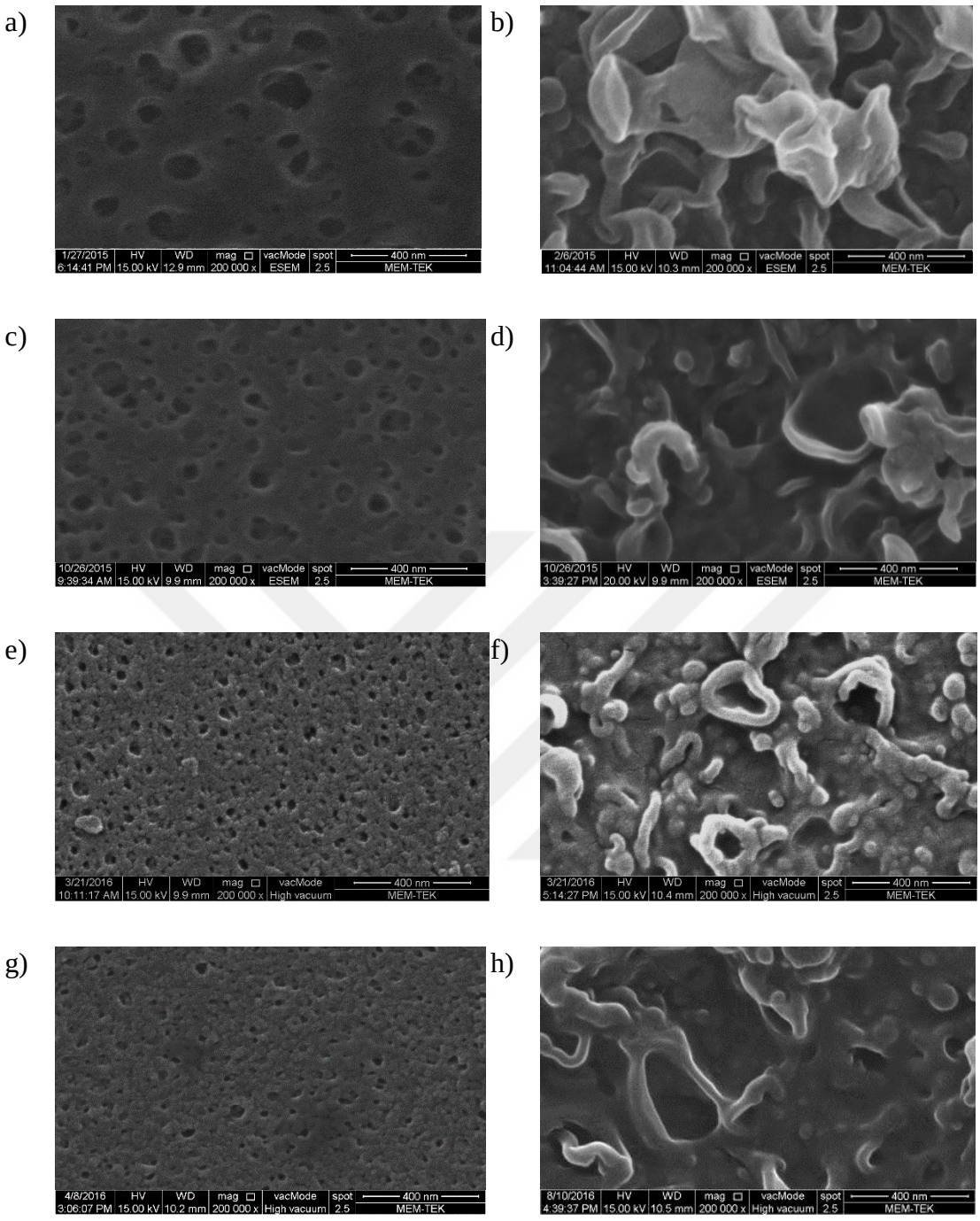

Figure 2.7 : SEM surface views of different types of polysulfone support layers (left) and corresponding polyamide active layers formed after interfacial polymerization (right). Micrographs a) and b) correspond to Type-1; c) and d) Type-3; e) and f) Type-5; g) and h) Type-6.

Figure 2.8 shows cross-sections of Type-3 and Type-6 TFC membranes taken from a small angle from top. The cross-sectional SEM micrographs suggest that the polyamide layer thickness of the Type-3 membrane is around 400 nm **(**Figure 2.8a) compared to approximately 200 nm (Figure 2.8c) in case of the Type-6 membrane. However, since the polyamide layer adheres to the underlying polysulfone support in

the heat curing process [10], the boundary between these two layers cannot be distinguished accurately. Therefore the polyamide layer thickness is estimated on the basis of the morphological differences between the polyamide and polysulfone layers observed in these micrographs.

SEM micrographs in Figure 2.8b and Figure 2.8d show a clear difference in the surface roughness of the two polyamide layers. In the Type-3 membrane, the protuberances extend out of the plane more significantly than in the Type-6 membrane. As a result, large ridge-like protuberances are observed to a lesser extent in membrane Type-6. These findings confirm that, when larger protuberances are more frequently observed horizontally (in x-y direction in Figure 2.7), they are also more frequently observed vertically (in z direction in Figure 2.8).

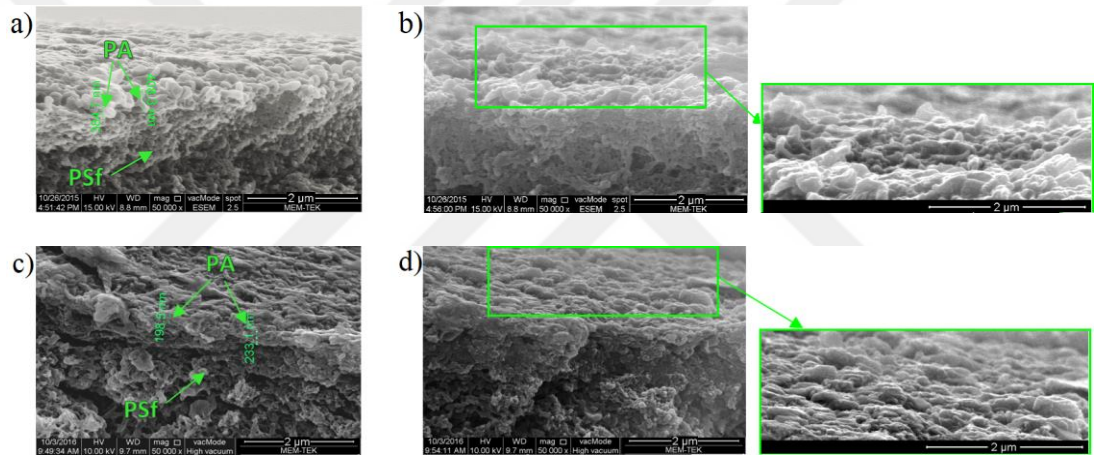

Figure 2.8 : SEM cross-sectional views of TFC membranes showing the polyamide (PA) and polysulfone (PSf) layers (left) and magnification of polyamide protuberances (right). a) and b) correspond to TFC-Type-3; c) and d) to TFC-Type-6.

Larger ridge-like protuberances were similarly observed in morphological studies about brackish water desalination and nanofiltration membranes in the literature [26,70–72]. In a number of studies, it is assumed that the ridge-and-valley structure is caused by an enhanced MPD transport during the interfacial polymerization reaction [17,73,74]. These studies state that MPD convection (diffusion and advection) can be caused by surface tension gradients between the aqueous and the organic phase (Marangoni instability). However, Buoyancy forces caused by density gradients (Rayleigh instability) may also play a critical role in my opinion. The hypothesis that both diffusion and advection can take place during interfacial polymerization is central to explaining the results of this study.

When the TMC organic solution is poured over the support layer with an adsorbed aqueous phase containing the MPD monomer, MPD molecules migrate to the interface and react with TMC. The reaction is expected to take place in the organic phase, due to the solubility of MPD in organic solutions and the hydration of TMC in water [28]. Because of the porous nature of the support layer surface, most of MPD monomers will be located in pores. However, in small pores, where the aqueous phase is thin, migration of MPD is not expected to be governed by advection, but by diffusion causing nodular structures to be formed (Figure 2.9a). The interfacial reaction produces a cross-linked film with small domain sizes, because diffusive transport processes do not favor the formation of larger polyamide structures. As a result, the TFC membrane surface is relatively smooth. In the case of larger pores, where the aqueous phase is thicker, perturbations promoted by the large movement of MPD towards the organic phase can be expected. Here, convection caused by density or surface tension gradients may play a superior role due to a larger contact area between the aqueous and organic phase (Figure 2.9b and Figure 2.9c). During this process, while interfacial reactions are continuously evolving between unreacted TMC and MPD, it is very likely that the early formed domains may be pushed and bent, forming ear-like and ridge-like structures. As a consequence, a rougher polyamide layer is expected to form.

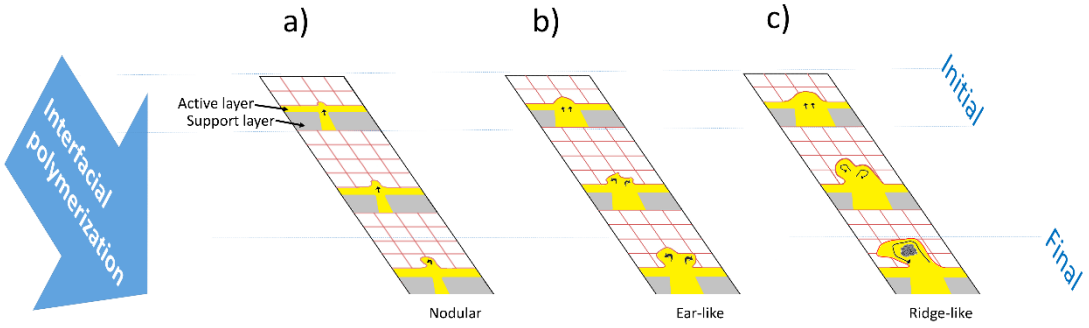

Figure 2.9 : Schematic formation of polyamide nodular structures during interfacial polymerization due to MPD diffusion in small pores a) and formation of larger polyamide protuberances due to convection in large pores b) and c).

2.2.2.3 Infrared absorbance

The ATR-FTIR spectrum of the Type-3 TFC membrane is representatively presented in Figure 2.10. All other TFC membranes exhibited the same absorbance peaks with varying intensities. Relative absorbance intensities of the band at 1542 cm-1 for polyamide and the band at 1504 cm-1 for polysulfone are reported in Figure 2.11 as their average ratios (1542 cm-1/1504 cm-1) as an indication of relative polyamide layer thicknesses of these membranes. These ratios suggest a general trend such that the polyamide layer thickness increases as a function of the average pore size of the corresponding support layer. The Type-6 TFC membrane with an 18 nm average pore size of the support layer has a polyamide layer thickness less than half of the polyamide layer thicknesses of membranes from Type-1 to Type-4 and is in the range of the commercial TFC membranes. As observed in the characterization of commercial membranes, the ATR-FTIR results for the fabricated TFC membranes agree with morphological observations by SEM analysis that the membranes with larger protuberances have higher polyamide absorbance intensities.

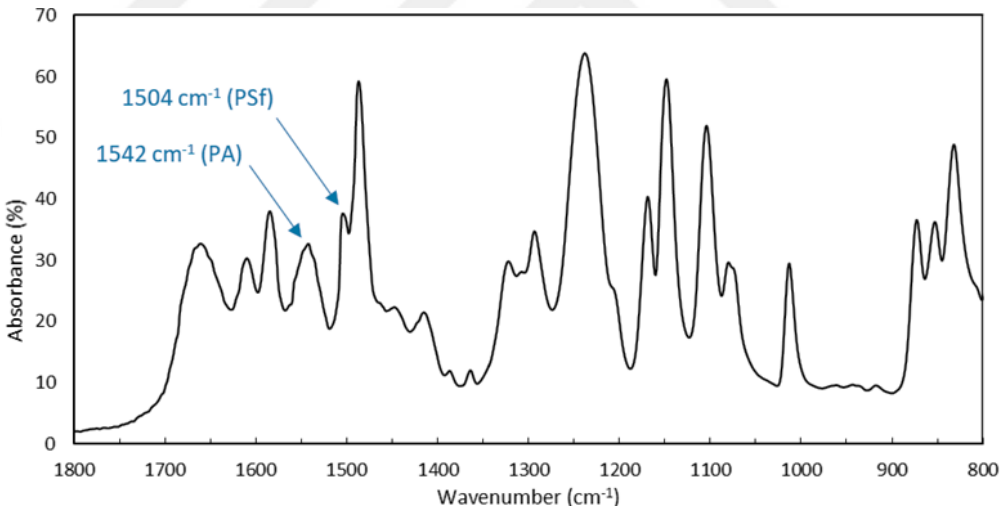

Figure 2.10 : ATR-FTIR spectrum of the Type-3 TFC membrane with characteristic polysulfone (PSf) and polyamide (PA) peaks selected to calculate relative polyamide layer thickness.

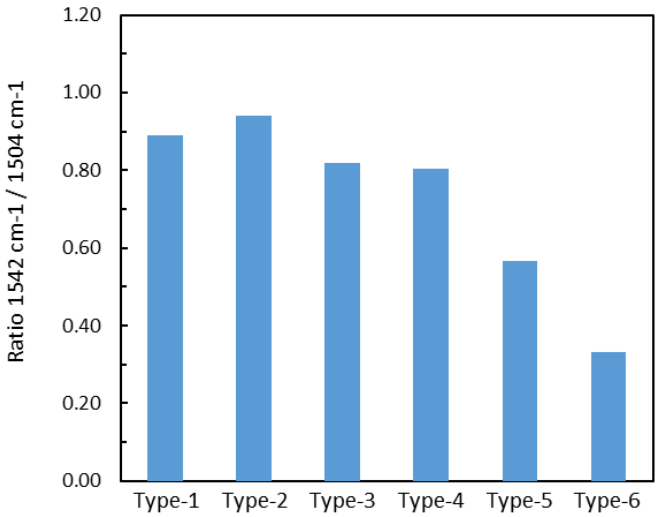

Figure 2.11 : Ratio of the 1542 cm-1 and 1504 cm-1 absorbance intensities corresponding to the TFC membrane's polyamide and polysulfone signals, respectively. A higher ratio corresponds to a relatively higher polyamide content, which indicates a thicker active layer.

2.2.2.4 Seawater desalination performance

Figure 2.12 illustrates the seawater desalination performance of each tested TFC membrane plotted by its support layer pore size on the x-axis. The correlation between the salt rejection and the support layer pore size was found to be high with a statistical factor value F of 25.3 (calculated with ANOVA as in section 2.2.2.1). It was revealed that with increasing support layer pore size, RO salt rejection decreases. The highest salt rejection (99.0 %) was achieved with the Type-6 support, which has an average pore size of 18 nm. The permeate flux of TFC membranes with support layer pore size from 18 nm to 42 nm were around 30 L m^{-2} h^{-1} ± 5 and did not correlate significantly with the average pore size. However, for TFC membranes with larger support pores (79 nm and 120 nm) a reduction in salt rejection was observed with a significant increase in flux, which was possibly due to the evolvement of defects in the active layer. A detailed theory on the damage mechanism is discussed in the following.

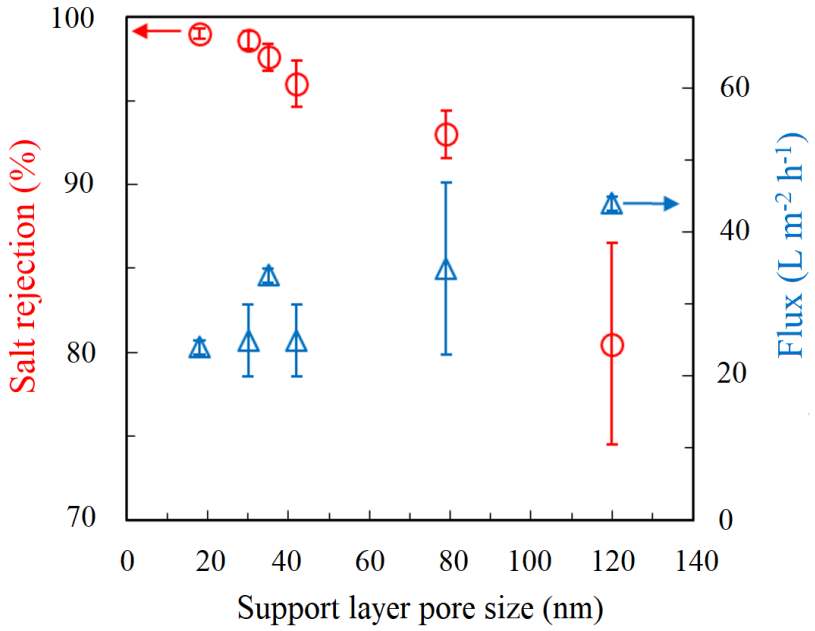

Figure 2.12 : RO-performance at seawater desalination conditions (32,000 ppm NaCl; 55.2 bar) of TFC membranes produced with different support layers as a function of their average pore size.

The findings in this chapter reveal a critical relationship between the morphology of polyamide layers and their RO-performances. This relationship suggests that a convective MPD transport during interfacial polymerization could cause defects in the salt rejecting polyamide layer. Moreover, Cadotte`s recommendation to use a support membrane with pore sizes around 20 nm in order to achieve high salt rejections is confirmed, as in the case of the Type-6 TFC membrane with an average support layer pore size of 18 nm, which exhibited the highest salt rejection of 99.0%. The Type-3 TFC membrane, fabricated with an average support pore size around 42 nm, on the other hand, exhibited a salt rejection of 96.0% under seawater desalination conditions. Singh et al. [23] found a similar salt rejection value for TFC membranes fabricated over support layers with 70 nm pore size tested under brackish water desalination conditions. They have compared these results with TFC membranes prepared with supports of larger pore size (150 nm) and found a decreased salt rejection of 65%. This result was explained by the deeper penetration of MPD into larger support layer pores, creating thinner overall polyamide layers as confirmed by their FTIR studies. The thinner polyamide layer was assumed to lead to a higher possibility of defects and consequently lower salt rejection. This explanation by Singh et al. is also valid in this study, but only in the case of membranes prepared with large support layer pore sizes (larger than 79 nm). FTIR results showed a slight decrease of polyamide layer

thickness from TFC Type-2 to Type-1, supporting the assumption that deeper penetration of the MPD is likely for membranes with pore sizes in the this particular range. However, higher salt rejections of membranes prepared with support layer pore sizes from 18 nm to 79 nm necessitate another explanation, because the FTIR results as well as the cross-section SEM images show a decrease of polyamide layer thickness for decreasing support layer pore sizes from 79 nm to 18 nm.

The explanation that the entire polyamide layer with its visible morphology is not responsible for the salt rejection, but it is more likely a byproduct of the polymerization reaction, has already been proposed [28]. It is hypothesized that only a highly cross-linked inner polyamide layer rejects the salts [70,71,75,76], which is further strengthened by our observations. In comparison to nanofiltration or brackish water desalination membranes, seawater desalination membranes stand out, because ridge-like protuberances are not observed on their surfaces, as it was confirmed from the SEM cross-sections in Figure 2.2, Figure 2.3 and from other studies [19,31,32,38]. This observation indicates that ridge-like protuberances may be undesired for the production of defect-free and high-performance membranes. The presence of a tightly packed nodular structure underneath the ridge-and-valley structure indicates that the observed protuberances originate from nodular structures, which has also been reported by other studies [26,72,77].

Thus, the initially formed inner polyamide layer can apparently be damaged due to twisting and bending of polyamide nodules, if for example the diffusion rate of MPD is relatively fast due to larger support layer pores, which act as MPD reservoirs during the interfacial polymerization reaction. Other studies that have observed cavities and voids in the back surface of polyamide films [26,71] and in their cross-section [78] indicate that observed protuberances are hollow, but eventually must be sealed in order to reject salts. A transmission electron microscope study from Freger [70] furthermore revealed that the ridge-and-valley surface structure consists of a carboxyl-rich phase on top of a carboxyl free phase, showing that this underlying layer is fully crosslinked. While Freger claimed that the structures of the underlying layer also include semicircular homogenous features with radii as large as 0.5 μm, Pacheco et al. [72] report that the underlying layer is only 30-60 nm thick, which is also indicated by our study. All these studies support the hypothesis that a dense crosslinked layer exists within the overall polyamide structure.

However, further quantitative evidence and thus analytical methods are needed for changes in the nanometer scale throughout the polyamide layer thickness regarding the chemical composition or the degree of crosslinking. If it can be confirmed that the structures caused by convection are not fully crosslinked, they can be identified as the defective sites responsible for the salt passage. Another cause for the membrane damage could be the occurrence of pinhole defects due to a reaction of TMC with water included in large pores or drops [26,27]. Such a reaction would reduce the reactivity of acid chloride groups of TMC with amino-groups of MPD and thus reduce the degree of polymerization or crosslinking.

3. ZWITTERIONIC POLYSILOXANE-POLYAMIDE HYBRID NETWORK AS ACTIVE LAYER FOR HIGH-PERFORMANCE AND CHLORINE-RESISTANT TFC MEMBRANES

In the previous chapter, it was described how polyamide TFC membranes with high performance for seawater desalination are produced by interfacial polymerization using MPD monomers in aqueous and TMC monomers in organic phase. This chapter investigates the in-situ polymerization of an additional zwitterionic monomer during the interfacial polymerization process for an enhanced desalination performance and better chlorine resistance. The trialkoxysilane-based zwitterionic monomer, (3-sulfopropylbetaine-propyl)-trimethoxysilane (SPPT), was added to the aqueous MPD solution at different concentrations. The aqueous solutions were adsorbed on polysulfone support layers and contacted with the organic TMC solution to create a polysiloxane-polyamide hybrid active layer (Figure 3.1). Comparison of streaming zeta potential measurements showed a pH-independent behavior of the zwitterionic membranes due to their strongly acidic and basic functional groups. Membranes produced with a SPPT/MPD ratio of 0.1 exhibited an increase in permeate flux from 25 L m^{-2} h^{-1} to 33 L m^{-2} h^{-1} (55.2 bar operating pressure; 3.2% NaCl feed) when compared to the control membrane prepared without SPPT. Furthermore, salt rejection was not compromised, but slightly increased from 98.8% to 98.9%. The highest resistance to chlorine was observed for membranes produced with a SPPT/MPD ratio of 1. It is postulated that electrostatic forces induced by the incorporated zwitterionic groups affect free volume and repulsion of mobile ions in the active layer.

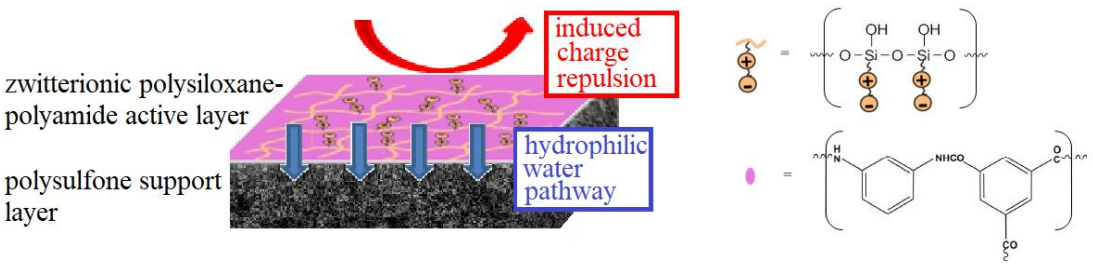

Figure 3.1 : Schematic drawing of the novel TFC membrane and its chemical structure. Orange color represents polysiloxane with its zwitterionic groups. Purple color represents polyamide.

3.1 Materials and Methods

3.1.1 Materials and reagents

Polysulfone (PSf), Udel P-3500 NT LCD (molecular weight mw: 80-86 kDa) was purchased from Solvay Specialty Polymers (USA). N,N-dimethyl formamide (DMF) was purchased from Akkim Chemicals (Turkey). (3-aminopropyl)trimethoxysilane (APS) (96%), (N,N-Dimethylaminopropyl)]trimethoxysilane (DMAPS) (96%), 1,3-propane sultone (≥99%), Polyvinylalcohol (PVA) (mw: 89-98 kDa), polyvinylpyrrolidone (PVP) PVP10 (mw: 10 kDa), m-phenylenediamine flakes (MPD) (99%), sodium dodecyl sulfate (SDS), triethylamine (TEA) (99.5%), (+)-10-camphor sulfonic acid (CSA) (98%), 1,3,5-benzene tricarboxylic acid chloride or trimesoyl chloride (TMC) (98%) were obtained from Sigma–Aldrich (Germany). Hexane or n-hexane Suprasolv, acetone, sodium chloride salt Emprove and hypochlorite solution (7-14% active chlorine) were purchased from Merck (Germany). CU424 type polyethylene terephthalate (PET) non-woven fabrics (thickness: 90 μm; width: 40 cm) from Neenah Papers (USA) were used as membrane backing material.

All chemicals were used as received, unless specified. Acetone was dried before use. All glassware, needles, and stirring bars were dried overnight in an oven at 150 °C and purged with nitrogen before monomer synthesis. Aqueous solutions were prepared with deionized (DI) water from Milli-Q ultrapure water system (Millipore, USA).

A seawater desalination membrane module from Hydranautics, type SWC5-4040 was used to extract membrane sheets for comparison in the chlorination experiments.

3.1.2 Membrane fabrication

3.1.2.1 Synthesis of (3-sulfopropylbetaine-propyl)-trimethoxysilane (SPPT)

The zwitterionic functional trialkoxysilane monomer (3-sulfopropylbetaine-propyl)-trimethoxysilane (SPPT) was synthesized according to the reaction in Figure 3.2. An empty reaction flask was fitted with a magnetic stirring bar, sealed with rubber septa and purged with nitrogen for 30 min. 6.22 g of DMAPS (30 mmol, 6.6 mL) and 3.91 g of 1,3-propane sultone (32 mmol, 2.8 mL) and 30 mL acetone were transferred into the reaction flask by syringe under nitrogen. The mixture was stirred under nitrogen at room temperature overnight. The crude white solid product was washed with anhydrous acetone for three times in order to remove unreacted reagents. The pure

product was dried under vacuum overnight at 30 °C and stored under vacuum in a desiccator (8.61 g, 87% yield). The nuclear magnetic resonance (NMR) ^{1}H NMR and ^{13}C NMR spectra of the product were performed on a Varian Unity Inova 500-MHz spectrometer. The spectra were recorded at room temperature with a 500MHz 1H-19F(15N-31P) 5mm PFG Switchable Probe. ^{1}H NMR ($CDCl_3$): δ 0.66 (t, 2H, Si-CH_2), 1.82 (m, 2H, Si-C-CH_2-C-N), 2.24 (m, 2H, N-C-CH_2-C-S), 2.89 (t, 2H, N-C-C-CH_2-S), 3.20 (s, 6H, 2xN-CH_3), 3.32 (t, 2H, Si-C-C-CH_2-N), 3.59 (s, 9H, 3xCH_3-O-Si), 3.73 (t, 2H, N-CH_2-C-C-S) ppm.^{13}C NMR ($CDCl_3$): 5.68 (Si-C-*C*-C-N), 16.48 (Si-*C*-C-C-N), 19.44 (N-C-*C*-C-S), 47.89 (*C*H_3-O-Si), 50.33 (N-C-C-*C*-S), 50.78 (N-*C*H_3), 63.55 (N-*C*-C-C-S), 65.96 (Si-C-C-*C*-N) ppm.

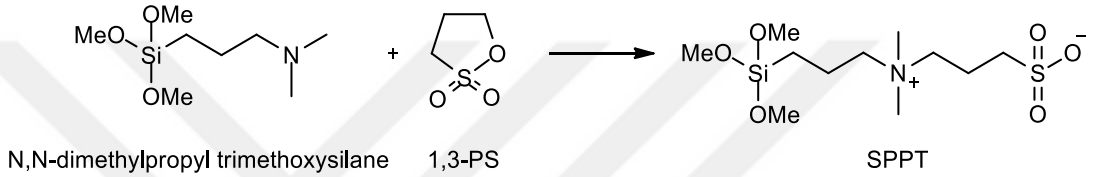

Figure 3.2 : Synthesis of the zwitterionic silane monomer (3-sulfopropylbetaine-propyl)-trimethoxysilane (SPPT).

3.1.2.2 Preparation of TFC RO membranes

The production of TFC RO membranes was carried out in two stages. First, the polysulfone support layer was produced by the nonsolvent-induced phase separation (NIPS) method [61] using a pilot scale casting system and according to the same parameters that were used for the fabrication of the Type-6 support layer in the previous chapter. An 18% (w/w) polysulfone solution with 4.5% (w/w) PVP10 additive was prepared using DMF as a solvent and stirring at 70 °C for 24 h. The casting solution was poured with a casting knife having a gap of 130 μm and homogenously cast onto the PET nonwoven fabric layer at a speed of 3 m/min. It was then coagulated in a water bath at 15 °C. The support layer membranes had a surface pore size around 18 nm and a sponge-like structure with a thickness of about 40 μm without the nonwoven fabric. Unlike finger-like structures, sponge-like structures are more resistant to membrane compaction during high pressure [62].

In the second stage, the active layer was produced in laboratory scale using the interfacial polymerization method [48] as outlined in Figure 3.3. The support membrane surface was contacted with a 2% (w/w) MPD aqueous solution including 2% (w/w) TEA, 5% (w/w) CSA, and 0.1% (w/w) SDS as additives. In order to produce

polysiloxane-polyamide crosslinked active layer membranes, different amounts of the zwitterionic functional trialkoxysilane monomer SPPT were added to this solution according to Table 3.1. Additionally, the two neutral silane compounds DMAPS and APS were used as co-monomers for the interfacial polymerization reaction at a concentration of 0.2 % (w/w) with MPD at 2% (w/w) in the aqueous phase.

Table 3.1 : Preparation of polyamide-polysiloxane TFC membranes by interfacial polymerization.

Membranes	SPPT addition[a] (%) (w/w)	SPPT/MPD ratio	Salt rejection[b] (%)	Flux[b] (L m^{-2} h^{-1})
TFC-0	0	0	98.8 ± 0.4	25 ± 1
TFC-1	0.1	0.05	98.4 ± 0.3	28 ± 2
TFC-2	0.2	0.10	98.9 ± 0.2	33 ± 2
TFC-3	0.5	0.25	98.9 ± 0.6	27 ± 1
TFC-4	1	0.50	98.8 ± 0.3	24 ± 2
TFC-5	2	1	98.3 ± 0.1	27 ± 2

[a]Final concentration of the zwitterionic silane monomer SPPT after addition to the 2% (w/w) MPD aqueous solution to be used for the interfacial polymerization reaction with the organic 0.1 w/v% TMC solution.

[b]Averaged performance of TFC membranes obtained with 3.2% NaCl feed solution at an operating pressure of 55.2 bar, cross flow rate of 5 L/min, and temperature of 25 °C.

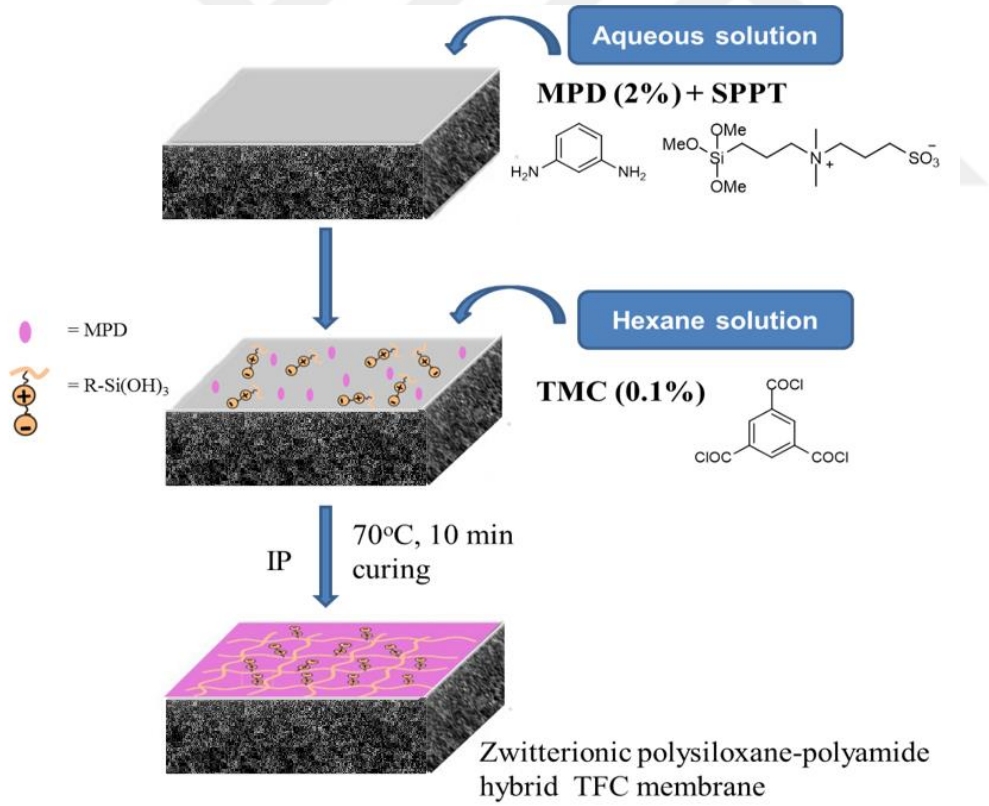

Figure 3.3 : In-situ incorporation of the zwitterionic silane polymer in the polyamide network of the TFC membrane by interfacial polymerization (IP).

Membranes were produced in triplicate for each silane concentration. After leaving the membranes in contact with the aqueous solution for 5 min, the excess of the solution

was removed using a silicone rubber, and the membranes were dried at room temperature for 2 min. The hexane solution of 0.1 % (w/v) TMC was then poured over the membranes and allowed to react with the adsorbed substances from the aqueous phase for 1 min. After pouring excess solution, the membranes were cured in an oven at 70 °C for 10 min. The prepared TFC membranes were washed with distilled water and immersed in an aqueous solution of 0.2% (w/w) PVA to adsorb a protective layer.

3.1.2.3 Coating experiments

Additional coating layers were applied on the TFC-2 membrane to further probe the effect of coatings on membrane flux and resistance to chlorination. The composition of the aqueous coating solutions are presented in Table 3.3.

Table 3.2 : Composition of coating solutions.

Membranes	SPPT content (%) (w/w)	MPD content (%) (w/w)
TFC-2_Coating 1	0.2 %	-
TFC-2_Coating 1	0.2 %	2 %

After leaving the membranes in contact with the coating solution for 1 min, the excess of the solution was removed using a silicone rubber poured and the membranes were cured in an oven at 70 °C for 10 min.

3.1.3 Synthesis of further polyamide and polysiloxane polymers for analysis

Zwitterionic polysiloxane-polyamide hybrid and polyamide polymers were synthesized by interfacial polymerizations in a glass bottom flask, analogously to the preparation of active layers of the membranes. 20 mL water solutions containing 2% (w/w) MPD and SPPT at certain ratios (0.1, 0.25, 0.5 and 1) were prepared for the synthesis. The pH of the solutions was adjusted to ~8 with TEA. The water solutions were transferred to the flask, then 20 mL of hexane solutions containing 0.1 % TMC were added to each of the water phases. The mixtures were stirred for 1 min. Polymers formed at the interfaces were taken and cured at a temperature of 70 ^{o}C. The resulting polymers were allowed to stand in water for 24 h and then dried again. Polyamide polymer was prepared similarly to the synthesis of polysiloxane-polyamide hybrid polymers. The only difference was that zwitterionic silane (SPPT) was not added to the water phase. For the preparation of polysiloxane polymer, 20 mL water solution with 2% (w/w) SPPT was prepared, then the solvent was removed and remaining polysiloxane polymer was dried at 120 ^{o}C.

3.1.4 Membrane characterization

3.1.4.1 Scanning electron microscopy (SEM) with energy dispersive spectroscopy (EDS)

Membrane surfaces were characterized using a FEI Quanta FEG 200 SEM. Samples were coated with 5 nm Palladium and Gold (Pd-Au) particles by using a Quorum SC7620 ion sputtering device. METEK EDAX Apollo X was used for EDS analysis of the samples.

3.1.4.2 Fourier transform infrared (FTIR) spectroscopy

Fourier transform infrared (FTIR) spectra were recorded to verify the chemical structure of the polymers. FTIR spectra were measured in the absorbance mode ranged 400–4000 cm^{-1} at room temperature using a PerkinElmer Spectrum 100 FTIR Spectrometer with a resolution of 4 cm^{-1}. The attenuated total reflectance (ATR) crystal is composed of a diamond ATR with a zinc selenide focusing element which is in direct contact with the diamond and has a refractive index (n_1) of 2.4. Before measuring samples, a background spectrum was conducted to decrease instrumental and atmospheric contributions to a minimum level.

3.1.4.3 Water contact angle

To examine the hydrophilicity of the membrane surfaces, water contact angle measurements were recorded using a tensiometer from KSV Instruments. A droplet of distilled water was formed at the tip of a stainless steel syringe needle and placed on the membrane surface. Ten images were picked out from three different places on each membrane surface and averaged to give the mean contact angle.

3.1.4.4 Zeta potential

Streaming zeta potential analysis as an indicator of membrane surface charge [58] was performed using a SurPASS analyzer from Anton Paar (Austria). Membranes were soaked in a 1 mM potassium chloride (KCl) electrolyte solution for at least 4 h before measurement. Measurement was performed while circulating the electrolyte at different pH at 25 °C. The solution was pumped at a target pressure of 100 mbar over two membrane samples (20 x 10 mm^2) placed in an adjustable gap cell. The streaming potential was measured with Ag/AgCl electrodes attached very closely to the

rectangular slit formed by the membranes. The gap between the two membrane samples was adjusted to 100 μm. The pH of the KCl solution was adjusted from pH 2.5 to pH 12 using sodium hydroxide (NaOH) and hydrogen chloride (HCl). The automated program included a thorough rinsing step with the measuring electrolyte after each titration step. The zeta potential is calculated according to the Helmholtz-Smoluchowski equation (3.1):

$$\zeta = \frac{d\varphi}{dP}\frac{\eta}{\varepsilon_r \varepsilon_0}\frac{L_S}{A_S}\frac{1}{Re} \tag{3.1}$$

where ζ is the zeta potential (V), $d\varphi/dP$ is the gradient of streaming potential with respect to pressure (A Pa^{-1}), η is the dynamic viscosity of the electrolyte (Pa s), ε_0 is the vacuum permittivity (F m^{-1}), ε_r is the dielectric constant of the electrolyte, L_s is the length of the streaming channel (m), A_s is the cross-section area of the streaming channel (m^2) and R_e is the electrical resistance across the medium.

3.1.5 Membrane performance

The same cross-flow filtration system was used as in chapter 2 (see Figure 2.1 on page 15). It consists of a feed tank with heat exchanger, cartridge filter, high pressure pump, membrane filtration cell, permeate collection vessel, computer with supervisory control and data acquisition (SCADA), flow meter, and pressure, pH, temperature and conductivity sensors. The effective filtration area of the membrane in the membrane filtration cell was 140 cm^2. The feed solution was subjected to coarse filtration with a cartridge filter (5 μm pore size) before entering the following pumping system.

3.1.5.1 Seawater desalination

The feed solution was prepared by dissolving NaCl in deionized water to a final concentration of 3.2% (w/w). Performance tests were conducted at an operating pressure of 55.2 bar, at a feed solution flow rate of 5 L/min, while the temperature was held at 25 ± 1 °C. Water flux and salt rejection of the membranes were measured after stabilization for 60 min. A digital conductivity meter (Multimeter 44, Crison Instruments, Spain) was used to measure the conductivities of feed and permeate. A calibration curve was used to relate the solution conductivity to the salt concentration. The salt rejection, R (%), was calculated from the salt concentrations in the permeate (C_P) and feed (C_F) solution according to equation (3.2):

$$R = \left(1 - \frac{C_p}{C_F}\right) \times 100\ \% \quad (3.2)$$

Permeate flux J (L m^{-2} h^{-1}), was calculated from the volume of permeated water (ΔV), the time for collecting fixed volume water (Δt), and the effective membrane surface area (A_m) according to equation (3.3):

$$J = \frac{\Delta V}{(\Delta t \times Am)} \quad (3.3)$$

The results were averaged from the measurement of three separately produced membranes for each silane concentration.

3.1.5.2 Chlorination tests

After measuring initial water flux and salt rejection, the system continued to operate under the same conditions as in the previous chapter, but with the addition of sodium hypochlorite in the sodium chloride feed tank, to a final concentration of 500 ppm. The conductivity of the feed was arranged to 44.5 mS to equal the conductivity of a 3.2% (w/w) sodium chloride concentration. The mixture with a pH > 9 contains mainly anionic hypochlorite as the active chlorine species. The system was operated for 8 h at 55 bar. Performance results were given after every 2 h which translates into an active chlorine exposition of 1000 ppm h. Chlorination results are reported as averages of three produced membranes for each silane concentration.

3.2 Results and Discussion

3.2.1 Membrane surface properties

3.2.1.1 Zeta potential

Figure 3.4 shows streaming zeta potential profiles as a function of the streaming solution pH. The polyamide membrane (TFC-0) is compared to the membranes produced with uncharged silane monomers (DMAPS and APS) and the zwitterionic silane monomer (SPPT). The hybrid membranes were produced at silane/MPD ratios of 0.1. The graph is plotted from pH 4 to pH 10 to emphasize the differences in the membranes. The isoelectric point of all membranes was below that scale at pH 3. All membranes display predominantly negative zeta potentials and a minor or major dependence on the pH value of the streaming potassium chloride (KCl) solution except for the profile of the zwitterionic SPPT, which shows a pH-independent behavior.

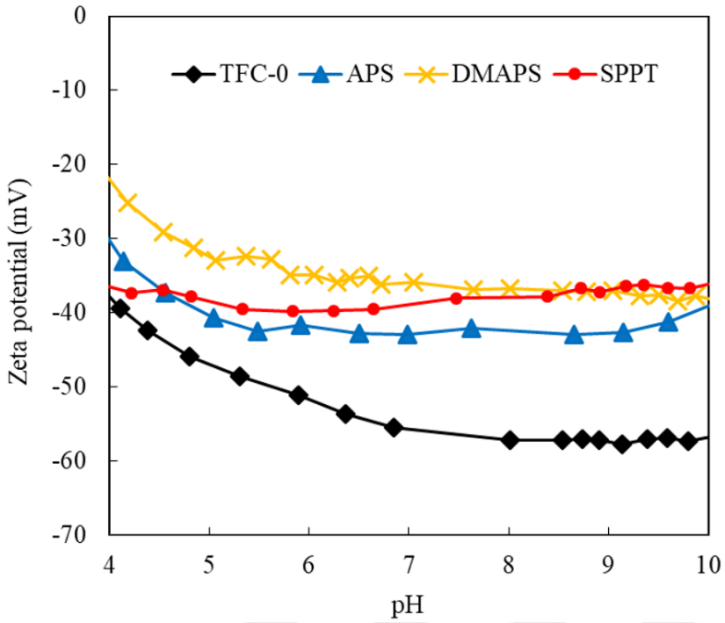

Figure 3.4 : Streaming zeta potential measurements of polyamide (TFC-0) and modified polyamide-polysiloxane hybrid membranes with neutral silanes (APS, DMAPS) and zwitterionic silane (SPPT) produced at a silane/MPD ratio of 0.1.

The pH-dependent behavior of the zeta potential can be explained with the presence of carboxylic acid and amide groups. The surface charge of the membrane is dependent on the degree of ionization of these groups and hence, the pH of the streaming KCl solution. Numerous studies have, furthermore, demonstrated that the surface charge is superposed by the pH-dependent adsorption of hydroxide and hydronium ions from the solution and that negatively charged hydroxide ions are more preferably adsorbed than positively charged hydronium ions, which in turn results in predominantly negative zeta potential values [79–83]. The polyamide surface has positive and negative but also neutral (non-ionogenic) sites where the adsorption of these ions is concentration-dependent. The pH-dependency of the zeta potential at low pH can be explained by the concentration-dependent adsorption of hydronium ions. At higher pH the negative zeta potential becomes more negative due to an increasing adsorption of hydroxide ions. This pH-dependent behavior is observed in the control membrane (TFC-0), but to a lesser degree in the modified membranes. Amongst the latter, the zwitterionic SPPT membrane does not display any pH-dependent behavior, which indicates that the surface is effectively covered with either negative or positive charges, leaving no place for an increased adsorption of hydroxide ions to neutral parts of the polyamide surface. The zeta potential value remains stable over most of the measured pH range with a weaker change of surface charge at high pH, which would result from the dissociation of amide groups and strong change at the isoelectric point

at pH 3. The overall negative value of the SPPT-modified membrane is therefore expected to result from the preferential adsorption of hydroxide ions.

Zwitterionic polymers with strongly acidic and strongly basic functional groups are expected to remain more dissociated in a broader pH range than weakly acidic and weakly basic groups in polyamide, which is described as being amphoteric in contrast [84,85]. Studies of zwitterionic polymers [86,87] have shown that the zeta potential is dependent on both the surface charge and the preferential adsorption of hydroxide ions. Zeta potential values closer to zero and the reduced dependency from the solution pH therefore indicate the successful integration of a strongly acidic and strongly basic zwitterionic polymer in this study.

3.2.1.2 Contact Angle

Contact angle measurements give an indication about the hydrophilicity of a material surface. Figure 3.5 shows contact angle measurements of the control polyamide membrane (TFC-0) and zwitterionic silane-modified polyamide-polysiloxane membranes produced at different SPPT/MPD ratios. The introduction of zwitterionic monomers into the membrane active layer did not appear to systematically affect the membrane contact angle. Up to an SPPT/MPD ratio of 0.1, the contact angle increased from 48.8° to 60.6°, indicating a more hydrophobic surface, due to the arrangement of the polysiloxane backbone. At higher SPPT/MPD ratios, the contact angle decreased and the lowest contact angle of 41.3° was observed when the SPPT/MPD ratio was 1.

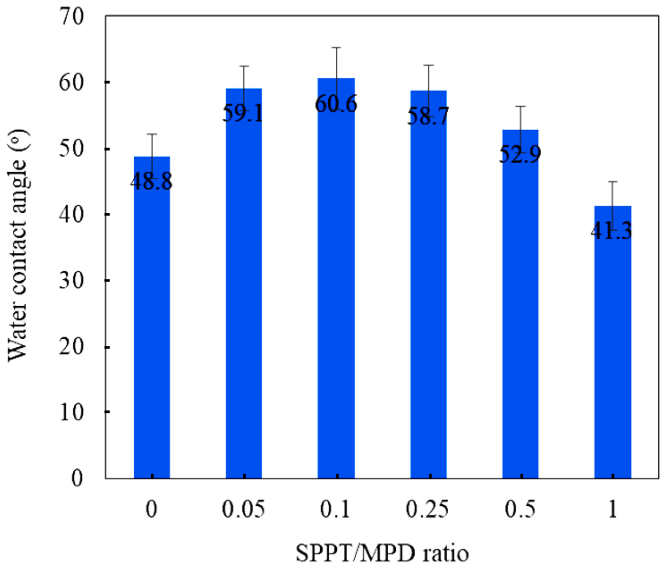

Figure 3.5 : Contact angle measurements of polyamide (TFC-0) and zwitterionic polyamide-polysiloxane membranes produced at different SPPT/MPD ratios.

The determination of the surface hydrophilicity by measuring the water contact angle is used in many studies [84]. However, since the contact angle depends on the surface energy, and thus the surface area, the issue of membrane surface roughness must be taken into account and makes water contact angles difficult to compare when the surface roughness is also altered due to membrane modification.

3.2.2 Membrane morphology and chemical composition

3.2.2.1 Secondary electron microscopy (SEM)

Figure 3.6 shows the SEM micrographs of the resulting TFC active layer, which were taken to characterize the surface morphologies. A comprehensive collection of SEM micrographs can be found in Figure B.1 in the appendix**,** where the active layers were also examined at a magnification of 50,000x to analyze a larger membrane area. The relatively rough surface, resembling a ridge-and-valley structure of the polyamide layer, is a general feature of aromatic polyamide RO membranes [63]. This morphology was observed in the SEM images of the different TFC membranes with the typical nodular structure and the ear-like and ridge like protuberances that result from the interfacial polymerization reaction as explained in chapter 2. Here again, the micrographs at high magnification (200,000x) show a tightly packed nodular structure underneath the ridge-and-valley layer. However, the size of the peak-and-valley structure is smaller and looser with increasing SPPT concentration used in the fabrication of the membranes, when compared with the standard polyamide membrane TFC-0. SEM micrographs at higher magnifications reveal that the valley structure between the peaks appears to be filled out with another polymer at high SPPT concentrations (red squares in TFC-4 and TFC-5). A closer examination of this polymer reveals a brittle structure, which is distinctively different to the nodular polyamide structure.

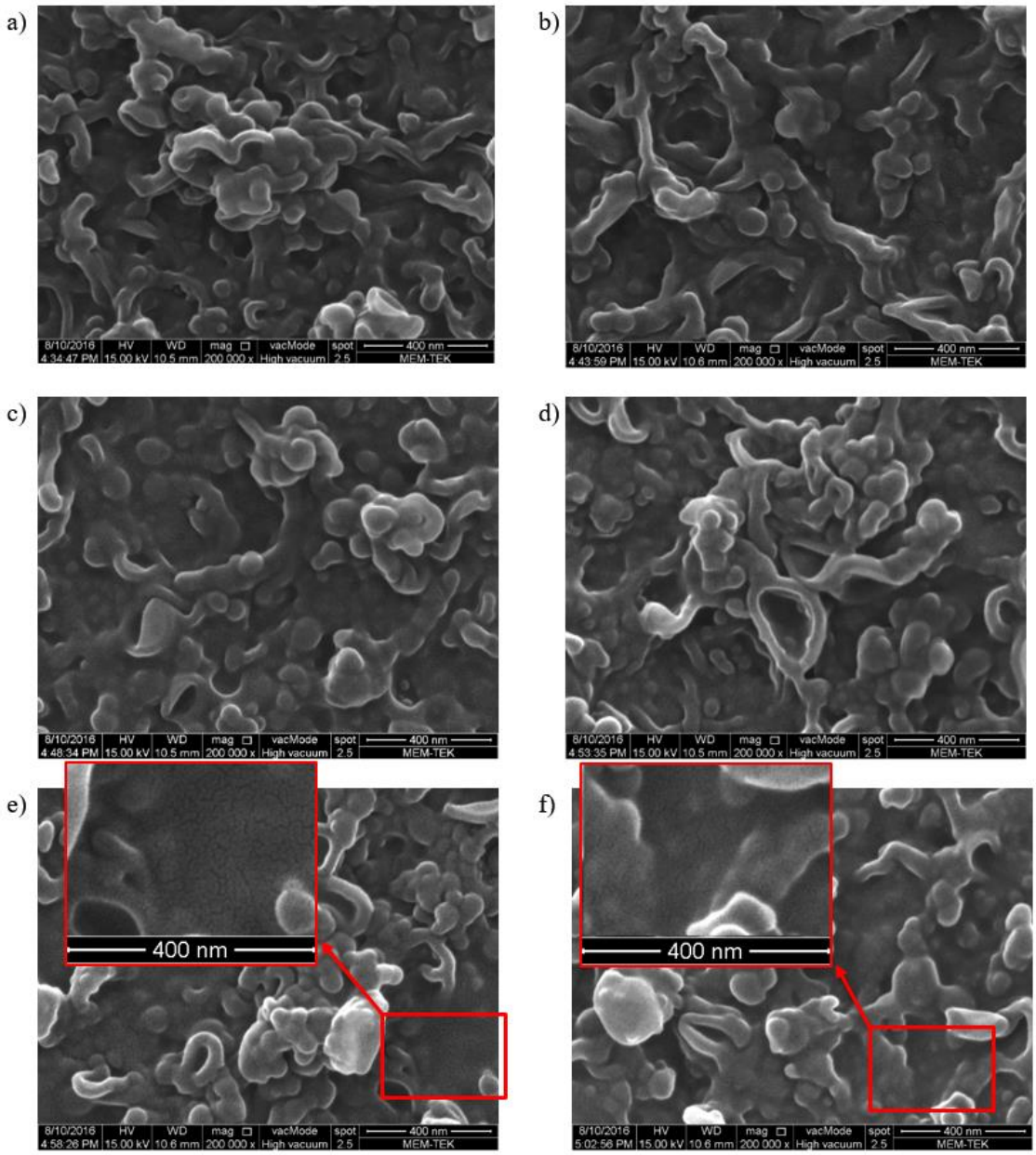

Figure 3.6 : SEM surface morphologies of control polyamide membrane TFC-0 (a) and the zwitterionic silane modified polyamide-polysiloxane membranes TFC-1 (b), TFC-2 (c), TFC-3 (d), TFC-4 (e) and TFC-5 (f), produced at SPPT/MPD ratios of 0.05, 0.1, 0.25, 0.5 and 1 respectively. Red rectangles mark proposed areas of polysiloxane between polyamide ridge structures.

3.2.2.2 Energy dispersive spectroscopy (EDS)

In the EDS analysis of the scanned areas in Table 3.3, the amount of silicon (Si) in the modified membranes was measured just above the value of the polyamide membrane (TFC-0). The silicon contents of the membranes prepared with higher SPPT/MPD ratios (TFC-3, TFC-4 and TFC-5) indicate a higher incorporation of polysiloxane into the polyamide layer.

Table 3.3: EDS analysis of scanned membrane areas.

Membrane	SPPT/MPD ratio [a]	C content (%w/w)	N content (%w/w)	O content (%w/w)	Si content (%w/w)
TFC-0	0	67.85 ± 2.33	8.15 ± 2.18	18.21 ± 6.67	0.10 ± 0.01
TFC-1	0.05	66.29 ± 0.47	10.26 ± 1.09	23.32 ± 0.62	0.21 ± 0.06
TFC-2	0.10	70.38 ± 5.17	7.19 ± 1.56	17.64 ± 10.34	0.24 ± 0.14
TFC-3	0.25	69.76 ± 4.73	7.99 ± 2.30	17.29 ± 9.35	0.30 ± 0.16
TFC-4	0.50	69.79 ± 5.38	8.62 ± 1.51	17.04 ± 10.05	0.27 ± 0.19
TFC-5	1	70.71 ± 3.63	7.62 ± 0.50	17.23 ± 10.28	0.34 ± 0.07

[a] Ratio of SPPT to MPD in aqueous phase solution used in the interfacial polymerization.

The SEM-EDS results signpost that the addition of the zwitterionic (sulfobetaine) functional trialkoxysilane monomer SPPT to the aqueous MPD solution is a result of the polymerization of an interpenetrating hybrid network. Additionally to the polyamide condensation reaction between MPD and TMC, other condensation reactions by silanol groups can occur. The alkoxy group of the silane compound becomes strongly reactive after hydrolysis, forming silanol (SiOH) groups. As a result, it can undergo condensation reactions with other silane monomers, the COCl group of TMC and amide linkages during interfacial polymerization and oven drying [30]. As a result, the formation of Si-O-C or Si-O-N bonds can act as a bridge to bond polysiloxane chains to polyamide chains. Ultimately, it produces an interpenetrating polyamide-polysiloxane network with amide (CO–NH), siloxane (RSi–O) and analogous bonds (RSi–O–N and RSi–O–C) between aromatic benzene (C_6H_n) subunits, whereby R represents the zwitterionic functionalized unit. The MPD monomers are uncharged and have a high solubility in organic solvents, as in contrast to the charged SPPT monomers, which due to the charged and partly inorganic nature have a much lower partitioning into the organic phase. Thus, because the polymerization can only take place in the organic phase and because the MPD monomer concentration is higher compared to the SPPT made membranes except for TFC-5, it is assumed that polyamide chains are longer than polysiloxane chains. The latter are assumed to be present in the oligomeric form inside the active layer.

3.2.3 Chemical composition of pure and hybrid polymers

Polyamides have a cross-linked structure and are therefore insoluble in most polar solvents. Moreover, the layer is very thin between 100-300 nm. So, it was not possible to separate the polyamide-polysiloxane active layer of the TFC membranes from the

polysulfone support layer for further analytical techniques. A Fourier transform infrared (FTIR) analysis for example did not show any differences between the different TFC membranes, because the active layer is very thin and the underlying polysulfone layer is also measured. Thus, in order to still be able to analyze the differences between polysiloxane and polyamide, the active layer polymers were produced separately in a glass beaker at different concentrations and analyzed further.

3.2.3.1 Fourier transform infrared (FTIR) spectroscopy

Figure 3.7 illustrates the FTIR spectra of a) a polysiloxane pure polymer, b) a polysiloxane-polyamide hybrid polymer and c) a pure polyamide polymer. By comparing the spectra, it can be confirmed that in case b) the zwitterionic polysiloxane-polyamide hybrid structure is obtained. The marked adsorption peak at 1039 cm^{-1} is ascribed to the symmetric stretch vibration of the SO^{3-} group coming from the sulfobetaine zwitterionic group. The SO^{3-} peak is only detectable in polysiloxane and polysiloxane-polyamide polymer spectrums, whereas it is undetectable in the polyamide polymer spectrum. Characteristic adsorptions of the zwitterionic polysiloxane polymer are supposed to appear in the polysiloxane-polyamide polymer spectrum, but these peaks are believed to be overlapped with the large and intense polyamide polymer IR bands.

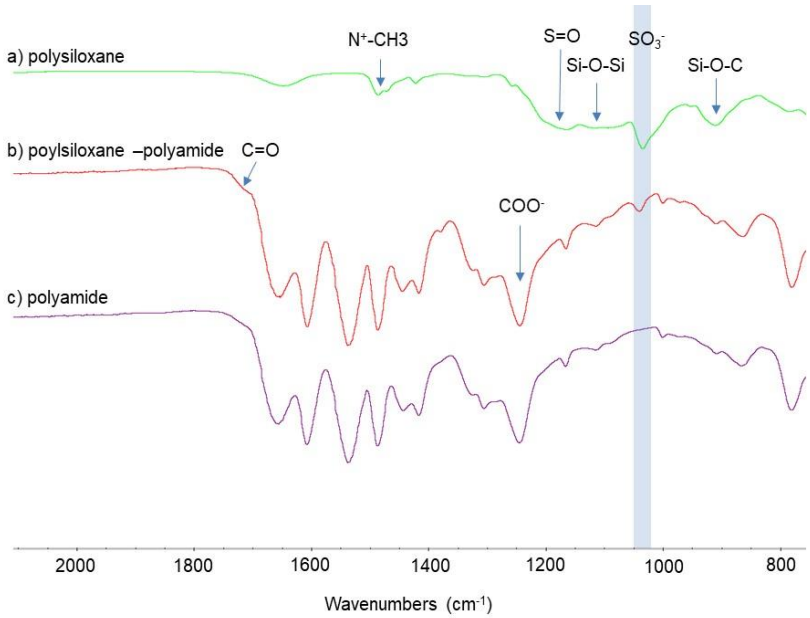

Figure 3.7 : Fourier transform infrared spectroscopy (FTIR) spectra of (a) polysiloxane polymer derived from SPPT, (b) polysiloxane-polyamide hybrid polymer prepared from SPPT, MPD (SPPT/MPD ratio of 0.25) and TMC, and (c) polyamide polymer prepared with MPD and TMC.

3.2.3.2 Energy dispersive spectroscopy (EDS)

Polymers at different SPPT/MPD ratios were also used for a further EDS analysis, which is presented in Table 3.4. In this case, the amount of silicon (Si) in the modified membranes was measured at values that were significantly above the value of the polyamide membrane (P-0). However, the silicon contents of the membranes prepared with higher SPPT/MPD ratios (P-2, P-3, P-4 and P-5) do not indicate a higher incorporation of polysiloxane into the polyamide layer.

Table 3.4 : EDS analysis of polyamide (P-0) and polyamide-polysiloxane polymers (P-2 to P-5).

Polymer	SPPT/MPD ratio [a]	C content (%w/w)	N content (%w/w)	O content (%w/w)	Si content (%w/w)
P-0	0	63.13	17.34	15.81	0.00
P-2	0.1	61.80	15.22	21.00	1.05
P-3	0.25	60.62	13.19	24.48	0.95
P-4	0.50	62.46	12.11	21.22	2.22
P-5	1	63.79	11.85	22.14	1.12

[a] Ratio of SPPT to MPD in aqueous phase solution used for polymerization.

3.2.4 Seawater desalination performance

3.2.4.1 Zwitterionic silane membranes

Using a crossflow RO test system, the membrane performances were evaluated for the polyamide (TFC-0) and the zwitterionic silane modified polyamide-polysiloxane membranes (TFC-1, TFC2, TFC-3, TFC-4 and TFC-5). The performance results are summarized in Figure 3.8 with the ratio of the final concentrations of SPPT and MPD in the aqueous solution plotted on the x-axis. The results for each ratio are given together with standard deviations as the average of the three membranes produced and tested separately. They demonstrate that water flux increases with the addition of SPPT showing a maximum value at the SPPT/MPD ratio of 0.1 (TFC-2), while salt rejection remained stable, similar to the control polyamide membrane. At that ratio, the flux increased from 25 to 33 L m^{-2} h^{-1}, which is a 31% increase, and the salt rejection increased slightly from 98.8% to 98.9%. SPPT addition at other SPPT/MPD ratios, however, did not change the membrane performance to an extent that is significantly greater than the standard deviation. The explanation of the results including the

mechanism of electrostatic repulsion that leads to an increased free volume in the active layer and the rejection of mobile ions will be addressed in the following.

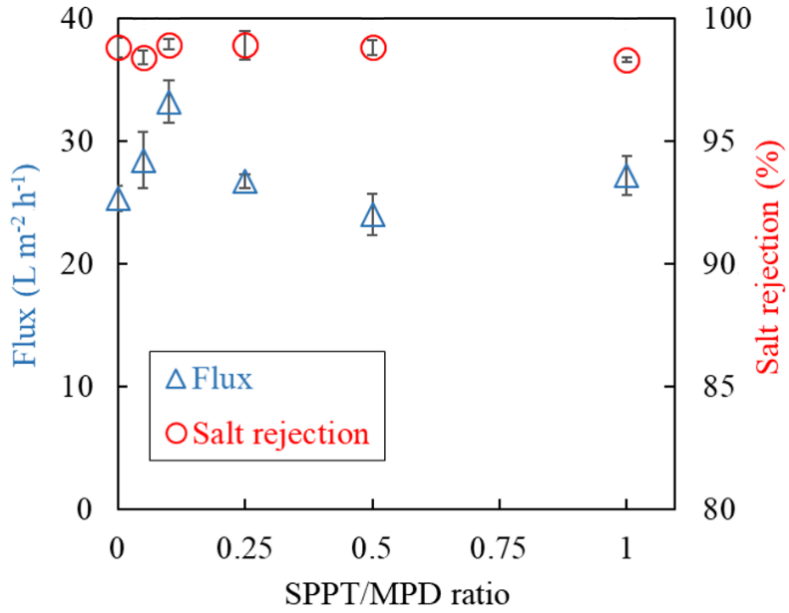

Figure 3.8 : Seawater desalination performance of polyamide membrane (TFC-0) and zwitterionic polyamide-polysiloxane membranes (TFC-1, TFC-2, TFC-3, TFC-4 and TFC-5). Zwitterionic SPPT monomers were added at different amounts to the aqueous 2% (w/w) MPD solution for interfacial polymerization with the organic 0.1% (w/v) TMC solution. Averaged results were obtained with 3.2% NaCl feed solution at an operating pressure of 55.2 bar, cross flow rate of 5 L/min at 25 °C.

The interfacial polymerization methods allows the in-situ polymerization of alkoxysilanes in the active layer. The sulfobetaine functionalized alkoxysilanes undergo condensation reactions among one another and, in addition, are also able to react with TMC [34-36]. As a result, an interpenetrating and crosslinked polysiloxane-polyamide network with zwitterionic moieties can be produced as the active layer of the TFC membrane and enhanced water flux can be obtained. The trialkoxysilane monomers were functionalized to contain sulfobetaine zwitterionic groups that induce electrostatic repulsion during RO operation. McKelvey et al. [88] were the first to introduced the idea of using Donnan rejection for the purpose of desalination. The use of ion exchange membranes as candidates to induce salt rejection by electrical forces was examined in further succeeding studies [89]. In principle, the separation characteristics of every membrane is influenced by the charge of its active layer. For example, it was found that commercial polyamide membranes reject more sodium ions than chloride ions, which was ascribed to their positively charged amine groups and that other commercial membranes such as the PEC1000 exhibit the opposite behavior

due to their negatively charged sulfonic acid groups [82]. It should be noted that amine groups in polyamide are expected to be present between each aromatic unit, whereas carboxylic acid groups are only comprised in linear polyamide chains that are not crosslinked. Many studies do not measure single salt species and claim that due to the overall negative zeta potential of the polyamide surface, the repulsion of negative ions is expected to be dominant [90,91]. However, it is not clear if the negative charge is only present on the surface due to the preferential adsorption of hydroxide ions and if the polyamide bulk has a positive charge instead.

The Donnan potential is based on electrical potential differences between two phases, one of which has a constant charge. The phase with a constant charge has more mobile ions of its opposite charge than the other phase. Without the Donnan potential, the mobile ions present in both phases would level out concentration differences by diffusion. But to maintain electroneutrality, ions are pulled back to the side with the opposite Donnan potential [92]. Rejection of co-ions (mobile ions with the same charge as the fixed charge) is established by the resulting electrostatic repulsion [93]. Because in this study the integrated polymer is zwitterionic and thus has an equal number of positive and negative fixed charges, an uniform Donnan potential between membrane and feed cannot be established. Yet, the occurrence of alternating local potentials in the membrane due to the fixed negative and positive charges in the active layer is expected to have an analogous effect in the range of the local potentials that results in an elongated diffusion path for mobile ions. Therefore, it is assumed that the resulting electrostatic forces are responsible for maintaining both the high salt rejection and the higher permeate flux in case of the TFC-2 membrane at a SPPT/MPD ratio of 0.1. Though, a further increase of the SPPT amount showed no improvement of the desalination performance. In other studies about the zwitterionization of carbon nanotubes (CNT), it is similarly hypothesized that zwitterionic groups block the entry of ionic species into the CNT pores, enhancing thereby the overall salt rejection of polyamide nanocomposite membranes [94].

3.2.4.2 Neutral silane membranes

The interfacial polymerization reaction was repeated in another experiment with the functional trialkoxysilane monomers DMAPS and APS that have neutral functional groups, in order to evaluate whether there could also be an increase in permeate flux

without the presence of zwitterionic moieties in the polysiloxane chain. Figure 3.9 shows the seawater desalination performance of the standard polyamide membrane (TFC-0) and the membranes that have been produced with the addition of 0.2% (w/w) neutral silane monomers (DMAPS and APS) to the aqueous MPD solution at a silane monomer to MPD ratio of 0.1. In that case, a decrease in the membrane desalination performance instead of an enhancement was observed. On the other hand, it was demonstrated in the previous section how the addition of SPPT at the same ratio resulted in a significant increase in the permeate flux, most probably due to the incorporated zwitterionic moieties.

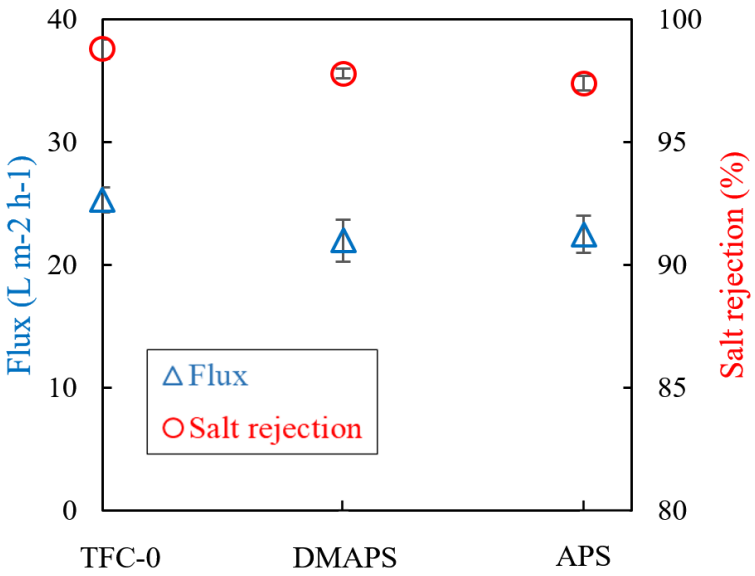

Figure 3.9 : Seawater desalination performance of polyamide membrane (TFC-0) and neutral polyamide-polysiloxane membranes. The neutral monomers DMAPS and APS were each added to a final concentration of 0.2% (w/w) to the aqueous 2% (w/w) MPD solution at a ratio of 0.1 for interfacial polymerization with the organic 0.1% (w/v) TMC solution. Averaged results were obtained with 3.2% NaCl feed solution at an operating pressure of 55.2 bar, cross flow rate of 5 L/min at 25 °C.

3.2.4.3 Coated silane membranes

The previous results have shown that the addition of the zwitterionic SPPT monomer to the aqueous MPD solution resulted in a maximum flux increase in the hybrid TFC membranes, when the SPPT/MPD ratio is 0.1, as in case of the TFC-2 membrane. The interfacial polymerization reaction of the aqueous monomeric solution with TMC in the organic phase produced a polyamide polysiloxane hybrid network as the active layer. Figure 3.10 illustrates the performance results of the TFC-2 membrane, compared to two membranes with additional coating layers on it (TFC-2_Coating-1 and TFC-2_Coating-2). The coating layers were applied over the hybrid active layer

to probe their effect on water flux and also to resistance to chlorination, as presented later. Coating 1 comprised a 0.2% aqueous SPPT solution that was allowed to prepolymerize before coating. When the zwitterionic oligomers adsorb on the TFC-2 active layer they are expected to further polymerize in the following oven curing step. However, the results showed that the coating resulted in a lowered salt rejection and a higher membrane flux, which indicates that the membranes had been damaged in the curing step. Coating 2 contained additionally to the SPPT 2 % MPD in the coating solution to crosslink polysiloxane oligomers with polyamide during prepolymerization and curing. The performance results showed that the resulting hybrid coating layer was observable in the permeate flux, which was lower due to the additional resistance of the coating layer, whereas the salt rejection did not change significantly.

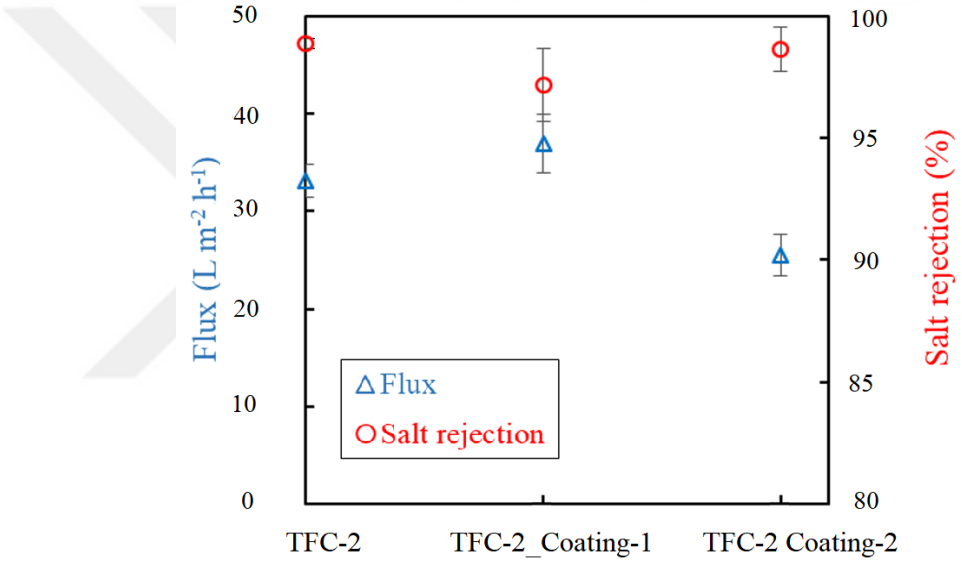

Figure 3.10 : Seawater desalination performance of the zwitterionic polysiloxane-polyamide membrane TFC-2 and of the same coated with SPPT (TFC-2_Coating-1) and with both SPPT and MPD (TFC-2_Coating-2). Averaged results were obtained with 3.2% NaCl feed solution at an operating pressure of 55.2 bar, cross flow rate of 5 L/min, and temperature of 25 °C.

3.2.5 Resistance to chlorination

The desalination performance tests were repeated with active chlorine added to the feed to investigate the chlorine resistance of the fabricated active layers. Figure 3.11 illustrates the course of the salt rejection with increasing exposure time to active chlorine, given as the product of active chorine concentration in ppm with time in h.

In Figure 3.11a, chlorination test results are given for standard polyamide membranes. TFC-0 was the TFC membrane fabricated without additional SPPT monomers. The commercial membrane was extracted from a seawater SWC5 desalination module

from Hydranautics for comparison. The chlorination tests reveal that salt rejection immediately decreases with increasing exposition to chlorine. After 1000 ppmh active chlorine, the salt rejection is already under 95%, which means that the membrane active layer is then severely damaged.

Figure 3.11b illustrates the chlorination experiment results for the polysiloxane-polyamide hybrid membranes. An improved resistance to chlorination was observed for the TFC-4 and TFC-5 membranes prepared wat SPPT/MPD ratios of 0.5 and 1 respectively. Significant membrane damage and consequent loss of salt rejection was only observed after exposure to 3000 ppmh chlorine, whereas the other hybrid membranes prepared at lower SPPT/MPD ratios are already prone to chlorine damage after 1000 ppmh, as it was the case with the standard polyamide membranes.

In Figure 3.11c, chlorination experiment results are given for the coated membranes as previously presented. The performance of the TFC-2_Coating-1 membrane, which was coated only with SPPT, showed a decrease in salt rejection after 1000 ppmh, similar as most of the tested membranes. In contrast, the TFC-2_Coating-2 membrane, which was coated with SPPT and MPD monomers, exhibited the highest resistance to chlorination of all tested membranes, which shows that only a crosslinked polysiloxane-polyamide network is effective as a protective layer.

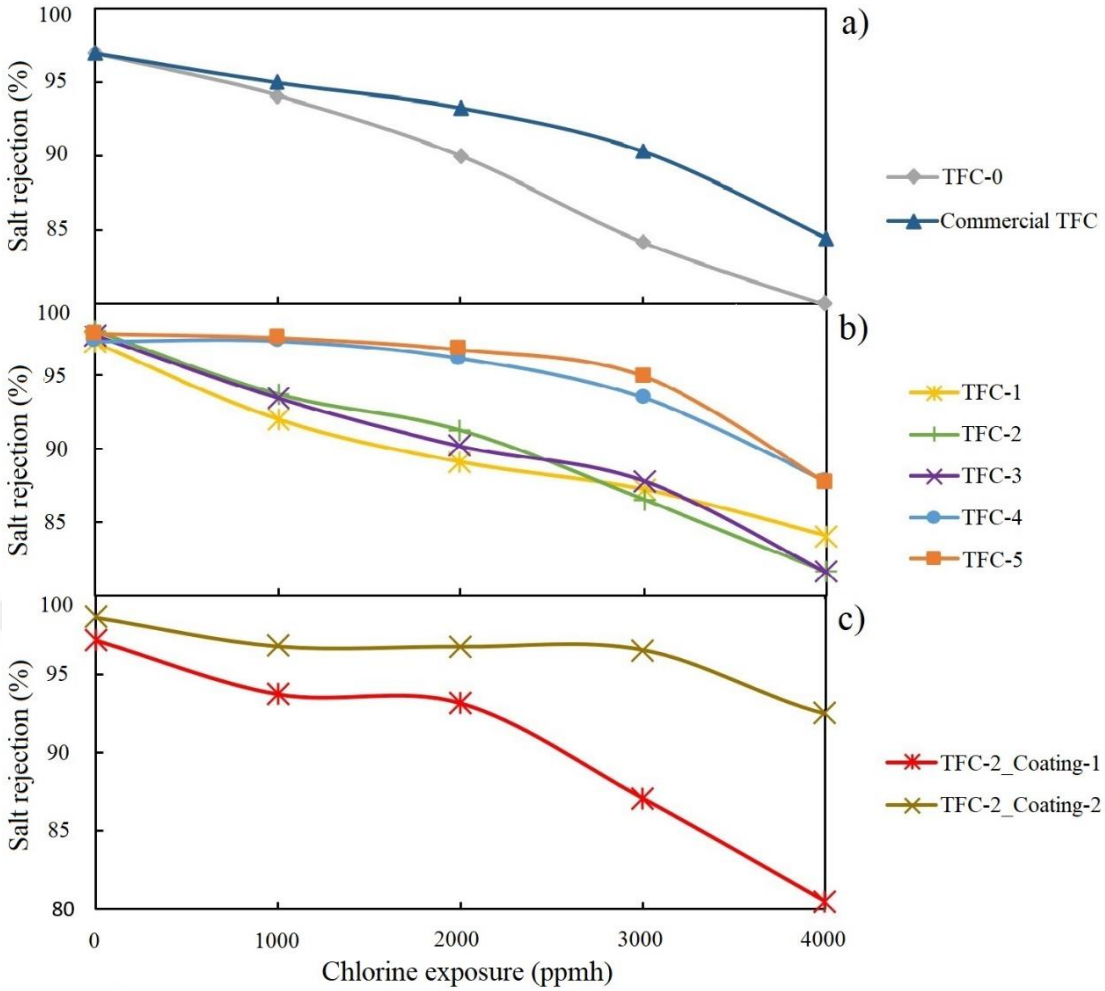

Figure 3.11 : Salt rejections after chlorination tests with a) standard polyamide membranes, b) polysiloxane-polyamide hybrid membranes and c) coated TFC-2 membranes. The active chlorine concentration was arranged to 500 ppm. Averaged results were obtained with 3.2% NaCl feed solution at an operating pressure of 55.2 bar, cross flow rate of 5 L/min, and temperature of 25 °C.

4. CONCLUSIONS

4.1 Role of Support Layer

This thesis demonstrated the important role of the support layer for the production of a defect-free active layer. The prevention of membrane defects is especially important for the fabrication of seawater desalination membranes. Selective properties of the produced polyamide active layers could be gradually improved by using polysulfone support layers with smaller average pore sizes. Cross-flow seawater desalination tests revealed that with decreasing average pore size of the support layer from 120 nm to 18 nm, salt rejection systematically increased from 80.5% to 99.0%. Morphological studies showed that the active layers of membranes prepared with larger pore size support layers exhibit more pronounced ridge-and-valley structures with many ridge-like protuberances, possibly due to convective MPD transport during interfacial polymerization. The mechanism leading to these structures is believed to cause defects in the inner polyamide layer and to result in a significant decrease in salt rejection. These findings further strengthen the hypothesis that a highly crosslinked inner polyamide layer is responsible for salt rejection and that the entire active layer with its visible morphology is more likely a byproduct of the polyamide polymerization reaction.

4.2 Effect of Zwitterionic Modification

The thesis, moreover, demonstrated the in-situ integration of zwitterionic moieties into the polyamide active layer by adding the zwitterionic trialkoxysilane monomer SPPT to the aqueous monomer solution for interfacial polymerization. This modification of the TFC membrane fabrication method resulted in the incorporation of zwitterionic polysiloxane polymers inside the polyamide active layer. It is, therefore, fundamentally different to other methods that involve a coating layer on top of the active layer, which would result in an additional resistance to membrane flux. In contrast to these methods, the modified membranes produced in this study exhibited a

higher flux at a certain SPPT/MPD ratio. They also showed a significant change in the membrane's active layer morphology and surface properties. The lack of a correlation between the streaming zeta potential of the membrane surface and the pH of the streaming solution is, furthermore, an indication for the successful integration of the strongly acidic and strongly basic zwitterionic groups.

It is hypothesized that the ionic solvation of free water molecules induced by the incorporated zwitterionic groups creates a more hydrophilic inner active layer that also has a larger free volume. As a result, a higher permeate flux is observed. Furthermore it is postulated that the zwitterionic properties of the used polymers cause an increase in electrostatic repulsion between membrane and feed solution and that, as a result, the diffusion path of both positive and negative solute ions will be longer. High salt rejection can only be maintained due to the elongated diffusion path of sodium and chloride ions even though the free volume of the hybrid polymer is expected to be larger. Furthermore, an increased rejection of charged chlorine species that are present at high pH, such as hypochlorite (ClO^-**)** mainly and also trichloride (Cl_3^-) is hypothesized. Because the acidity of hypochlorous acid i.e. the pK_a is 7.53, uncharged chlorine species will not be present at a significant concentration at pH > 7.5, as in the chlorination experiments. As a consequence, the electrostatic repulsion of charged chlorine species will occur and the polyamide layer is shielded from chlorination. The highest resistance to chlorine was observed at the highest amount of zwitterionic monomers added to the aqueous monomer solution. In that case, the salt rejection of the modified membrane stayed stable up to an active chlorine concentration of 3000 ppmh under seawater desalination conditions (55.2 bar; 3.2% NaCl feed), which is a threefold improvement compared to the control membranes. Zwitterionic polymers can therefore be regarded as competitive active layers for high performance membranes.

It has to be mentioned that the presence of a high ionic strength during seawater desalination is expected to diminish the effects of the proposed electrostatic repulsion due to ion shielding effects. However, in this work the zwitterionic side groups were incorporated into the active layer, where lower ionic strengths are present when solutes diffuse to the permeate side. Therefore, it is suggested that zwitterionic groups can be effective in the course of salt rejection during the RO process. High salt rejection can only be achieved when the sodium chloride concentration is reduced to below 400

ppm. To achieve this goal, the contribution of electrostatic repulsion to the salt rejection by solution diffusion differences is assumed to be critical for polymer networks with a larger free volume than crosslinked aromatic polyamides.

The study demonstrated that membrane properties strongly depend on the ratio of the monomers used for the interfacial polymerization process. Hydrophilicity, hypochlorite ion rejection and permeate flux are extremely sensitive to the amount of added SPPT. Because the polymerization can only take place in the organic phase for which the partitioning of MPD is higher than SPPT, it is assumed that polyamide chains are generally longer than polysiloxane chains. The zwitterionic polysiloxane is assumed to be present in the oligomeric form at different lengths according to the amount of added SPPT. In theory, the length of the polysiloxane chain should have a significant influence on the structure of polysiloxane inside the polyamide network. Shorter polysiloxane chains are expected to be present in a coiled form with hydrophobic and hydrophilic regions, where the zwitterionic groups interact with one another and with the opposite poles of water molecules to form water layers by electrostatic attractions. The effect of this phenomenon on water flux can be attributed to the ionic solvation of free water molecules, as explained in this and also in other studies. On the other hand, longer polysiloxane chains are expected to be present in an uncoiled structure, in which the zwitterionic groups are more evenly distributed. The higher resistance to charged chlorine species and the lower water contact angle of the membrane surface at higher SPPT additions can be explained by the more uniform effect of electrostatic repulsion and attraction. The coating experiments showed that an effectively salt rejecting and chlorine resisting active layer can only be produced, when both SPPT and MPD monomers are used. Together with the membrane characterization results they reflect the hybrid nature of the produced active layer and the importance of crosslinking between the zwitterionic polysiloxane oligomers and the polyamide polymers.

4.3 Future Prospect

According to the results of this study, it is assumed that the postulated electrostatic forces during RO operation are fundamental for maintaining a high salt rejection, a higher permeate flux and an improved chlorine resistance. Similar strategies using the principle of electrostatic rejection were already proposed, but had not yet been realized

with high salt rejections for seawater desalination. Moreover, the use of trialkoxysilane (organic/inorganic) coupling reagents in interfacial polymerization to produce polyamide-polysiloxane hybrid networks, as in this work, had not been proposed in the literature before. To the best of our knowledge, neither zwitterionic functional trialkoxysilanes, nor other functional alkoxysilanes have been used as reactants for interfacial polymerization in other published works. As an outcome of the collaboration between the universities a patent was filed for our unique method of organic/inorganic hybrid membrane fabrication. This study and the patented method for in-situ zwitterionization are, therefore, important steps for implementing the idea of using charged functional groups in membranes for the purpose of desalination, as it had been first introduced by McKelvey and his coworkers.

However, the membrane fabrication conditions have still to be further improved to reach better performance levels. In order to balance out the polymerization of the two polymers, polyamide and polysiloxane, it is very important to choose the exact monomer concentrations and polymerization conditions until permeate flux and salt rejection are fully optimized. It is, furthermore, important to decrease membrane surface roughness and thickness so that zwitterionic membranes become more competitive than commercial seawater desalination membranes. A synergistic cooperation between industry and academia would be very promising in this regard, because it could develop the full potential of zwitterionic membranes and pave the way for their commercialization. Membrane manufacturers have the expertise to produce thinner and smoother membranes than those fabricated by academic researchers in the laboratory to provide a proof of concept. The membranes produced in this study exhibited a 31% increase in permeate flux when compared to the control membrane prepared without the zwitterionic monomer. It would be a significant achievement, if an equivalent increase can be realized for commercial polyamide membranes. Their commercial fabrication would only involve an additional step and a minor modification to the active layer polymerization process, i.e. the synthesis of zwitterionic trialkoxysilanes and their addition to the interfacial polymerization aqueous monomer solution. In this manner, a major breakthrough in the field of membrane technology could be achieved, if membranes can be developed that have even a higher resistance to chlorine than the membranes presented in this thesis.

REFERENCES

[1] **Elimelech, M.** & **Phillip, W. A.** (2011). The Future of Seawater and the Environment: Energy, Technology, and the Environment, *Science*, *333*, 712–718.

[2] **Ismail, A. F.**, **Padaki, M.**, **Hilal, N.**, **Matsuura, T.** & **Lau, W. J.** (2015). Thin film composite membrane — Recent development and future potential, *Desalination*, *356*, 140–148.

[3] **Koyuncu, I.**, **Wiesner, M. R.**, **Bele, C.**, **Coriton, G.**, **Djafer, M.** & **Cavard, J.** (2006). Bench-scale assessment of pretreatment to reduce fouling of salt-rejecting membranes, *Desalination*, *197* (1–3), 94–105.

[4] **Koyuncu, I.** & **Wiesner, M. R.** (2007). Morphological Variations of Precipitated Salts on NF and RO Membranes, *Environ. Eng. Sci.*, *24* (5), 602–614.

[5] **Koyuncu, I.**, **Brant, J.**, **Lüttge, A.** & **Wiesner, M. R.** (2006). A comparison of vertical scanning interferometry (VSI) and atomic force microscopy (AFM) for characterizing membrane surface topography, *J. Memb. Sci.*, *278* (1–2), 410–417.

[6] **Tarabara, V. V.**, **Koyuncu, I.** & **Wiesner, M. R.** (2004). Effect of hydrodynamics and solution ionic strength on permeate flux in cross-flow filtration: Direct experimental observation of filter cake cross-sections, *J. Memb. Sci.*, *241* (1), 65–78.

[7] **World Health Organization** (2017). Guidelines for drinking-water quality.

[8] **Loeb, S.** (1981). The Loeb-Sourirajan Membrane: How It Came About, *ACS Symp. Ser. Am. Chem. Soc. Washington, DC*, 1–9.

[9] **Mudler, M.** (1996). Basic principles of membrane technology. .

[10] **Tomaschke, J. E.** (2000). *Membrane Preparation | Interfacial Composite Membranes. in: Encycl. Sep. Sci.*, pp. 3319–3331.

[11] **Baker, R.** (2004). *Membrane technology and applications. 2nd ed.* John Wiley & Sons Ltd, .

[12] **Cadotte, J. E.** & **Petersen, R. J.** (1981). *Thin-film composite reverse-osmosis membranes: Origin, development, and recent advances*, 305–326.

[13] **Cadotte, J. E.** (1981). *Interfacially synthesized reverse osmosis membrane*, *US Patent 4,277,344*, 1981.

[14] **Rozelle, L. T.**, **Cadotte, J.E.**, **Corneliussen, R. D.** & **Erickson, E. E.** (1967). Development of new reverse osmosis membranes for desalination, *Spring-Reld, VA Natl. Tech. Inf. Serv.*

[15] **Cadotte, J. E.** (1977). *Reverse Osmosis Membran*e, *US Patent 4,039,440*, 1977.

[16] **Lee, K. P.**, **Arnot, T. C.** & **Mattia, D.** (2011). A review of reverse osmosis membrane materials for desalination-Development to date and future potential, *J. Memb. Sci.*, *370* (1–2), 1–22.

[17] **Zhu, S., Zhao, S., Wang, Z., Tian, X., Shi, M.** & **Wang, J.** (2015). Improved performance of polyamide thin-film composite nanofiltration membrane by using polyetersulfone/polyaniline membrane as the substrate, *J. Memb. Sci.*, *493*, 263–274.

[18] **Singh, P. S.**, **Joshi, S. V.**, **Trivedi, J. J.**, **Devmurari, C. V.**, **Rao, A. P.** & **Ghosh, P. K.** (2006). Probing the structural variations of thin film composite RO membranes obtained by coating polyamide over polysulfone membranes of different pore dimensions, *J. Memb. Sci.*, *278* (1–2), 19–25.

[19] **Misdan, N.**, **Lau, W. J.**, **Ismail, A. F.** & **Matsuura, T.** (2013). Formation of thin film composite nanofiltration membrane: Effect of polysulfone substrate characteristics, *Desalination*, *329*, 9–18.

[20] **Peyravi, M.**, **Rahimpour, A.**, & **Jahanshahi, M.** (2012). Thin film composite membranes with modified polysulfone supports for organic solvent nanofiltration, *J. Memb. Sci.*, *423–424*, 225–237.

[21] **Ghosh, A. K.** & **Hoek, E. M. V** (2009). Impacts of support membrane structure and chemistry on polyamide-polysulfone interfacial composite membranes, *J. Memb. Sci.*, *336* (1–2), 140–148.

[22] **Yoon, K.**, **Hsiao, B. S.** & **Chu, B.** (2009). High flux nanofiltration membranes based on interfacially polymerized polyamide barrier layer on polyacrylonitrile nanofibrous scaffolds, *J. Memb. Sci.*, *326* (2), 484–492.

[23] **Singh, P. S.**, **Joshi, S. V.**, **Trivedi, J. J.**, **Devmurari, C. V**, **Rao, A. P.** & **Ghosh, P. K.** (2006). Probing the structural variations of thin film composite RO membranes obtained by coating polyamide over polysulfone membranes of different pore dimensions, *J. Memb. Sci.*, *278*, 19–25.

[24] **Lau, W. J.**, **Ismail, A. F.**, **Misdan, N.** & **Kassim, M. A.** (2012). A recent progress in thin film composite membrane: A review, *Desalination*, *287*, 190–199.

[25] **Singh, P. S., Rao, A. P., Ray, P., Bhattacharya, A., Singh, K., Saha, N. K. et al.** (2011). Techniques for characterization of polyamide thin film composite membranes, *Desalination*, *282*, 78–86.

[26] **Pacheco, F.**, **Sougrat, R.**, **Reinhard, M.**, **Leckie, J. O.** & **Pinnau, I.** (2016). 3D visualization of the internal nanostructure of polyamide thin films in RO membranes, *J. Memb. Sci.*, *501*, 33–44.

[27] **Xie, W.**, **Geise, G. M.**, **Freeman, B. D.**, **Lee, H. S.**, **Byun, G.** & **McGrath, J. E.** (2012). Polyamide interfacial composite membranes prepared from m-phenylene diamine, trimesoyl chloride and a new disulfonated diamine, *J. Memb. Sci.*, *403–404*, 152–161.

[28] **Ghosh, A. K.**, **Jeong, B. H.**, **Huang, X.**, & **Hoek, E. M. V** (2008). Impacts of reaction and curing conditions on polyamide composite reverse osmosis membrane properties, *J. Memb. Sci.*, *311* (1–2), 34–45.

[29] **Deborde, M.** & **von Gunten, U.** (2008). Reactions of chlorine with inorganic and organic compounds during water treatment-Kinetics and mechanisms: A critical review, *Water Res.*, *42* (1–2), 13–51.

[30] **Shin, D. H.**, **Kim, N.** & **Lee, Y. T.** (2011). Modification to the polyamide TFC RO membranes for improvement of chlorine-resistance, *J. Memb. Sci.*, *376* (1–2), 302–311.

[31] **Glater, J.**, **Hong, S. K.** & **Elimelech, M.** (1994). The search for a chlorine-resistant reverse osmosis membrane, *Desalination*, *95* (3), 325–345.

[32] **Shenvi, S. S.**, **Isloor, A. M.**, & **Ismail, A. F.** (2015). A review on RO membrane technology: Developments and challenges, *Desalination*, *368*, 10–26.

[33] **Gohil, J. M.** & **Ray, P.** (2017). A review on semi-aromatic polyamide TFC membranes prepared by interfacial polymerization: Potential for water treatment and desalination, *Sep. Purif. Technol.*, *181*, 159–182.

[34] **Zhao, Y.**, **Zhang, Z.**, **Dai, L.**, **Mao, H.** & **Zhang, S.** (2017). Enhanced both water flux and salt rejection of reverse osmosis membrane through combining isophthaloyl dichloride with biphenyl tetraacyl chloride as organic phase monomer for seawater desalination, *J. Memb. Sci.*, *522*, 175–182.

[35] **Yu, S.**, **Liu, M.**, **Liu, X.** & **Gao, C.** (2009). Performance enhancement in interfacially synthesized thin-film composite polyamide-urethane reverse osmosis membrane for seawater desalination, *J. Memb. Sci.*, 342 (1–2), 313–320.

[36] **Moon, J. H.**, **Katha, A. R.**, **Pandian, S.**, **Kolake, S. M.** & **Han, S.** (2014). Polyamide-POSS hybrid membranes for seawater desalination: Effect of POSS inclusion on membrane properties, *J. Memb. Sci.*, *461*, 89–95.

[37] **Zhao, L.** & **Ho, W. S. W.** (2014). Novel reverse osmosis membranes incorporated with a hydrophilic additive for seawater desalination, *J. Memb. Sci.*, *455*, 44–54.

[38] **Goh, P. S.**, **Matsuura, T.**, **Ismail, A. F.**, & **Hilal, N.** (2016). Recent trends in membranes and membrane processes for desalination, *Desalination*, *391*, 43–60.

[39] **Ni, L.**, **Meng, J.**, **Geise, G. M.**, **Zhang, Y.**, & **Zhou, J.** (2015). Water and salt transport properties of zwitterionic polymers film, *J. Memb. Sci.*, *491*, 73–81.

[40] **Zhang, Y.**, **Wang, Z.**, **Lin, W.**, **Sun, H.**, **Wu, L.** & **Chen, S.** (2013). A facile method for polyamide membrane modification by poly(sulfobetaine methacrylate) to improve fouling resistance, *J. Memb. Sci.*, *446*, 164–170.

[41] **Azari, S.** & **Zou, L.** (2013). Fouling resistant zwitterionic surface modification of reverse osmosis membranes using amino acid l-cysteine, *Desalination*, *324*, 79–86.

[42] **Eisenberg, D.** & **Kauzmann, W.** (2005). *The Structure and Properties of Water*. Oxford University Press, .

[43] **Jenniskens, P.**, **Banham, S. F.**, **Blake, D. F.**, **Mccoustra, M. R. S.** & **Jenniskens, P.** (1997). Liquid water in the domain of cubic crystalline ice I c, *J. Chem. Phys.*, *107*.

[44] **Rowland, B.** & **Devlin, J. P.** (1991). Spectra of dangling OH groups at ice cluster surfaces and within pores of amorphous ice, *J. Chem. Phys.*, *94* (1), 812.

[45] **Kitano, H., Mori, T., Takeuchi, Y., Tada, S., Gemmei-Ide, M., Yokoyama, Y. et al.** (2005). Structure of water incorporated in sulfobetaine polymer films as studied by ATR-FTIR, *Macromol. Biosci.*, *5* (4), 314–321.

[46] **Mi, Y.-F.**, **Zhao, Q.**, **Ji, Y.-L.**, **An, Q.-F.** & **Gao, C.-J.** (2015). A novel route for surface zwitterionic functionalization of polyamide nanofiltration membranes with improved performance, *J. Memb. Sci.*, *490*, 311–320.

[47] **Kim, S. G.**, **Park, S. Y.**, **Chun, J. H.**, **Chun, B.-H.** & **Kim, S. H.** (2012). Novel thin-film composite membrane for seawater desalination with sulfonated poly(arylene ether sulfone) containing amino groups, *Desalin. Water Treat.*, *43* (1–3), 230–237.

[48] **Xie, W.**, **Geise, G. M.**, **Freeman, B. D.**, **Lee, H. S.**, **Byun, G.** & **McGrath, J. E.** (2012). Polyamide interfacial composite membranes prepared from m-phenylene diamine, trimesoyl chloride and a new disulfonated diamine, *J. Memb. Sci.*, *403–404*, 152–161.

[49] **Chiang, Y. C.**, **Chang, Y.**, **Chuang, C. J.** & **Ruaan, R.C.** (2012). A facile zwitterionization in the interfacial modification of low bio-fouling nanofiltration membranes, *J. Memb. Sci.*, *389*, 76–82.

[50] **Ma, R.**, **Ji, Y. L.**, **Weng, X. D.**, **An, Q. F.**, & **Gao, C. J.** (2016). High-flux and fouling-resistant reverse osmosis membrane prepared with incorporating zwitterionic amine monomers via interfacial polymerization, *Desalination*, *381*, 100–110.

[51] **Belov, N.**, **Nizhegorodova, Y.**, **Bermeshev, M.** & **Yampolskii, Y.** (2015). Detailed study of the gas permeation parameters of a glassy poly(tricyclononene) with Si-O-Si side groups, *J. Memb. Sci.*, *483*, 136–143.

[52] **Heile, S.**, **Rosenberger, S.**, **Parker, A.**, **Jefferson, B.** & **McAdam, E. J.** (2014). Establishing the suitability of symmetric ultrathin wall polydimethylsiloxane hollow-fibre membrane contactors for enhanced CO2 separation during biogas upgrading, *J. Memb. Sci.*, *452*, 37–45.

[53] **Nie, F.**, **He, G.**, **Zhao, W.**, **Ju, J.**, **Liu, Y.** & **Dai, Y.** (2014). Improving CO2 separation performance of the polyethylene glycol (PEG)/polytrifluoropropylsiloxane (PTFPMS) blend composite membrane, *J. Polym. Res.*, *21* (1), 319.

[54] **Femmer, T., Kuehne, A. J. C., Wessling, M., Smolders, C., Huang, C.-Y., Chen, K.-N. et al.** (2014). Print your own membrane: direct rapid prototyping of polydimethylsiloxane, *Lab Chip*, *14* (15), 2610.

[55] **Baker, R. W.** & **Low, B. T.** (2014). Gas Separation Membrane Materials: A Perspective, *Macromolecules*, 47 6999–7013.

[56] **Raaijmakers, M. J. T., Hempenius, M. A., Schön, P. M., Vancso, G. J., Nijmeijer, A.** & **Wessling, M.** (2014). Sieving of hot gases by hyper-cross-linked nanoscale-hybrid membranes, *J. Am. Chem. Soc.*, *136* (1), 330–335.

[57] **Duan, J.**, **Litwiller, E.** & **Pinnau, I.** (2015). Preparation and water desalination properties of POSS-polyamide nanocomposite reverse osmosis membranes, *J. Memb. Sci.*, *473*, 157–164.

[58] **Bauman, M.**, **Košak, A.**, **Lobnik, A.**, **Petrinić, I.** & **Luxbacher, T.** (2013). Nanofiltration membranes modified with alkoxysilanes: Surface characterization using zeta-potential, *Colloids Surfaces A Physicochem. Eng. Asp.*, *422*, 110–117.

[59] **Kim, N.**, **Shin, D. H.** & **Lee, Y. T.** (2007). Effect of silane coupling agents on the performance of RO membranes, *J. Memb. Sci.*, *300* (1–2), 224–231.

[60] **Jee, K. Y.**, **Shin, D. H.** & **Lee, Y. T.** (2016). Surface modification of polyamide RO membrane for improved fouling resistance, *Desalination*, *394*, 131–137.

[61] **Guillen, G. R.**, **Pan, Y.**, **Li, M.** & **Hoek, E. M. V** (2011). Preparation and Characterization of Membranes Formed by Nonsolvent Induced Phase Separation : A Review, *Ind. Eng. Chem. Res.*, *50* (7) 3798–3817.

[62] **Cadotte, J. E.** (1985). Evolution of composite reverse osmosis membranes., *ACS Symp. Ser.*, *269* (Mater. Sci. Synth. Membr.), 273–294.

[63] **Porter, M. C.** (1990). *Handbook of industrial membrane technology*. Noyes Publications, .

[64] **Saravanan, P.**, **Ramana, G. V.**, **Rao, K. S.**, **Sreedhar, B.**, **Vinod, V. T. P.** & **Chandrasekaran, V.** (2011). Structural and magnetic properties of self-assembled Sm – Co spherical aggregates, *J. Magn. Magn. Mater.*, *323* (15), 2083–2089.

[65] **Soltani, N.**, **Saion, E.**, **Erfani, M.**, **Rezaee, K.** & **Bahmanrokh, G.** (2012). Influence of the Polyvinyl Pyrrolidone Concentration on Particle Size and Dispersion of ZnS Nanoparticles Synthesized by Microwave Irradiation, *Int. J. Mol. Sci.*, *13* (10), 12412–12427.

[66] **Mulder, M. H. V.**, **Hendrikman, J. O.**, **Wijmans, J. G.** & **Smolders, C. A.** (1985). A rationale for the preparation of asymmetric pervaporation membranes, *J. Appl. Polym. Sci.*, *30* (7), 2805–2820.

[67] **Wienk, I. M.**, **Boom, R. M.**, **Beerlage, M. A. M.**, **Bulte, A. M. W.**, **Smolders, C. A.** & **Strathmann, H.** (1996). Recent advances in the formation of phase inversion membranes made from amorphous or semi-crystalline polymers, *J. Memb. Sci.*, *113*, 361–371.

[68] **Wijmans, J. G.**, **Kant, J.**, **Mulder, M. H. V.** & **Smolders, C.A.** (1985). Phase separation phenomena in solutions of polysulfone in mixtures of a solvent and a nonsolvent: relationship with membrane formation, *J. Polym. Sci. Part A-2, Polym. Phys.*, *26* (9), 1539–1545.

[69] **Tiraferri, A.**, **Yip, N. Y.**, **Phillip, W. A.**, **Schiffman, J. D.** & **Elimelech, M.** (2011). Relating performance of thin-film composite forward osmosis membranes to support layer formation and structure, *J. Memb. Sci.*, *367* (1–2), 340–352.

[70] **Freger, V.** (2003). Nanoscale heterogeneity of polyamide membranes formed by interfacial polymerization, *Langmuir*, *19* (11), 4791–4797.

[71] **Yan, H., Miao, X., Xu, J., Pan, G., Zhang, Y., Shi, Y. et al.** (2015). The porous structure of the fully-aromatic polyamide film in reverse osmosis membranes, *J. Memb. Sci.*, *475*, 504–510.

[72] **Pacheco, F.**, **Pinnau, I.**, **Reinhard, M.** & **Leckie, J.O.** (2010). Characterization of isolated polyamide thin films of RO and NF membranes using novel TEM techniques, *J. Memb. Sci., 358* (1–2), 51–59.

[73] **Klaysom, C., Hermans, S., Gahlaut, A., Craenenbroeck, S. Van, Vankelecom, I. F. J. J., Van Craenenbroeck, S. et al.** (2013). Polyamide/Polyacrylonitrile (PA/PAN) thin film composite osmosis membranes: Film optimization, characterization and performance evaluation, *J. Memb. Sci., 445* 25–33.

[74] **Li, X.**, **Wang, K. Y.**, **Helmer, B.**, & **Chung, T.S.** (2012). Thin-film composite membranes and formation mechanism of thin-film layers on hydrophilic cellulose acetate propionate substrates for forward osmosis processes, *Ind. Eng. Chem. Res., 51* (30), 10039–10050.

[75] **Tsuru, T., Sasaki, S., Kamada, T., Shintani, T., Ohara, T., Nagasawa, H. et al.** (2013). Multilayered polyamide membranes by spray-assisted 2-step interfacial polymerization for increased performance of trimesoyl chloride (TMC)/m-phenylenediamine (MPD)-derived polyamide membranes, *J. Memb. Sci., 446,* 504–512.

[76] **Ridgway, H.F.**, **Orbell, J.** & **Gray, S.** (2017). Molecular simulations of polyamide membrane materials used in desalination and water reuse applications: Recent developments and future prospects, *J. Memb. Sci., 524,* 436–448.

[77] **Kwak, S. Y.**, **Jung, S. G.**, **Yoon, Y. S.** & **Ihm, D.W.** (1999). Details of surface features in aromatic polyamide reverse osmosis membranes characterized by scanning electron and atomic force microscopy, *J. Polym. Sci. Part B Polym. Phys., 37* (13), 1429–1440.

[78] **Lin, L.**, **Lopez, R.**, **Ramon, G. Z.** & **Coronell, O.** (2016). Investigating the void structure of the polyamide active layers of thin-film composite membranes, *J. Memb. Sci., 497,* 365–376.

[79] **Zimmermann, R.**, **Dukhin, S.** & **Werner, C.** (2001). Electrokinetic measurements reveal interracial charge at polymer films caused by simple electrolyte ions, *J. Phys. Chem. B, 105* (36), 8544–8549.

[80] **Tang, C.Y.**, **Kwon, Y.N.** & **Leckie, J.O.** (2009). Effect of membrane chemistry and coating layer on physiochemical properties of thin film composite polyamide RO and NF membranes. II. Membrane physiochemical properties and their dependence on polyamide and coating layers, *Desalination, 242* (1–3), 168–182.

[81] **Birkner, M.** & **Ulbricht, M.** (2015). Ultrafiltration membranes with markedly different pH- and ion-responsivity by photografted zwitterionic polysulfobetain or polycarbobetain, *J. Memb. Sci., 494,* 57–67.

[82] **Nakagawa, Y.**, **Edogawa, K.**, **Kurihara, M.** & **Tonomura, T.** (1985). Solute separation and transport characteristics through polyether composite (PEC)-1000 reverse-osmosis membranes., *ACS Symp. Ser., 281,* 187–199.

[83] **Vrijenhoek, E. M.**, **Hong, S.** & **Elimelech, M.** (2001). Influence of membrane surface properties on initial rate of colloidal fouling of reverse osmosis and nanofiltration membranes, *J. Memb. Sci., 188* (1), 115–128.

[84] **Breite, D.**, **Went, M.**, **Prager, A.** & **Schulze, A.** (2017). Tailoring Membrane Surface Charges : A Novel Study on Electrostatic Interactions during Membrane Fouling, *Polymers, 7* (10), 2017–2030.

[85] **Childress, A.E.** & **Elimelech, M.** (1996). Effect of solution chemistry on the surface charge of polymeric reverse osmosis and nanofiltration membranes, *J. Memb. Sci., 119* (2), 253–268.

[86] **Zimmermann, R., Küttner, D., Renner, L., Kaufmann, M., Zitzmann, J., Müller, M. et al.** (2009). Charging and structure of zwitterionic supported bilayer lipid membranes studied by streaming current measurements, fluorescence microscopy, and attenuated total reflection Fourier transform infrared spectroscopy, *Biointerphases*, *4* (1), 1–6.

[87] **Zhou, Y.** & **Raphael, R.M.** (2007). Solution pH alters mechanical and electrical properties of phosphatidylcholine membranes: Relation between interfacial electrostatics, intramembrane potential, and bending elasticity, *Biophys. J.*, *92* (7), 2451–2462.

[88] **McKelvey, J.G.** & **Spiegler, K.S.** (1964). Ultrafiltration of Electrolyte Solutions Through Ion-Exchange Membranes, US3132094, 1964.

[89] **Kimura, S.G.** (1971). Reverse osmosis performance of sulfonated poly(2,6-dimethylphenylene ether) ion exchange membranes., *Ind. Eng. Chem. Prod. Res. Dev.*, *10* (3), 335–339.

[90] **Hagmeyer, G.** & **Gimbel, R.** (1998). Modelling the salt rejection of nanofiltration membranes for ternary ion mixtures and for single salts at different pH values, *Desalination, 117*, 247–256.

[91] **Wang, D.**, **Su, M.**, **Yu, Z.**, **Wang, X.** & **Masaaki, A.** (2005). Separation performance of a nanofiltration membrane influenced by species and concentration of ions, *175*, 219–225.

[92] **Friedrich G. Helfferich** (1962). Ion Exchange. Dover Publications.

[93] **Nicolini, J. V.**, **Borges, C. P.** & **Ferraz, H. C.** (2016). Selective rejection of ions and correlation with surface properties of nanofiltration membranes, *Sep. Purif. Technol.*, *171*, 238–247.

[94] **Chan, W., Chen, H., Surapathi, A., Taylor, M. G., Shao, X.** & **Marand, E.** (2013). Zwitterion Functionalized Carbon Nanotube / Polyamide Nanocomposite, *ACS Nano, 7* (6), 5308–5319.

APPENDICES

APPENDIX A: Polyamide membranes with different support layers

APPENDIX B: Polysiloxane-polyamide hybrid membranes

APPENDIX A: Polyamide membranes with different support layers

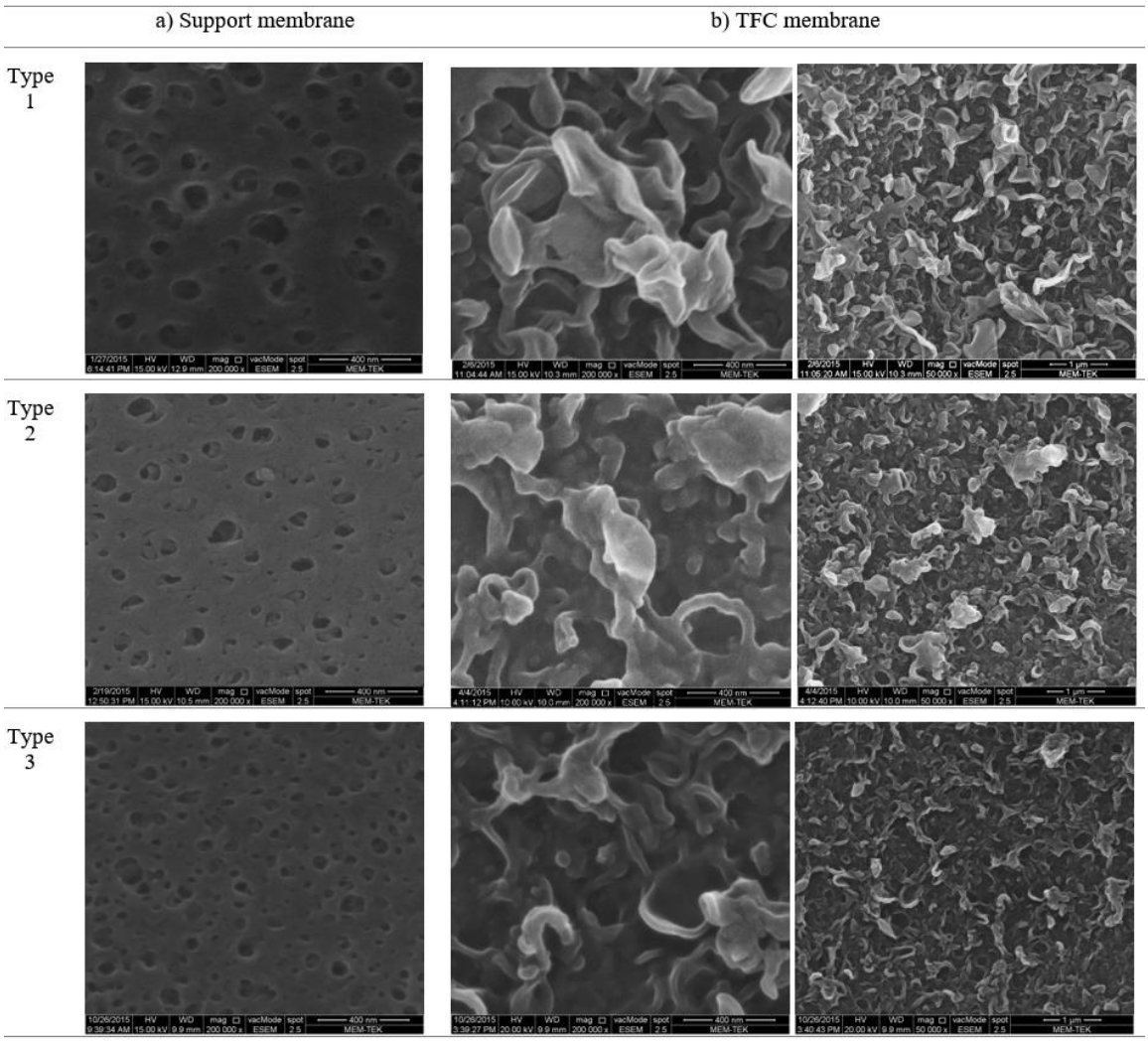

Figure A.1 : SEM surface view of different types of a) polysulfone support layers and b) fabricated polyamide active layers formed by interfacial polymerization.

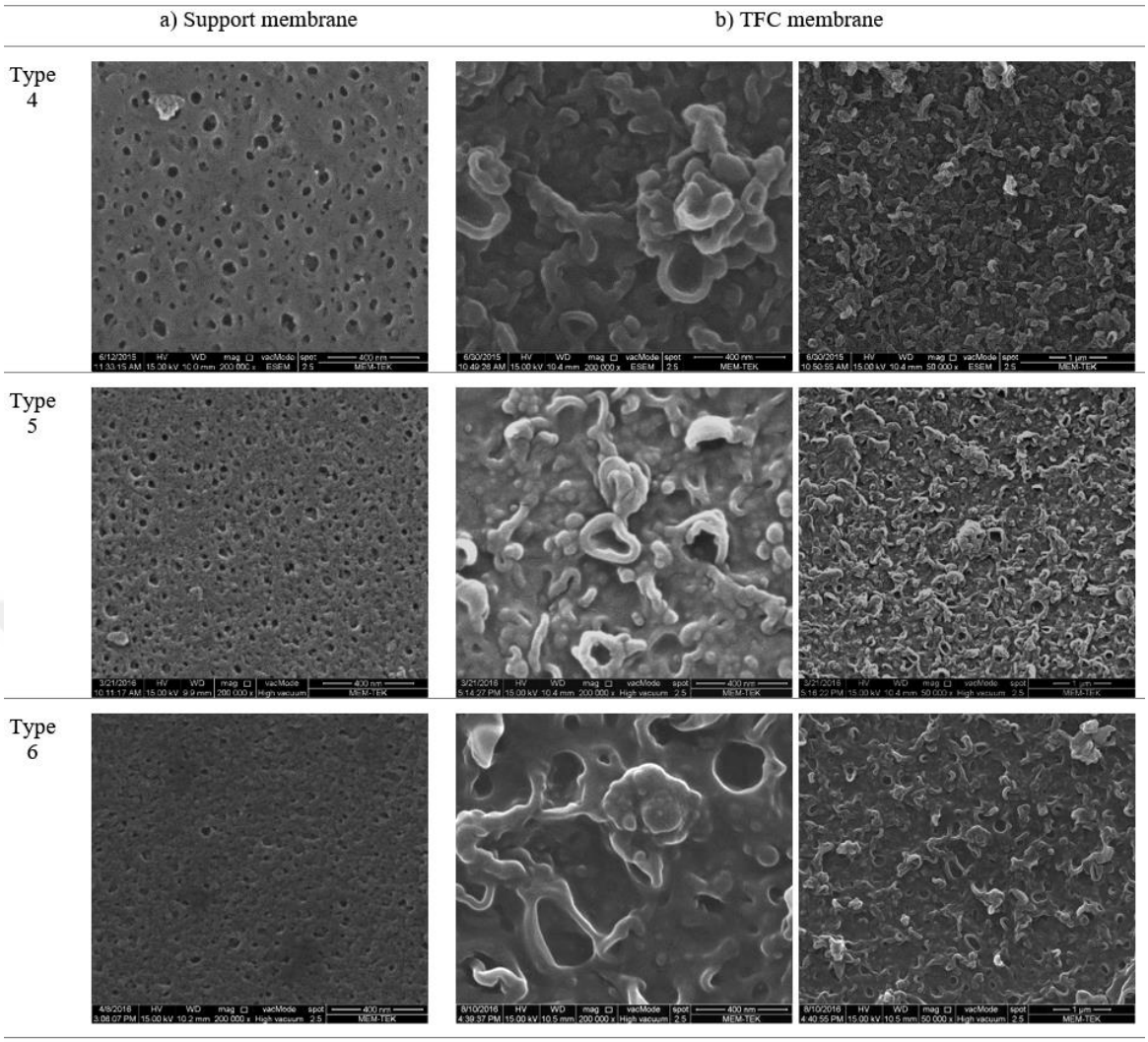

Figure A.1 (continued) : SEM surface view of different types of (a) polysulfone support layers and (b) fabricated polyamide active layers formed by interfacial polymerization

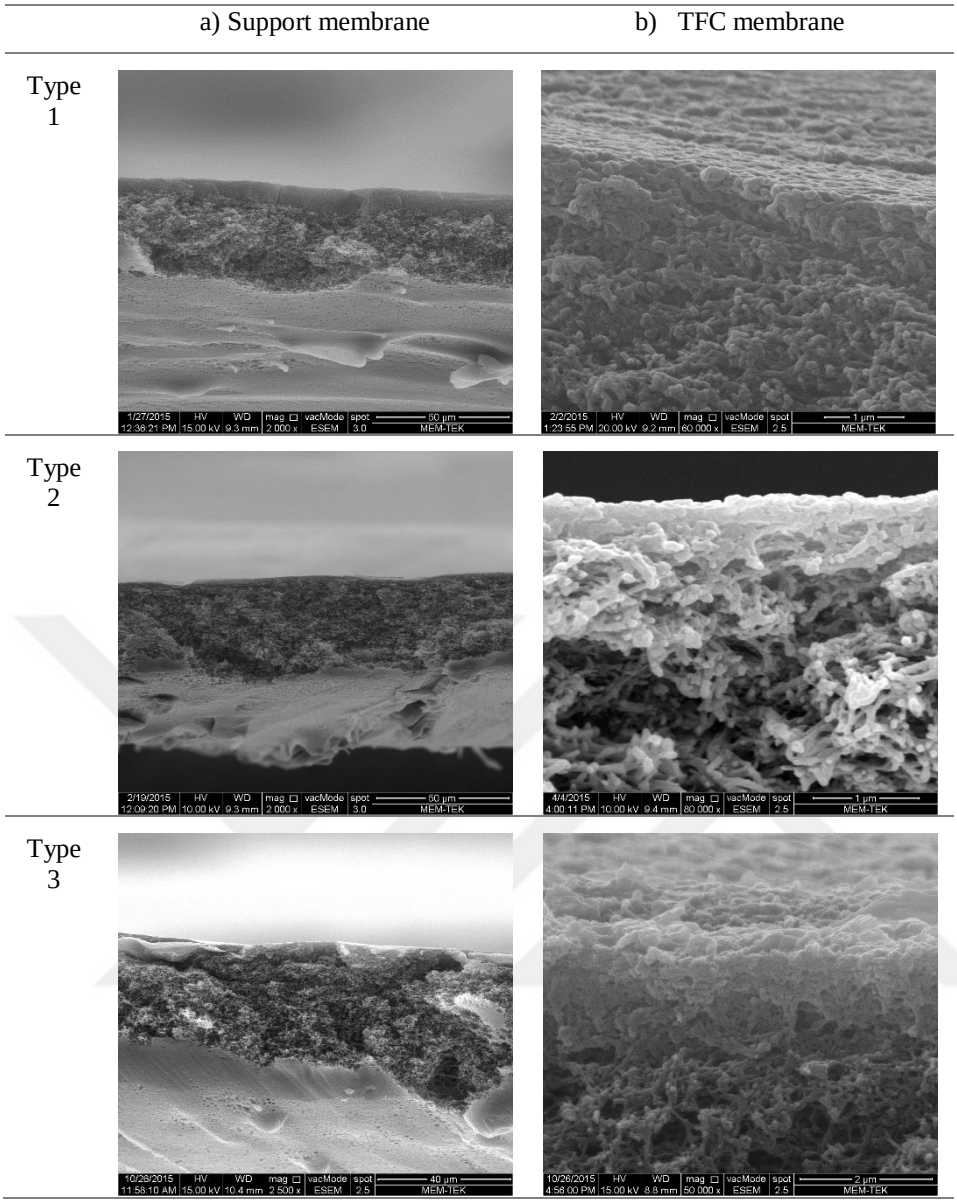

Figure A.2 : SEM cross-sectional view of different types of a) polysulfone support layers and b) polyamide active layers formed by interfacial polymerization.

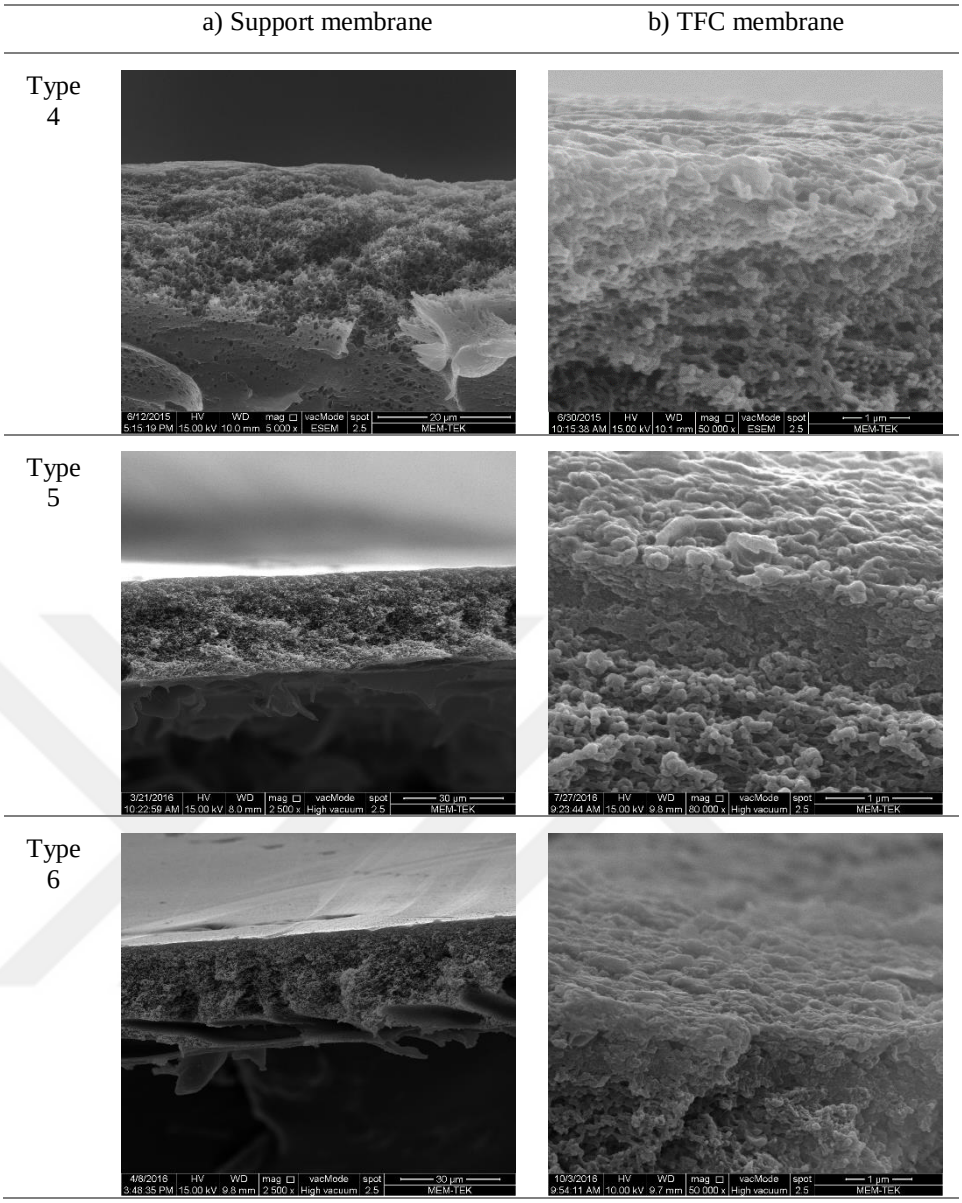

Figure A.2 (continued) : SEM cross-sectional view of different types of (a) polysulfone support layers and (b) polyamide active layers formed by interfacial polymerization

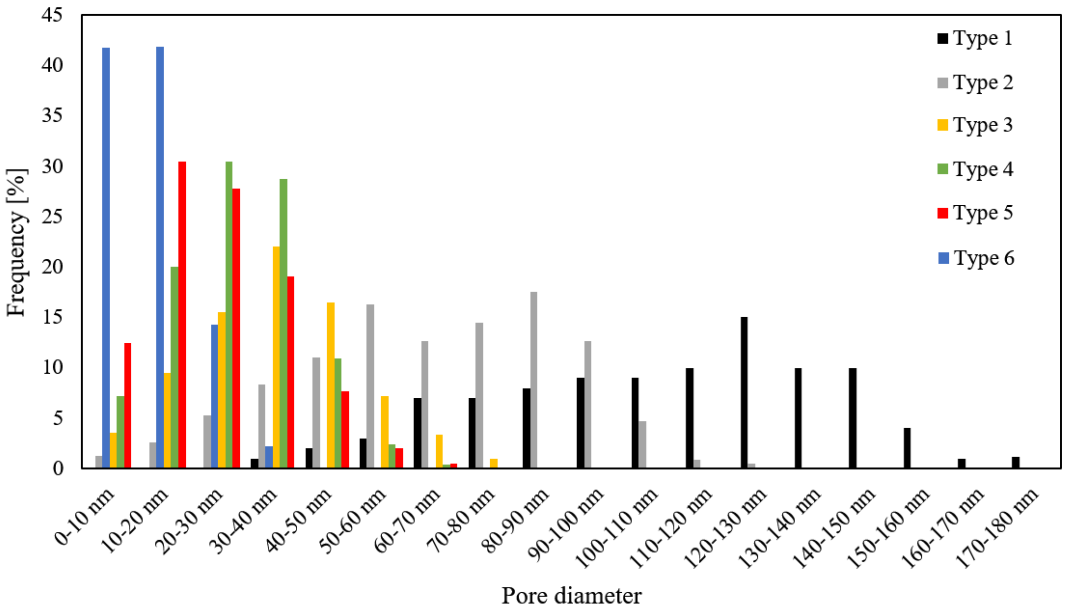

Figure A.3 : Pore size distribution for different types of polysulfone support layers. Pore diameters were determined with imaging software ImageJ from corresponding SEM images.

APPENDIX B: Polysiloxane-polyamide hybrid membranes

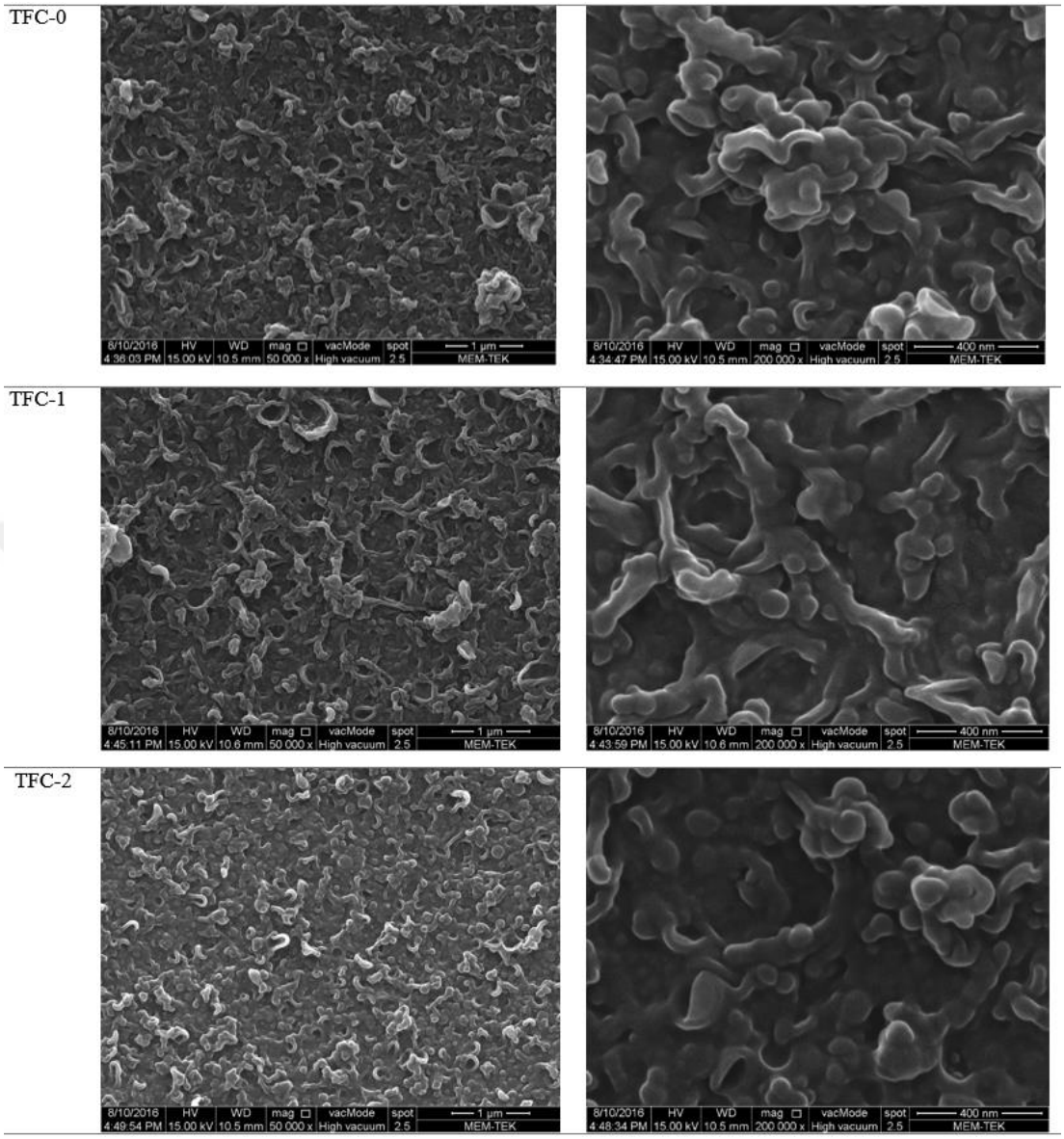

Figure B.1 : SEM surface morphologies of the control polyamide membrane TFC-0 and the zwitterionic silane modified polyamide-polysiloxane membranes TFC-1, TFC-2, TFC-3, TFC-4 and TFC-5, produced at SPPT/MPD ratios of 0.05, 0.1, 0.25, 0.5 and 1 respectively.

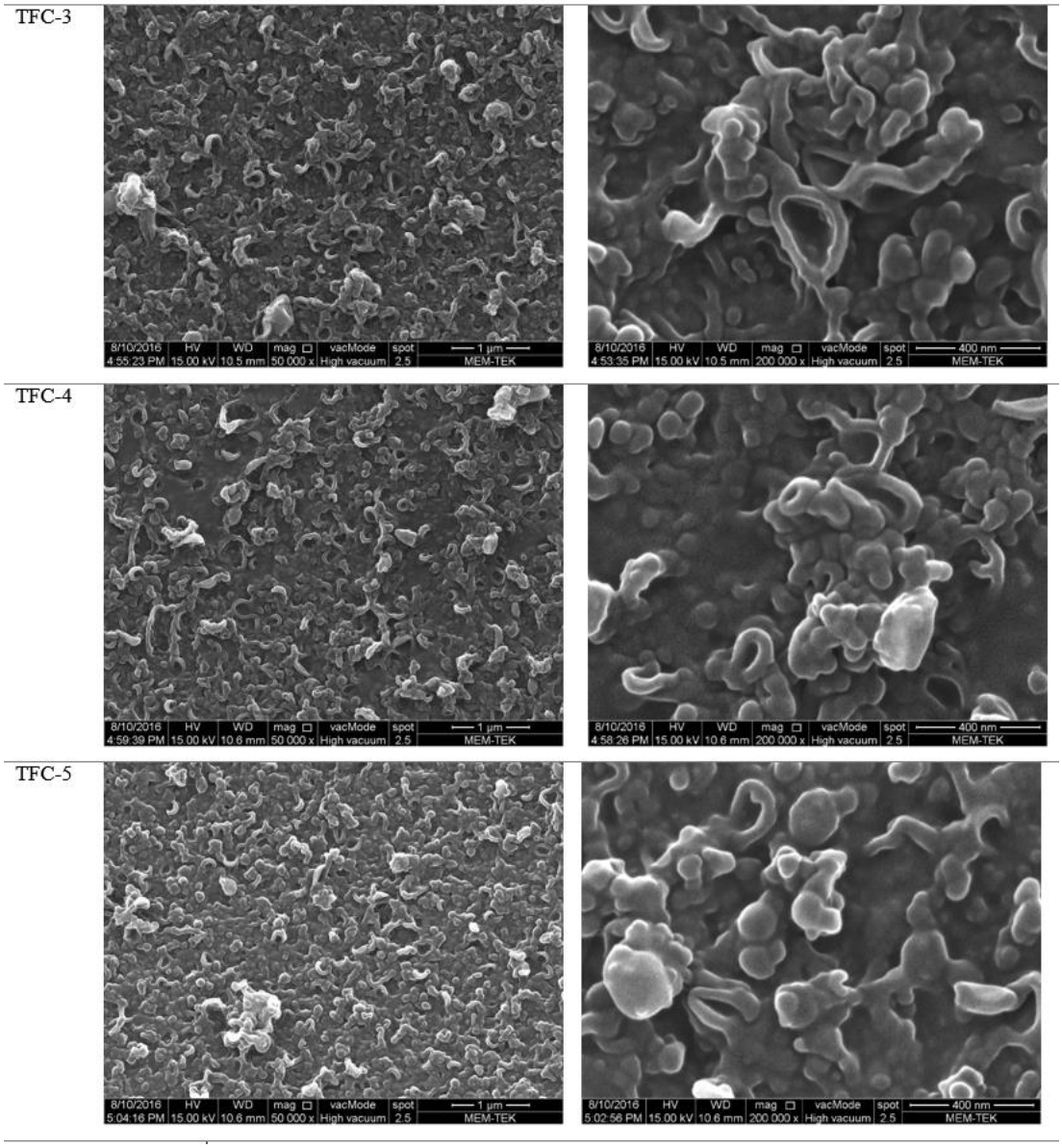

Figure B.1 (continued) : SEM surface morphologies of the control polyamide membrane TFC-0 and the zwitterionic silane modified polyamide-polysiloxane membranes TFC-1, TFC-2, TFC-3, TFC-4 and TFC-5, produced at SPPT/MPD ratios of 0.05, 0.1, 0.25, 0.5 and 1 respectively.

CURRICULUM VITAE

Name Surname **:** Jalal-Al-Din SHARABATI

Place and Date of Birth **:** Freiburg im Breisgau, 08.08.1986

E-Mail **:** sharabati@outlook.com

EDUCATION **:**

- **B.Sc.** **:** 2010, University of Duisburg-Essen, Water-Science
- **M.Sc.** **:** 2013, University of Duisburg-Essen, Water-Science

PROFESSIONAL EXPERIENCE:

- 2012-2013 University of Duisburg-Essen, Technical Chemistry II
- 2014-2018 Istanbul Technical University, MEM-TEK Research Center
- 2018 Completed Doctorate at Istanbul Technical University

PUBLICATIONS, PRESENTATIONS AND PATENTS ON THE THESIS:

- **Sharabati, J.,** Guclu, S., Erkoc-Ilter, S., Koseoglu-Imer, D.Y., Unal, S., Menceloglu, Y.Z., Ozturk, I., Koyuncu, I. 2018. Interfacially polymerized thin-film composite membranes: Impact of support layer pore size on active layer polymerization and seawater desalination performance, *Seperation and Purification Technology*, 212, 438–448
- Guclu, S., **Sharabati, J.**, Eris, C., Imer, D.Y., Menceloglu, Y., Ozturk, I., Koyuncu, I. 2017. Effect of support layer pore size on active layer morphology and RO salt rejection of interfacially polymerized TFC membranes, *3rd International Conference on Desalination Using Membrane Technology*, 2-5 April 2017, Las Palmas, Spain.

- **Sharabati, J.**, Erkoc-Ilter, S., Guclu, S., Saffarimiandoab, F., Imer, D.Y., Unal, S., Menceloglu, Y., Ozturk, I., Koyuncu, I. 2017. Zwitterionic Polysiloxane-polymamide interpenetrating network as active layer for high performance RO Membranes, *8th IWA Membrane Technology Conference & Exhibition for Water and Wastewater Treatment and Reuse*, 5-9 Sept. 2017, Suntec Singapore International Convention & Exhibtion Centre, Singapore.
- Guclu, S., **Sharabati, J.**, Saffarimiandoab F., Agtas, M., Koseoglu-Imer, D.Y., Pasaoglu, M.E., Menceloglu, Y.Z., Unal, S., Koyuncu, I., 2018. Investigation of pilot scale manufacturing of polysulfone (PSf) membranes by wet phase inversion method, *Desalination and Water Treatment*, 131, 66–74.
- **Sharabati, J.**, Erkoc-Ilter, S., Guclu, S., Saffarimiandoab, F., Koseoglu-Imer, D.Y., Unal, S., Menceloglu, Y., Ozturk, I, Koyuncu, I. (2017). Zwitteriyonik Monomer Katkılı Poliamid Aktif Tabakalı Ters Ozmos Membranları. MEMTEK Çalıştayı 2017, Istanbul.
- **Sharabati, J.**, Erkoc-Ilter, S., Guçlu, S., Saffarimiandoab, F., Koseoglu-Imer, D.Y., Unal, S., Menceloglu, Y., Ozturk, I., Koyuncu, I. (2017). Poliamid Aktif Tabaka İçerisine Zwitteriyonik Monomer Katkısının Performans Değerlendirmesi. Desalinasyon Teknolojileri Çalıştayı 2017, Istanbul.
- **Sharabati, J.**, Erkoc-Ilter, S., Guclu S., Koseoglu-Imer, D.Y., Unal, S., Menceloglu, Y.Z., Ozturk, I., Koyuncu, I. (2019). High-performance and chlorine-resistant thin-film composite membrane with zwitterionic polysiloxane-polyamide active layer. Under review.
- High Performance Thin Film Composite Membranes. Patent application number 2017/13140.

OTHER PUBLICATIONS, PRESENTATIONS AND PATENTS:

- Racyte, J.**, Sharabati**, **J.**, Paulitsch-Fuchs, A.H., Yntema, D.R., Mayer, M.J.J., Bruning, H., Rijnaarts, H.H.M. (2011). Combining fluidized activated carbon with weak alternating electric fields for disinfection, *Carbon, 49* (2011) 5321-5328.

- **Sharabati, J.,** Birkner, M., Ulbricht, M., (2013). Fouling and cleaning test system for stimuli-responsive membranes. 29th European Membrane Summerschool 2013, Essen, Germany.